Studies of Lattice Fermion-Scalar Interactions

Andrew M. Thornton

PhD, University of Edinburgh, 1989.

Abstract

Lattice models of quantum field theories are studied numerically and analytically where scalar fields interact with fermionic fields. The results of these studies are discussed in the context of the Higgs mechanism and the lattice fermion doubling problem. An introduction to the analytical and numerical techniques used in these studies is given. Some suggestions are given as to how this work could be extended.

Declaration

The composition of this thesis is my own work.

The work on the radially fixed Higgs-Yukawa model, as described in chapter 2, was done in collaboration with David Stephenson. Richard Kenway suggested the semi-classical treatment described in section 1.6.2 and used in the study of the models described in chapters 2 and 3. The rest of the work described in this thesis is my own.

Some material used in this thesis has previously been published [1,2,3,4].

Contents

1 Introduction **8**

1.1 Introduction 8

1.2 Path Integrals on the Lattice 10

1.3 Fermions on the Lattice 15

1.3.1 Chiral Symmetry 16

1.3.2 Fermion Doubling 16

1.3.3 Pseudo-Fermions 19

1.4 Hybrid Monte Carlo 20

1.5 Inversion Algorithms 23

1.5.1 Standard Conjugate Gradient 23

1.5.2 Least Norm Conjugate Gradient 24

1.5.3 Predictor 25

1.6 Analytical Methods 26

1.6.1 Lattice Perturbation Theory 27

1.6.2 Semi-Classical Treatment 33

1.6.3 Large Y Expansion 34

1.6.4 Mean Field Theory 35

2 Lattice Higgs-Yukawa Model **39**

2.1 Introduction 39

2.2 Action 42

2.2.1 Phases of the Model 44

2.2.2 $Y = 0$ Limit 45

2.3 Observables 46

2.4 Simulation 50

2.4.1 Algorithm 50

2.4.2 Implementation 52

2.4.3 Program Checks 53

2.5 Results 59

2.6 Analytical Study 71

2.6.1 Semi-Classical Study 71

2.6.2 $Y = \infty$ 73

2.6.3 Effective Scalar Potential 75

2.7 Discussion 76

3 Lattice Yukawa-Wilson Model **80**

3.1 Introduction 80

3.2 Action 82

3.3 Observables 84

3.4 Phase Diagram 86

3.4.1 Program Checks 86

3.4.2 Results 87

3.4.3 Analytical Study 92

3.4.4 Discussion 93

3.5 Fermion Propagators 94

3.5.1 Implementation 95

3.5.2 Program Checks 97

3.5.3 Results 97

3.5.4 Discussion 108

4 Prospects **111**

A Conventions Used **114**

A.1 Fourier Transforms 114

A.2 Gamma Matrices 115

Acknowledgements **118**

Bibliography **119**

Chapter 1

Introduction

1.1 Introduction

It is widely believed that all the known forces of nature can be described in terms of quantum field theories. At all energy scales at which observations have been made of the physical universe around us, it is seen that the basic building blocks of matter are fermions, and the forces between them are mediated by bosons according to quantum mechanical rules. It may well be the case, at some finer scale than has been possible so far to study, that Supersymmetry, Superstrings or some other Super-phenomenon may be required to describe what happens, but this is pure speculation at this time.

In our intuitive understanding of nature (so-called 'ping-pong physics'), we try to use our knowledge of the world around us to come to terms with quantum field theories, and thus we attempt to label these bosons and fermions as particles. Such a description is sometimes useful, because of the comforting analogy with everyday experience, but, for the most part, the intuitive notion of the particle is, at best, misleading, and often just plain wrong at small enough scales of observation. Although it is often possible to construct operators in quantum mechanics which create and annihilate states, which we try to interpret as operators which create and annihilate particles, quantum mechanics as applied to quantum field theories tells us that it is actually impossible to count the number

of particles in a physical quantum field state.

The quantum vacuum, for instance, far from being empty, is in fact the ground state of the quantum field, that is the allowed state of the system with the lowest energy. In our (literally) particular view of the world, we attempt to understand this vacuum state in terms of the possibility of the creation and then annihilation of virtual particle pairs, allowed by the Heisenberg uncertainty principle, as some kind of particle 'sea', whilst there are no permanent or 'valence' particles in the vacuum state. Another example is the proton, which is often described as consisting of three 'valence' quarks, which are fermions, held together by gluons, which are bosons, with some 'sea' quark anti-quark pairs occasionally being created and annihilated.

Quantum field theories are not bounded to such concepts, however. Instead, there is the formal mathematics of the effect of field operators on field states to consider. In practice, when physicists attempt to use mathematics to predict the behaviour of quantum field theories, the problems they encounter are so intractable that they tend to resort to methods owing much to the human intuitive particle view of nature. This is most apparent in the use of Feynman diagrams for evaluating some quantum field theory prediction for some quantity as a series expansion in one of the parameters of the theory. Whilst much has been achieved in the last few decades using such 'perturbative' methods, it is widely accepted that these are limited in what can be achieved with them.

With the recent availability of high performance computers, it is not surprising that physicists have attempted to use such machines in 'non-perturbative' studies of quantum field theories. To do this, physicists attempt to model quantum field theories by replacing the continuous dimensions of space and (usually) time with a lattice, on which models are defined which, in some 'continuum' limit, when the lattice spacing is reduced to zero, have the same properties as the real quantum field theories. This discretisation is necessary to give the system a finite number of degrees of freedom.

Although computers today can be made to perform many millions of calculations per second, simulations of quantum field theories on lattices, especially where

fermions are involved, as will be described later, are so numerically intensive that at present only extremely simple models on very small lattices have been studied. The work described in this thesis takes this into account, in that the models studied are ones in which fermionic fields interact with scalar fields in a simple way, and the numerical simulations performed on the computer are done on very small lattices. Scalar fields are the simplest form of bosonic fields. Despite these limitations, it is still possible to make qualitative statements about some aspects of quantum field theories in which scalar fields interact with fermions, which occurs for instance in the Standard Model, where the Higgs mechanism is thought to account for the generation of masses for the fermions (electrons) and some of the bosons (the W and Z bosons recently observed in the SPS collider at CERN).

Such computer simulations can only ever give answers to specific questions we humans ask about the quantum field theory models being studied, they cannot in themselves improve our understanding of the models. Knowledge, however, leads to insight, and thus computational physics in the field of quantum field theories can be viewed as a discipline in its own right, as well as a bridge between the long established disciplines of theoretical and experimental physics.

1.2 Path Integrals on the Lattice

The formalism by which quantum field theories are transcribed into lattice models will not be discussed here. Interested readers are invited to consult texts such as that by Creutz [5]. Instead, an intuitive 'recipe' will be given.

Classical field theories can be formulated in terms of classical dynamics. The action for a particular theory is written down and the allowed classical states of the system, which are the states which extremise the action, are given by the 'equations of motion', which are the Euler-Lagrange equations involving the functional derivatives of the action with respect to the classical fields and their space-time derivatives. It is usually possible to discretise a classical field theory on a lattice, in which derivatives of the fields are replaced by finite differences

between field variables on neighbouring lattice sites, so that the continuum action is regained when the lattice spacing is taken to zero. Then the lattice equations of motion, which are obtained by setting the functional derivatives of the action with respect to the lattice field variables equal to zero, will represent the true continuum behaviour of the field when the lattice spacing is taken to zero.

In the quantum version of a classical field theory, the field variables in the classical action are replaced by field operators in the quantum action, so it is not possible to assign values to them in any classical way. Instead, it is possible to write down a partition function which is a weighted integral over all possible classical field values, the so called path integral. Such an integration procedure is well defined on a lattice, where there is a finite number of degrees of freedom, which are the classical values of the fields at every point on the lattice, to integrate over.

So, given a classical lattice action $\mathcal{S}[\phi]$ which is a functional of fields $\phi(x)$ defined on lattice sites x, the classical state, which is represented by the set of values of $\phi(x)$ which extremise this action, is obtained by the 'equations of motion', which is the set of equations:

$$\frac{\delta \mathcal{S}[\phi]}{\delta \phi(x)} = 0 \tag{1.1}$$

for all sites on the lattice, x.

In Minkowski space-time, the partition function for the quantum version of the field theory on the lattice is:

$$\int \mathcal{D}\phi \, e^{\frac{i}{\hbar}\mathcal{S}[\phi]} \tag{1.2}$$

where the integration measure, $\mathcal{D}\phi$, is an abbreviation for the integration measure of the set of classical field variables, $\phi(x)$:

$$\mathcal{D}\phi = \prod_x \mathrm{d}\phi(x) \tag{1.3}$$

and $\hbar$ is Planck's constant divided by 2π. Note that in the 'classical' limit as $\hbar \to 0$, then the partition function becomes dominated more and more by the contribution from the set of field values which extremise the action, that is the set of field values which represents the classical field state. For small but finite $\hbar$, the dominant contribution to the partition function comes from a distribution of

sets of field variables more or less centered around that set which represents the classical field state - this is what is meant by the term 'quantum fluctuations.'

If the classical action is real, however, it is much more convenient to define the quantum version of the lattice field theory in Euclidean space, that is Minkowski time equals i times Euclidean time. After the rotation into Euclidean time, then the partition function, $\mathcal{Z}$, becomes:

$$\mathcal{Z} = \int \mathcal{D}\phi \, e^{-\frac{1}{\hbar}\mathcal{S}_E[\phi]} \tag{1.4}$$

where $\mathcal{S}_E$ is the Euclidean version of the action, which is conventionally defined as minus the Minkowski action with the change in the definition of time taken into consideration in the differentials with respect to time.

If there is an observable of the quantum field theory, O, which depends on field operators, then its expectation value can be evaluated using the path integral formulation as the weighted average of the classical version of the operator, $O[\phi]$, in which the field operators are replaced by the field variables, $\phi(x)$, over all possible sets of values of $\phi(x)$:

$$\langle O[\phi] \rangle = \frac{1}{\mathcal{Z}} \int \mathcal{D}\phi \, O[\phi] \, e^{-\frac{1}{\hbar}\mathcal{S}_E[\phi]} \tag{1.5}$$

In this way the weight factor $e^{-\frac{1}{\hbar}\mathcal{S}_E[\phi]}$ in the integral, which is real if the action is real, can be interpreted in terms of a Boltzmann-like probability density factor, and hence $\hbar$ can be interpreted in terms of a temperature. Thus a connection can be made between quantum field theories and statistical mechanical systems, though the action is used in one case and the Hamiltonian in the other.

In future in this thesis, as is the general convention, natural units will be used in which $\hbar = 1$. Unless otherwise stated, four dimensional Euclidean space will be assumed.

Thus to perform a computer simulation of the quantum field theory to find the expectation value of $O[\phi]$ on the lattice, the integrations of equation (1.5) are performed by Monte Carlo numerical methods. This can be done if a computer program generates sets of field values, $\phi(x)$, called 'configurations', with probability density $e^{-\mathcal{S}[\phi]}$, and the expectation value of the operator O will then just be the simple average over these configurations of the classical value of $O[\phi]$.

For example, consider a simple real scalar field theory with a continuum Minkowski action, $\mathcal{S}_M$:

$$\mathcal{S}_M = \int \mathrm{d}^4x \frac{1}{2} \left[(\partial_\mu \phi(x)) (\partial^\mu \phi(x)) - m^2 \phi(x)^2 \right] \tag{1.6}$$

where the summation of repeated indices is assumed, which has the equations of motion:

$$\partial_\mu \partial^\mu \phi(x) + m^2 \phi(x) = 0 \tag{1.7}$$

If $\phi(x)$ is interpreted in terms of a particle wave function of energy E and momentum $\mathbf{p}$, then this means that:

$$-E^2 + \mathbf{p}^2 + m^2 = 0 \tag{1.8}$$

that is the scalar 'particles' have mass m.

In Euclidean space, the continuum action becomes:

$$\mathcal{S} = \int \mathrm{d}^4x \frac{1}{2} \left[(\partial_\mu \phi(x)) (\partial_\mu \phi(x)) + m^2 \phi(x)^2 \right] \tag{1.9}$$

which can be discretised on the lattice to give, after a convenient change of scale, the lattice action:

$$\mathcal{S} = -\frac{\kappa}{2} \sum_{x\mu} \phi(x) \left[\phi(x+\mu) + \phi(x-\mu) \right] + \frac{1}{2} \sum_x (\phi(x))^2 \tag{1.10}$$

where site $x + \mu$ is the next lattice site from site x in the μ direction. The 'hopping parameter', κ, is related to the mass of the scalar field, m, in units of the inverse lattice spacing:

$$\kappa = \frac{1}{8 + m^2} \tag{1.11}$$

The partition function of this lattice model can be calculated. Using the abbreviation for the lattice action, $\mathcal{S}$:

$$\mathcal{S} = \frac{1}{2} \phi P \phi \tag{1.12}$$

then the partition function, $\mathcal{Z}$ is:

$$\begin{aligned} \mathcal{Z} &= \int \mathcal{D}\phi \, e^{-\mathcal{S}} \\ &\sim \mathrm{Det}\,[P]^{-\frac{1}{2}} \end{aligned} \tag{1.13}$$

which can be derived by diagonalising the matrix P and then performing the Gaussian integrations. This result easily generalises to lattice models involving complex scalar fields.

When a particle interpretation is put on a quantum field theory, information is obtained by studying the 'propagator' for that particle, which in essence shows how a particle would move from point to point in the background vacuum state of the quantum field. This propagator is a correlation function, it is the expectation value of the time ordered product of field operators at different points in space and time. In the path integral formulation, the propagator is just the expectation value of the given product with the operators replaced by the field variables. For example, the Euclidean propagator for the above real one-component scalar field theory on the lattice can easily be evaluated as the inverse of the matrix P using techniques described in section 1.6.1:

$$\begin{aligned} \langle \phi(x_1)\,\phi(x_2)\rangle &= \frac{1}{\mathcal{Z}}\int \mathcal{D}\phi\,\phi(x_1)\,\phi(x_2)\,e^{-\mathcal{S}} \\ &= P^{-1}(x_1,x_2) \\ &= \frac{1}{V}\sum_p \frac{e^{ip(x_1-x_2)}}{\left[1-2\kappa\sum_\mu \cos p_\mu\right]} \end{aligned} \tag{1.14}$$

See appendix A.1 for details of the conventions used here for the sum over the V lattice momentum states, p, where V is the number of sites on the lattice.

Setting x_1 to be the origin of the lattice and summing over the spatial components of x_2, x, leaving the Euclidean time parameter, t, then for values of t far from zero and from the size of the lattice in the Euclidean time direction, L, if periodic boundary conditions are used for the scalar fields:

$$\sum_{\mathbf{x}} \langle \phi(0)\,\phi(x_2)\rangle \sim e^{-mt} + e^{-m(L-t)} \tag{1.15}$$

where m is the mass of the scalar fields in inverse lattice units. This is an example of a general theorem for the zero spatial momentum Euclidean propagators of physical particles that states that at large Euclidean time separation they take on this exponential form with decay constant equal to the mass of the particle. This will be used in chapter 3 to fit masses to measured fermionic propagators.

1.3 Fermions on the Lattice

It is possible to construct a 'classical' spinor field theory that represents fermionic fields on a Euclidean lattice by naively discretising the Euclidean version of Dirac's equation, giving:

$$\frac{1}{2}\sum_{\mu}\gamma_{\mu}\left[\psi\left(x+\mu\right)-\psi\left(x-\mu\right)\right]+m\psi\left(x\right)=0 \tag{1.16}$$

which can be written in a shorthand matrix-vector notation:

$$M\Psi=0 \tag{1.17}$$

Thus a naive lattice fermionic action, S, can be constructed:

$$\begin{aligned} S &= \overline{\Psi}M\Psi \\ &= \frac{1}{2}\sum_{x\mu}\overline{\psi}\left(x\right)\gamma_{\mu}\left[\psi\left(x+\mu\right)-\psi\left(x-\mu\right)\right]+m\sum_{x}\overline{\psi}\left(x\right)\psi\left(x\right) \end{aligned} \tag{1.18}$$

which has the 'equation of motion' given in equation (1.16). See appendix A.2 for details of the gamma matrices used. The spinor degrees of freedom are represented using anticommuting Grassmann variables.

To go from 'classical' mechanics to a quantum field theory, the same path integral prescription can be used as was used for the bosonic field theory in the previous section. The partition function for the corresponding quantum field theory, Z, can be found:

$$\begin{aligned} Z &= \int \mathcal{D}\overline{\Psi}\mathcal{D}\Psi\, e^{-S} \\ &\sim \mathrm{Det}\left[M\right] \end{aligned} \tag{1.19}$$

using the definitions of the integrals over Grassmann degrees of freedom:

$$\begin{aligned} \int \mathrm{d}\psi &= 0 \\ \int \mathrm{d}\psi\psi &= 1 \\ \int \mathrm{d}\psi\left(\psi\right)^{n} &= 0 \quad \text{if } n>1 \end{aligned} \tag{1.20}$$

1.3.1 Chiral Symmetry

When $m = 0$, the naive fermionic action (1.18) is invariant under the set of global transformations:

$$\begin{aligned} R\psi(x) &\rightarrow e^{i\alpha_R\gamma_5} R\psi(x) \\ L\psi(x) &\rightarrow e^{i\alpha_L\gamma_5} L\psi(x) \\ \overline{\psi}(x) R &\rightarrow \overline{\psi}(x) R e^{i\alpha_L\gamma_5} \\ \overline{\psi}(x) L &\rightarrow \overline{\psi}(x) L e^{i\alpha_R\gamma_5} \end{aligned} \tag{1.21}$$

for arbitrary constants α_L and α_R where:

$$\begin{aligned} R &= \frac{1}{2}(1+\gamma_5) \\ L &= \frac{1}{2}(1-\gamma_5) \end{aligned} \tag{1.22}$$

are matrix operators which project out 'left-handed' and 'right-handed' fermion states when $m = 0$. This is called chiral symmetry.

An explicit fermion mass term in the action of the form:

$$m \sum_x \overline{\psi}(x)\psi(x) \tag{1.23}$$

breaks this chiral symmetry. This means that when interactions between the fermions and other fields are included when $m = 0$, then it is not possible for the fermions to gain an effective mass from those interactions unless either those interactions explicitly break the chiral symmetry of the action or if the symmetry is broken 'dynamically', where the ground state of the model does not possess the same symmetries as the action. This is the subject of much of this thesis.

1.3.2 Fermion Doubling

The expectation values of fermionic observables, for instance the fermionic propagator, can be evaluated analytically using the path integral formalism by doing

the integral of the 'classical' operator for the observable over the fermionic degrees of freedom with weight e^{-S}, using techniques described in section 1.6.1:

$$\begin{aligned}\left\langle \psi(x_1)\overline{\psi}(x_2)\right\rangle &= \frac{1}{Z}\int \mathcal{D}\overline{\Psi}\mathcal{D}\Psi\,\psi(x_1)\overline{\psi}(x_2)\,e^{-S} \\ &= M^{-1}(x_1,x_2) \\ &= \frac{1}{V}\sum_p \frac{e^{ip(x_1-x_2)}}{i\sum_\mu \gamma_\mu \sin p_\mu + m}\end{aligned} \tag{1.24}$$

using suitable conventions for the sum of the allowed lattice momentum states, p, (see appendix A.1), where V is the number of sites on the lattice.

Unfortunately, when the lattice spacing goes to zero, this propagator does not correspond to the continuum fermionic propagator in Euclidean space, which in momentum space is proportional to:

$$\left(i\sum_\mu \gamma_\mu p_\mu + m\right)^{-1} \tag{1.25}$$

because $\sin p_\mu$ is zero not only when $p_\mu = 0$, but also when $p_\mu = \pi$. This means that for every lattice direction, the effective number of fermion species is doubled. On a four dimensional lattice, that means there are sixteen such fermion species, only one of which corresponds to a physical continuum fermion when the lattice spacing is taken to zero. This is known as fermion doubling.

A number of methods have been tried to cure, or at least reduce, this fermion doubling. The two most popular formulations of lattice fermions used are Staggered and Wilson fermions.

Staggered Fermions

In many systems it is seen that the spinor degrees of freedom can be diagonalised by a spinor transformation [6], leaving four independent fermionic systems. Three of these can be discarded leaving a fermionic field with four fermion species. These are known as 'Staggered fermions' [7] as the spinor degrees of freedom are spread over binary hypercubic sublattices.

Define:

$$\begin{aligned} \psi(x) &= \gamma_0^{x_0}\gamma_1^{x_1}\gamma_2^{x_2}\gamma_3^{x_3}\chi(x) \\ \overline{\psi}(x) &= \overline{\chi}(x)\gamma_3^{x_3}\gamma_2^{x_2}\gamma_1^{x_1}\gamma_0^{x_0} \end{aligned} \tag{1.26}$$

where:

$$x_\mu = (x_0, x_1, x_2, x_3) \tag{1.27}$$

Thus, using the properties of the Euclidean gamma matrices used as described in appendix A.2, equation (1.18) can be rewritten as:

$$S = \frac{1}{2}\sum_{x_\mu}\overline{\chi}(x)\,\eta_\mu\left[\chi(x+\mu) - \chi(x-\mu)\right] + m\sum_x \overline{\chi}(x)\chi(x) \tag{1.28}$$

where:

$$\eta_\mu = \left(1, (-1)^{x_0}, (-1)^{x_0+x_1}, (-1)^{x_0+x_1+x_2}\right) \tag{1.29}$$

In this formulation, the four spinor degrees of freedom are independent, thus three of them can be dropped leaving four species of fermions, three of which are unphysical.

These Staggered fermions have the advantage that the resulting fermionic action is chirally invariant when $m = 0$, as described above. Another advantage is that the reduction by a factor of four of the fermionic degrees of freedom means that simulations using them tend to be much faster and use less computer memory than the corresponding simulations using other formulations of lattice fermions. It is the speed factor which accounts for their popularity.

Wilson Fermions

Wilson fermions [8] remove the unwanted fermionic species by giving them an excess mass. This is done by adding an extra momentum dependent term into the action:

$$\begin{aligned} \overline{\Psi} M \Psi &= \frac{1}{2}\sum_{x\mu}\overline{\psi}(x)\left[(\gamma_\mu - 1)\psi(x+\mu) - (\gamma_\mu + 1)\psi(x-\mu) + 2\psi(x)\right] \\ &\quad + m\sum_x \overline{\psi}(x)\psi(x) \end{aligned} \tag{1.30}$$

leading to a propagator:

$$\begin{aligned}\left\langle \psi(x_1)\overline{\psi}(x_2)\right\rangle &= M^{-1}(x_1,x_2) \\ &= \frac{1}{V}\sum_p \frac{e^{ip(x_1-x_2)}}{\sum_\mu (i\gamma_\mu \sin p_\mu + 1 - \cos p_\mu) + m}\end{aligned} \tag{1.31}$$

When the lattice spacing is taken to zero, this is equal to the continuum fermion propagator as required.

The addition of the extra momentum dependent term to the action to remove the doubled species of fermions in the Wilson formulation of the action (1.30) explicitly breaks the chiral symmetry which was present in the naive formulation when $m = 0$. When interactions with other fields are included, there is then no chiral symmetry to stop effective fermion mass terms being induced by the interactions, meaning that a zero fermion mass, m, in the action, called the 'bare' fermion mass, does not necessarily correspond to zero mass fermions in the model. In practice, to simulate interacting massless Wilson fermions, it is found that the bare fermion mass parameter, m, has to be tuned.

In fact, there is a general theorem [9,10] which states that any local extra momentum dependent fermionic term in the action for a fermionic system on a lattice, which gives all of the doubled fermion states an excess mass over the physical state, must break chiral symmetry.

1.3.3 Pseudo-Fermions

Classical fermionic fields are represented using anticommuting Grassmann variables. Unfortunately, there is no computer variable type **GRASSMANN**, and so these fermionic fields cannot be represented directly on a computer. Instead, pseudo-fermions can be used.

Using the definition of the partition function for a fermionic quantum field theory on a lattice, $\mathcal{Z}$:

$$Z = \int \mathcal{D}\overline{\Psi}\mathcal{D}\Psi\, e^{-\overline{\Psi}M\Psi}$$

$$\begin{aligned} &\sim \text{Det}\,[M] \\ &\sim \int \mathcal{D}\chi^\dagger \mathcal{D}\chi\, e^{-\chi^\dagger M^{-1}\chi} \end{aligned} \tag{1.32}$$

where the χ fields are complex scalars, called pseudo-fermions. Note that the fermionic matrix, M, in the fermionic action has been replaced by its inverse, M^{-1}, in the pseudo-fermionic action.

It is often the case that $M^\dagger$ is as suitable a fermionic matrix in the action as M. This is the case for naive fermions, because if a suitable Hermitian representation of the Euclidean gamma matrices, γ_μ, is used, then the representation, $-\gamma_\mu$, is also suitable. Thus two sets of fermionic fields can be used in the form:

$$\begin{aligned} Z &= \int \mathcal{D}\overline{\Psi}_1 \mathcal{D}\Psi_1 \mathcal{D}\overline{\Psi}_2 \mathcal{D}\Psi_2 \exp - \left[\overline{\Psi}_1 M \Psi_1 + \overline{\Psi}_2 M^\dagger \Psi_2\right] \\ &\sim \text{Det}\left[M^\dagger M\right] \\ &\sim \int \mathcal{D}\chi^\dagger \mathcal{D}\chi\, e^{-\chi^\dagger (M^\dagger M)^{-1}\chi} \end{aligned} \tag{1.33}$$

requiring only one set of pseudo-fermions, χ.

1.4 Hybrid Monte Carlo

In this section, the Hybrid Monte Carlo algorithm [11] is described, as used in this thesis to perform computer simulations of lattice models of quantum field theories where fermions interact with scalar fields. The fermionic degrees of freedom are simulated by using pseudo-fermions generated from a heatbath distribution and the scalar degrees of freedom are evolved using a molecular dynamics algorithm with a Monte Carlo accept/reject test to remove Monte Carlo time discretisation errors. This process generates scalar configurations with the required probability distribution over Monte Carlo time.

Suppose the model to be simulated has an action, $\mathcal{S}$, which is a function of a real scalar field Φ and fermion fields Ψ_1 and Ψ_2:

$$\mathcal{S} = S[\Phi] + \overline{\Psi}_1 M \Psi_1 + \overline{\Psi}_2 M^\dagger \Psi_2 \tag{1.34}$$

where the fermionic matrix, M, is a function of Φ so that the fermions interact with the scalar fields. Two sets of fermionic fields are included for reasons

described below. The pseudo-fermion representation is used, as described in section 1.3.3, so that the actual model simulated on the computer has action $\mathcal{S}'$:

$$\mathcal{S}' = S[\Phi] + \chi^\dagger \left(M^\dagger M\right)^{-1} \chi \tag{1.35}$$

for pseudo-fermion vector χ, which is generated with the correct distribution from a gaussian noise vector, η, generated with a probability density $e^{-\eta^\dagger \eta}$, by the relation $\chi = M^\dagger \eta$.

The scalar fields are evolved in Monte Carlo time, τ, by creating dynamics for Φ, whilst keeping the pseudo-fermions, χ, fixed. A random momentum vector, Π, is generated with probability distribution $e^{-\frac{1}{2}\Pi^2}$, and is used to define the dynamics of the scalar variables. There is some freedom in the choice of the coefficient of Π^2, corresponding to different definitions of the Monte Carlo time, τ. Thus a Hybrid Monte Carlo Hamiltonian, $\mathcal{H}$, can be written as:

$$\mathcal{H} = \frac{1}{2}\Pi^2 + S[\Phi] + \chi^\dagger \left(M^\dagger M\right)^{-1} \chi \tag{1.36}$$

The fact that two sets of fermionic fields, Ψ_1 and Ψ_2, are used ensures that the Hybrid Monte Carlo Hamiltonian, $\mathcal{H}$, is real, and thus a probabilistic interpretation can be made of the factor $e^{-\mathcal{H}}$, as in statistical mechanical systems.

In a continuous Monte Carlo time variable, τ, this Hamiltonian is conserved by the corresponding Hamilton's equations of motion:

$$\begin{aligned}
\frac{\mathrm{d}\Phi}{\mathrm{d}\tau} &= \frac{\partial \mathcal{H}}{\partial \Pi} \\
&= \Pi \\
\frac{\mathrm{d}\Pi}{\mathrm{d}\tau} &= -\frac{\partial \mathcal{H}}{\partial \Phi} \\
&= -\frac{\partial S[\Phi]}{\partial \Phi} + \chi^\dagger \left(M^\dagger M\right)^{-1} \left[M^\dagger \frac{\partial M}{\partial \Phi} + \frac{\partial M^\dagger}{\partial \Phi} M\right] \left(M^\dagger M\right)^{-1} \chi
\end{aligned} \tag{1.37}$$

In practice, τ is discretised into N intervals of size $\delta\tau$, and a discrete molecular dynamics algorithm, in this case the Leapfrog algorithm, is used:

1. The value of the momentum vector, Π, at time $\frac{\delta\tau}{2}$ is calculated, along with Φ at time $\delta\tau$:

$$\Pi\left(\frac{\delta\tau}{2}\right) = \Pi(0) - \frac{\partial \mathcal{H}}{\partial \Phi}(0) \times \frac{\delta\tau}{2} \tag{1.38}$$

$$\Phi(\delta\tau) = \Phi(0) + \Pi\left(\frac{\delta\tau}{2}\right) \times \delta\tau \tag{1.39}$$

2. For the number of steps required, $n = 1, \cdots, N-1$:

$$\Pi\left(\left(n+\frac{1}{2}\right)\delta\tau\right) = \Pi\left(\left(n-\frac{1}{2}\right)\delta\tau\right) - \frac{\partial\mathcal{H}}{\partial\Phi}(n\delta\tau) \times \delta\tau \tag{1.40}$$

$$\Phi((n+1)\,\delta\tau) = \Phi(n\delta\tau) + \Pi\left(\left(n+\frac{1}{2}\right)\delta\tau\right) \times \delta\tau \tag{1.41}$$

3. Finally, the value of the momentum vector, Π, at the end of the molecular dynamics steps is required:

$$\Pi(N\delta\tau) = \Pi\left(\left(N-\frac{1}{2}\right)\delta\tau\right) - \frac{\partial\mathcal{H}}{\partial\Phi}(N\delta\tau) \times \frac{\delta\tau}{2} \tag{1.42}$$

Over the required number of steps, because of the discretisation of the Monte Carlo time, τ, $\mathcal{H}$ changes by an amount $\delta\mathcal{H}$, and the new scalar configuration is accepted with a probability of one if this is negative, and with a probability of $e^{-\delta\mathcal{H}}$ if it is positive. The Leapfrog algorithm is reversible and is area preserving in the extended phase space, and thus the procedure satisfies detailed balance.

In this way, configurations are generated with probability density $e^{-\mathcal{H}}$ in the configuration space extended to include the momentum states represented by Π, and hence with the required probability density in the configuration space when Π is ignored.

The random vectors η and Π, along with the accept/reject test, are the stochastic elements of this algorithm, the molecular dynamics steps ensure that the scalar configuration evolves rapidly through phase space.

So an iteration of Hybrid Monte Carlo consists of the following steps:

1. Generate a gaussian noise vector η and set the pseudo-fermion vector $\chi = M^{\dagger}\eta$.

2. Measure any fermionic observables required. This is done independently of whether or not the next scalar configuration is accepted.

3. Do the requisite number of Molecular Dynamics steps using the Leapfrog algorithm keeping the pseudo-fermion vector χ constant.

4. Accept or reject the scalar configuration according to the change in $\mathcal{H}$ over the Molecular Dynamics steps as described above.

5. If the new configuration is accepted, then measure the new scalar observables, otherwise use the previous values.

The generalisation of this Hybrid Monte Carlo algorithm to lattice models with complex rather than real scalar fields is straightforward.

1.5 Inversion Algorithms

When simulating a lattice quantum field theory on a computer using the Hybrid Monte Carlo algorithm, the vast majority of computer time is spent in solving large sparse sets of linear equations to find the vector X, where:

$$M^\dagger M X = \chi \tag{1.43}$$

In the simulations described in this thesis, this is done by using two variants of the conjugate gradient algorithm [12,13,14,15,16,17], which solves the sets of linear equations (1.43) iteratively.

1.5.1 Standard Conjugate Gradient

The Standard Conjugate Gradient algorithm [18] solves for the vector X by minimising the modulus squared of the residual vector, R_i:

$$R_i = \chi - M^\dagger M X_i \tag{1.44}$$

where X_i is the approximation to X after the ith iteration.

Given some first approximate solution, X_0, to the required solution, X, the algorithm improves this approximate solution by proceeding as follows:

$$
\begin{aligned}
&R_0 = \chi - M^\dagger M X_0 \\
&P_0 = R_0 \\
&\text{while converging, } n = 0, 1, \cdots \\
&\quad \alpha_i = \frac{|R_i|^2}{|MP_i|^2} \\
&\quad X_{i+1} = X_i + \alpha_i P_i \\
&\quad R_{i+1} = R_i - \alpha_i M^\dagger M P_i \\
&\quad \beta_i = \frac{|R_{i+1}|^2}{|R_i|^2} \\
&\quad P_{i+1} = R_{i+1} + \beta_i P_i
\end{aligned}
$$

The algorithm is stopped when the modulus squared of R_i drops below a predetermined tolerance, and then the algorithm is restarted using the final value of X to be the first value of X in the restarted case to check that this tolerance has been achieved in practice. This is done because rounding errors are cumulative in this algorithm - the only time that the right hand side of equation (1.43) occurs in this algorithm is at the beginning.

1.5.2 Least Norm Conjugate Gradient

The first time equation (1.43) is to be solved in the Hybrid Monte Carlo algorithm, then it is known that:

$$\chi = M^\dagger \eta \tag{1.45}$$

Thus, in this case, equation (1.43) can be rewritten:

$$MX = \eta \tag{1.46}$$

enabling the Least Norm Conjugate Gradient algorithm to be used, which is known to be quicker and better conditioned [19] than the algorithm used above.

The algorithm iteratively improves the first guess, X_0, to the solution, X, of equations (1.46) by proceeding as follows:

$$R_0 = \eta - M X_0$$

$$
\begin{aligned}
&P_0 = 0 \\
&\text{while converging, } n = 0, 1, \cdots \\
&\quad \alpha_i = |R_i|^{-2} \\
&\quad P_{i+1} = P_i + \alpha_i M^\dagger R_i \\
&\quad \beta_i = |P_{i+1}|^{-2} \\
&\quad X_{i+1} = X_i + \beta_i P_{i+1} \\
&\quad R_{i+1} = R_i - \beta_i M P_{i+1}
\end{aligned}
$$

Again, the algorithm is stopped and then restarted when the modulus squared of R_i drops below a pre-determined tolerance.

1.5.3 Predictor

As so much time is spent in solving equations (1.43) when simulating lattice quantum field theories involving fermions using the Hybrid Monte Carlo algorithm, then some method of choosing the starting vector, X_0, close to the correct solution of the equations, X, will result in large savings in computer time.

The vector X, the solution of equations (1.43), is evaluated at regular intervals in Monte Carlo time. The pseudo-fermion vector, χ, is kept fixed throughout the Monte Carlo iteration, but the definition of the fermionic matrices M and $M^\dagger$ varies as the scalar fields are evolved. Given a sequence of past solutions of equations (1.43), then a Taylor expansion in $\delta\tau$, the Monte Carlo timestep, can be used to find an approximate value of X in terms of these previous values.

Given the last value of X at Monte Carlo time $\tau - \delta\tau$, $X(\tau - \delta\tau)$, then the vector X at Monte Carlo time τ, $X(\tau)$, can be evaluated as:

$$X(\tau) = X(\tau - \delta\tau) + O(\delta\tau) \tag{1.47}$$

Similarly, given the last two vectors, $X(\tau - \delta\tau)$ and $X(\tau - 2\delta\tau)$, Taylor's expansion can be used to show that:

$$X(\tau) = 2X(\tau - \delta\tau) - X(\tau - 2\delta\tau) + O\left(\delta\tau^2\right) \tag{1.48}$$

Error in prediction of $X(\tau)$	Coefficients of previous solutions			
	$X(\tau-\delta\tau)$	$X(\tau-2\delta\tau)$	$X(\tau-3\delta\tau)$	$X(\tau-4\delta\tau)$
$O(\delta\tau)$	1			
$O(\delta\tau^2)$	2	-1		
$O(\delta\tau^3)$	3	-3	1	
$O(\delta\tau^4)$	4	-6	4	-1

Table 1.1: Coefficients of solutions of the linear equations at previous Monte Carlo times used to find an approximate solution at this time.

Given the last three vectors, $X(\tau-\delta\tau)$, $X(\tau-2\delta\tau)$ and $X(\tau-3\delta\tau)$, Taylor's expansion can be used to show that:

$$X(\tau) = 3X(\tau-\delta\tau) - 3X(\tau-2\delta\tau) + X(\tau-3\delta\tau) + O\left(\delta\tau^3\right) \qquad (1.49)$$

Table 1.1 gives the coefficients of previous solutions and the error in the expression for the approximate new solution to the set of equations (1.43). It is clear that this can be generalised to arbitrary order if an arbitrary number of the previous solutions, X, are known, the coefficients of the previous solutions in the expression for the approximate new solution are just plus or minus a binomial coefficient. In this way, a good approximation to the required solution of equations (1.43) can be found from previous solutions. In practice, the number of previous solutions that can be used is limited by the number of steps done in that trajectory of the Molecular Dynamics part of the Hybrid Monte Carlo algorithm and ultimately by the size of computer memory used, as each of the previous solutions has to be remembered.

1.6 Analytical Methods

This section introduces and explains the analytical methods for studying models of quantum field theories on lattices as used in this thesis. These analytical

methods are perturbation theory, a semi-classical treatment, a large Y expansion and mean field theory.

To illustrate the techniques used, a simple lattice model will be studied as an example where a real one-component scalar field interacts with naive fermions via a Yukawa coupling. The action for this model, $\mathcal{S}$, is:

$$\begin{aligned}\mathcal{S} &= -\frac{1}{2}\kappa\sum_{x\mu}\phi(x)\left[\phi(x+\mu)+\phi(x-\mu)\right]+\frac{1}{2}\sum_{x}\left(\phi(x)\right)^2 \\ &+\frac{1}{2}\sum_{x\mu}\overline{\psi}(x)\gamma_\mu\left[\psi(x+\mu)-\psi(x-\mu)\right]+m\sum_{x}\overline{\psi}(x)\psi(x) \\ &+Y\sum_{x}\overline{\psi}(x)\phi(x)\psi(x) \qquad (1.50)\end{aligned}$$

1.6.1 Lattice Perturbation Theory

In this section, an introduction is given to the lattice perturbative methods used in this thesis. The general idea is to produce expressions for the expectation values of observables of the lattice quantum field theory model as an expansion in powers of some parameter of the model, where the expectation values of observables of the model can be evaluated analytically when that expansion parameter is zero. These perturbative expressions can then be evaluated, and their values compared with the expectation values measured from the computer simulation. This is used in this thesis as a check on the validity of the results obtained from the computer simulation.

To illustrate the techniques used, perturbative expressions to order Y^2 will be derived for the scalar and fermion propagators for the simple lattice model with action, $\mathcal{S}$, given in equation (1.50). By using the abbreviations:

$$\begin{aligned}\Phi P\Phi &= -\kappa\sum_{x\mu}\phi(x)\left[\phi(x+\mu)+\phi(x-\mu)\right]+\sum_{x}\left(\phi(x)\right)^2 \\ \overline{\Psi}F\Psi &= \frac{1}{2}\sum_{x\mu}\overline{\psi}(x)\gamma_\mu\left[\psi(x+\mu)-\psi(x-\mu)\right]+m\sum_{x}\overline{\psi}(x)\psi(x) \\ \overline{\Psi}U[\Phi]\Psi &= Y\sum_{x}\overline{\psi}(x)\phi(x)\psi(x) \qquad (1.51)\end{aligned}$$

the action can be written in the shorter and more convenient form:

$$\mathcal{S}=\frac{1}{2}\Phi P\Phi+\overline{\Psi}F\Psi+\overline{\Psi}U[\Phi]\Psi \qquad (1.52)$$

The partition function for the model when $Y = 0$, Z_0, can be found directly, as described in sections 1.2 and 1.3:

$$\begin{aligned} \mathcal{Z}_0 &= \int \mathcal{D}\overline{\Psi}\mathcal{D}\Psi\mathcal{D}\Phi \exp - \left[\frac{1}{2}\Phi P\Psi + \overline{\Psi}F\Psi\right] \\ &\sim \mathrm{Det}\,[P]^{-\frac{1}{2}}\,\mathrm{Det}\,[F] \end{aligned} \tag{1.53}$$

It is useful to define a partition function for the model with $Y = 0$ in the presence of 'source fields' $\overline{\eta}$, η and J for the fermion fields Ψ, $\overline{\Psi}$ and Φ respectively. This can also be evaluated explicitly:

$$\begin{aligned} \mathcal{Z}_0\left[\overline{\eta},\eta,J\right] &= \int \mathcal{D}\overline{\Psi}\mathcal{D}\Psi\mathcal{D}\Phi \exp - \left[\frac{1}{2}\Phi P\Psi + \overline{\Psi}F\Psi - \overline{\eta}\Psi - \overline{\Psi}\eta - J\Phi\right] \\ &= \int \mathcal{D}\overline{\Psi}\mathcal{D}\Psi\mathcal{D}\Phi \exp - \left[\frac{1}{2}\left(\Phi - JP^{-1}\right)P\left(\Phi - P^{-1}J\right) - \frac{1}{2}JP^{-1}J\right] \\ &\quad \times \exp - \left[\left(\overline{\Psi} - \overline{\eta}F^{-1}\right)F\left(\Psi - F^{-1}\eta\right) - \overline{\eta}F^{-1}\eta\right] \\ &\sim \mathrm{Det}\,[P]^{-\frac{1}{2}}\,\mathrm{Det}\,[F] \exp\left[\frac{1}{2}\left(JP^{-1}J\right) + \left(\overline{\eta}F^{-1}\eta\right)\right] \end{aligned} \tag{1.54}$$

Noting that functionally differentiating $\mathcal{Z}_0\left[\overline{\eta},\eta,J\right]$ with respect to $\overline{\eta}$, η and J respectively brings down a factor Ψ, $-\overline{\Psi}$ and Φ from the exponential, then the full partition function for the model for all values of Y in the presence of the sources can be written:

$$\begin{aligned} \mathcal{Z}\left[\overline{\eta},\eta,J\right] &\sim \mathrm{Det}\,[P]^{-\frac{1}{2}}\,\mathrm{Det}\,[F] \exp\left[-\frac{\delta}{\delta\eta}U\left[\frac{\delta}{\delta J}\right]\frac{\delta}{\delta\overline{\eta}}\right] \\ &\quad \times \exp\left[\frac{1}{2}\left(JP^{-1}J\right) + \left(\overline{\eta}F^{-1}\eta\right)\right] \\ &= \exp\left[-\frac{\delta}{\delta\eta}U\left[\frac{\delta}{\delta J}\right]\frac{\delta}{\delta\overline{\eta}}\right]\mathcal{Z}_0\left[\overline{\eta},\eta,J\right] \end{aligned} \tag{1.55}$$

The scalar propagator can thus be evaluated as:

$$\begin{aligned} \left\langle\phi\left(x_1\right)\phi\left(x_2\right)\right\rangle &= \int \mathcal{D}\overline{\psi}\mathcal{D}\psi\mathcal{D}\phi\,\phi\left(x_1\right)\phi\left(x_2\right)e^{-\mathcal{S}} \\ &= \frac{1}{\mathcal{Z}_0\left[\overline{\eta},\eta,J\right]}\frac{\delta}{\delta J\left(x_1\right)}\frac{\delta}{\delta J\left(x_2\right)}\exp\left[-\frac{\delta}{\delta\eta}U\left[\frac{\delta}{\delta J}\right]\frac{\delta}{\delta\overline{\eta}}\right]\mathcal{Z}_0\left[\overline{\eta},\eta,J\right]\Big|_0 \end{aligned} \tag{1.56}$$

where the symbol $X\,|_0$ means 'evaluate expression X when the source fields are set to zero.' The perturbative expression will be found by expanding the exponential involving U to second order in Y, and evaluating those non-zero terms in the limit where the sources are set to zero.

These non-zero terms, dropping terms which are divided out by the factor of $\frac{1}{Z_0}$ as they arise, are:

$$\begin{aligned}\frac{\delta}{\delta J(x_1)}\frac{\delta}{\delta J(x_2)}\frac{1}{2}\left(JP^{-1}J\right) &= P^{-1}(x_1,x_2)\\ &= \frac{1}{V}\sum_p \frac{e^{ip(x_1-x_2)}}{\left[1-2\kappa\sum_\mu \cos p_\mu\right]}\end{aligned} \tag{1.57}$$

$$\begin{aligned}&\frac{\delta}{\delta J(x_1)}\frac{\delta}{\delta J(x_2)}\frac{Y^2}{2}\sum_{y_1y_2}\frac{\delta}{\delta\eta(y_1)}\frac{\delta}{\delta J(y_1)}\frac{\delta}{\delta\overline{\eta}(y_1)}\frac{\delta}{\delta\eta(y_2)}\frac{\delta}{\delta J(y_2)}\frac{\delta}{\delta\overline{\eta}(y_2)}\\ &\times\frac{1}{8}\left(JP^{-1}J\right)^2\frac{1}{2}\left(\overline{\eta}F^{-1}\eta\right)^2\\ &= Y^2\sum_{y_1y_2}P^{-1}(x_1,y_1)\mathrm{Tr}\left[F^{-1}(y_1,y_1)\right]P^{-1}(y_2,x_2)\mathrm{Tr}\left[F^{-1}(y_2,y_2)\right]\\ &\quad -Y^2\sum_{y_1y_2}P^{-1}(x_1,y_1)\mathrm{Tr}\left[F^{-1}(y_1,y_2)F^{-1}(y_2,y_1)\right]P^{-1}(y_2,x_2)\end{aligned} \tag{1.58}$$

The first term gives:

$$\begin{aligned}&Y^2\sum_{y_1y_2}\frac{1}{V^4}\sum_{pqab}\frac{e^{ia(x_1-y_1)}}{\left[1-2\kappa\sum_\mu\cos a_\mu\right]}\mathrm{Tr}\left[\frac{1}{m+i\sum_\mu\gamma_\mu\sin p_\mu}\right]\\ &\times\frac{e^{ib(y_2-x_2)}}{\left[1-2\kappa\sum_\mu\cos b_\mu\right]}\mathrm{Tr}\left[\frac{1}{m+i\sum_\mu\gamma_\mu\sin q_\mu}\right]\\ &= \frac{Y^2}{V^2}\sum_{pqab}\frac{\delta(a)}{\left[1-2\kappa\sum_\mu\cos a_\mu\right]}\frac{4m}{\left[m^2+\sum_\mu\sin^2 p_\mu\right]}\frac{\delta(b)}{\left[1-2\kappa\sum_\mu\cos b_\mu\right]}\\ &\quad\times\frac{4m}{\left[m^2+\sum_\mu\sin^2 q_\mu\right]}e^{iax_1}e^{ibx_2}\\ &= \frac{16m^2Y^2}{V^2}\left[\sum_p\frac{1}{\left[1-8\kappa\right]\left[m^2+\sum_\mu\sin^2 p_\mu\right]}\right]^2\end{aligned} \tag{1.59}$$

The second gives:

$$-Y^2\sum_{y_1y_2}\frac{1}{V^4}\sum_{abpq}\frac{e^{ia(x_1-y_1)}}{\left[1-2\kappa\sum_\mu\cos a_\mu\right]}\frac{e^{ib(y_2-x_2)}}{\left[1-2\kappa\sum_\mu\cos b_\mu\right]}$$

$$
\begin{aligned}
&\times \mathrm{Tr}\left[\frac{e^{ip(y_1-y_2)}}{\left[m+i\sum_\mu \gamma_\mu \sin p_\mu\right]}\frac{e^{iq(y_2-y_1)}}{\left[m+i\sum_\mu \gamma_\mu \sin q_\mu\right]}\right] \\
&= -\frac{4Y^2}{V^2}\sum_{abpq}\delta(-a+p-q)\delta(-p+q+b)\frac{e^{iax_1}e^{-ibx_2}}{\left[1-2\kappa\sum_\mu \cos a_\mu\right]\left[1-2\kappa\sum_\mu \cos b_\mu\right]} \\
&\times\frac{\left[m^2-\sum_\mu \sin p_\mu \sin q_\mu\right]}{\left[m^2+\sum_\mu \sin^2 p_\mu\right]\left[m^2+\sum_\mu \sin^2 q_\mu\right]} \\
&= -\frac{4Y^2}{V^2}\sum_{pq}\frac{\left[m^2-\sum_\mu \sin p_\mu \sin q_\mu\right]e^{i((p-q)(x_1-x_2))}}{\left[m^2+\sum_\mu \sin^2 p_\mu\right]\left[m^2+\sum_\mu \sin^2 q_\mu\right]\left[1-2\kappa\sum_\mu \cos(p-q)_\mu\right]^2}
\end{aligned}
\tag{1.60}
$$

Thus:

$$
\begin{aligned}
\langle\phi(x_1)\phi(x_2)\rangle &= \frac{1}{V}\sum_p \frac{e^{ip(x_1-x_2)}}{\left[1-2\kappa\sum_\mu \cos p_\mu\right]} \\
&+\frac{16m^2Y^2}{V^2}\left[\sum_p \frac{1}{\left[1-8\kappa\right]\left[m^2+\sum_\mu \sin^2 p_\mu\right]}\right]^2 \\
&-\frac{4Y^2}{V^2}\sum_{pq}\frac{\left[m^2-\sum_\mu \sin p_\mu \sin q_\mu\right]e^{i((p-q)(x_1-x_2))}}{\left[m^2+\sum_\mu \sin^2 p_\mu\right]\left[m^2+\sum_\mu \sin^2 q_\mu\right]\left[1-2\kappa\sum_\mu \cos(p-q)_\mu\right]^2} \\
&+O(Y^4)
\end{aligned}
\tag{1.61}
$$

In the case $Y = 0$, this is equivalent to equation (1.14).

Similarly, the fermion propagator can be evaluated:

$$
\begin{aligned}
\left\langle\psi(x_1)\overline{\psi}(x_2)\right\rangle &= \int \mathcal{D}\overline{\psi}\mathcal{D}\psi\mathcal{D}\phi\,\psi(x_1)\overline{\psi}(x_2)\,e^{-\mathcal{S}} \\
&= -\frac{1}{\mathcal{Z}_0[\overline{\eta},\eta,J]}\frac{\delta}{\delta\overline{\eta}(x_1)}\frac{\delta}{\delta\eta(x_2)}\exp\left[-\frac{\delta}{\delta\eta}U\left[\frac{\delta}{\delta J}\right]\frac{\delta}{\delta\overline{\eta}}\right]\mathcal{Z}_0[\overline{\eta},\eta,J]\Big|_0
\end{aligned}
\tag{1.62}
$$

The non-zero terms from expanding the exponential in U, again dropping terms which are divided out by the factor of $\frac{1}{Z_0}$ as they arise, are:

$$\begin{aligned}
-\frac{\delta}{\delta\overline{\eta}(x_1)}\frac{\delta}{\delta\eta(x_2)}\left(\overline{\eta}F^{-1}\eta\right) &= F^{-1}(x_1,x_2) \\
&= \frac{1}{V}\sum_p \frac{e^{ip(x_1-x_2)}}{\left[m+i\sum_\mu \gamma_\mu \sin p_\mu\right]} \\
&= \frac{1}{V}\sum_p \frac{\left[m-i\sum_\mu \gamma_\mu \sin p_\mu\right] e^{ip(x_1-x_2)}}{\left[m^2+\sum_\mu \sin^2 p_\mu\right]} \qquad (1.63)
\end{aligned}$$

$$\begin{aligned}
&-\frac{\delta}{\delta\overline{\eta}(x_1)}\frac{\delta}{\delta\eta(x_2)}\frac{Y^2}{2}\sum_{y_1y_2}\frac{\delta}{\delta\eta(y_1)}\frac{\delta}{\delta J(y_1)}\frac{\delta}{\delta\overline{\eta}(y_1)}\frac{\delta}{\delta\eta(y_2)}\frac{\delta}{\delta J(y_2)}\frac{\delta}{\delta\overline{\eta}(y_2)} \\
&\times\frac{1}{2}\left(JP^{-1}J\right)\frac{1}{6}\left(\overline{\eta}F^{-1}\eta\right)^3 \\
&= Y^2\sum_{y_1y_2}F^{-1}(x_1,y_1)F^{-1}(y_1,y_2)F^{-1}(y_2,x_2)P^{-1}(y_1,y_2) \\
&\quad -Y^2\sum_{y_1y_2}F^{-1}(x_1,y_1)F^{-1}(y_1,x_2)P^{-1}(y_1,y_2)\mathrm{Tr}\left[F^{-1}(y_2,y_2)\right] \qquad (1.64)
\end{aligned}$$

The first of the above terms gives:

$$\begin{aligned}
&Y^2\sum_{y_1y_2}\frac{1}{V^4}\sum_{pqra}\frac{e^{ip(x_1-y_1)}}{\left[m+i\sum_\mu\gamma_\mu\sin p_\mu\right]}\frac{e^{iq(y_1-y_2)}}{\left[m+i\sum_\mu\gamma_\mu\sin q_\mu\right]}\frac{e^{ir(y_2-x_2)}}{\left[m+i\sum_\mu\gamma_\mu\sin r_\mu\right]} \\
&\times\frac{e^{ia(y_1-y_2)}}{\left[1-2\kappa\sum_\mu\cos a_\mu\right]} \\
&= \frac{Y^2}{V^2}\sum_{pqra}\frac{\left[m-i\sum_\mu\gamma_\mu\sin p_\mu\right]}{\left[m^2+\sum_\mu\sin^2 p_\mu\right]}\frac{\left[m-i\sum_\mu\gamma_\mu\sin q_\mu\right]}{\left[m^2+\sum_\mu\sin^2 q_\mu\right]}\frac{\left[m-i\sum_\mu\gamma_\mu\sin r_\mu\right]}{\left[m^2+\sum_\mu\sin^2 r_\mu\right]} \\
&\quad\times\frac{e^{ipx_1}e^{-irx_2}}{\left[1-2\kappa\sum_\mu\cos a_\mu\right]}\delta(-p+q+a)\delta(-q+r-a) \\
&= \frac{Y^2}{V^2}\sum_{pq}\frac{\left[m-i\sum_\mu\gamma_\mu\sin p_\mu\right]\left[m-i\sum_\mu\gamma_\mu\sin q_\mu\right]\left[m-i\sum_\mu\gamma_\mu\sin p_\mu\right]}{\left[m^2+\sum_\mu\sin^2 p_\mu\right]^2\left[m^2+\sum_\mu\sin^2 q_\mu\right]}
\end{aligned}$$

$$\times \frac{e^{ip(x_1-x_2)}}{\left[1-2\kappa\sum_\mu \cos(p-q)_\mu\right]} \tag{1.65}$$

The other gives:

$$\begin{aligned}
&-Y^2\sum_{y_1y_2}\frac{1}{V^4}\sum_{pqra}\frac{e^{ip(x_1-y_1)}}{\left[m+i\sum_\mu\gamma_\mu\sin p_\mu\right]}\frac{e^{ir(y_1-x_2)}}{\left[m+i\sum_\mu\gamma_\mu\sin r_\mu\right]}\\
&\times\mathrm{Tr}\left[\frac{1}{\left[m+i\sum_\mu\gamma_\mu\sin q_\mu\right]}\right]\frac{e^{ia(y_1-y_2)}}{\left[1-2\kappa\sum_\mu\cos a_\mu\right]}\\
&=-\frac{Y^2}{V^2}\sum_{pqra}\frac{\left[m-i\sum_\mu\gamma_\mu\sin p_\mu\right]}{\left[m^2+\sum_\mu\sin^2 p_\mu\right]}\frac{\left[m-i\sum_\mu\gamma_\mu\sin r_\mu\right]}{\left[m^2+\sum_\mu\sin^2 r_\mu\right]}\\
&\quad\times\frac{4m}{\left[m^2+\sum_\mu\sin^2 q_\mu\right]}\frac{e^{ipx_1}e^{-irx_2}}{\left[1-2\kappa\sum_\mu\cos a_\mu\right]}\delta(-p+r+a)\delta(a)\\
&=-\frac{4mY^2}{V^2}\sum_{pq}\frac{\left[m^2-2i\sum_\mu\gamma_\mu\sin p_\mu-\sum_\mu\sin^2 p_\mu\right]e^{ip(x_1-x_2)}}{\left[m^2+\sum_\mu\sin^2 p_\mu\right]^2\left[m^2+\sum_\mu\sin^2 q_\mu\right]\left[1-8\kappa\right]}
\end{aligned} \tag{1.66}$$

Thus:

$$\begin{aligned}
\left\langle\psi(x_1)\overline{\psi}(x_2)\right\rangle &= \frac{1}{V}\sum_p\frac{\left[m-i\sum_\mu\gamma_\mu\sin p_\mu\right]e^{ip(x_1-x_2)}}{\left[m^2+\sum_\mu\sin^2 p_\mu\right]}\\
&+\frac{Y^2}{V^2}\sum_{pq}\frac{\left[m-i\sum_\mu\gamma_\mu\sin p_\mu\right]\left[m-i\sum_\mu\gamma_\mu\sin q_\mu\right]\left[m-i\sum_\mu\gamma_\mu\sin p_\mu\right]}{\left[m^2+\sum_\mu\sin^2 p_\mu\right]^2\left[m^2+\sum_\mu\sin^2 q_\mu\right]}\\
&\times\frac{e^{ip(x_1-x_2)}}{\left[1-2\kappa\sum_\mu\cos(p-q)_\mu\right]}
\end{aligned}$$

$$-\frac{4mY^2}{V^2}\sum_{pq}\frac{\left[m^2-2i\sum_\mu\gamma_\mu\sin p_\mu-\sum_\mu\sin^2 p_\mu\right]e^{ip(x_1-x_2)}}{\left[m^2+\sum_\mu\sin^2 p_\mu\right]^2\left[m^2+\sum_\mu\sin^2 q_\mu\right]\left[1-8\kappa\right]}$$
$$+O\left(Y^4\right) \tag{1.67}$$

In the case $Y=0$, this is equivalent to equation (1.24).

1.6.2 Semi-Classical Treatment

In this section, a semi-classical treatment will be given to the simple lattice model with action given in equation (1.50) in the case $m=0$ for the sake of simplicity. The fermionic degrees of freedom will be integrated out analytically and the resulting effective scalar model will be treated classically, as described below.

Writing the action for the model, as given in equation (1.50), $\mathcal{S}$, as:

$$\mathcal{S}=\mathcal{S}\left[\phi\right]+\overline{\Psi}M\left[\phi\right]\Psi \tag{1.68}$$

where $\mathcal{S}\left[\phi\right]$ and the fermionic matrix $M\left[\phi\right]$ are functionals of the set of scalar field variables, $\phi(x)$, then the fermionic degrees of freedom can be integrated out analytically in the partition function, $\mathcal{Z}$:

$$\begin{aligned}\mathcal{Z} &= \int\mathcal{D}\overline{\psi}\mathcal{D}\psi\mathcal{D}\phi\, e^{-\mathcal{S}}\\ &= \int\mathcal{D}\phi\,\mathrm{Det}\left[M\left[\phi\right]\right]e^{-\mathcal{S}[\phi]}\\ &= \int\mathcal{D}\phi\, e^{-\mathcal{S}[\phi]+\mathrm{Tr}[\log_e M[\phi]]}\end{aligned} \tag{1.69}$$

Thus the model is equivalent to a scalar model with action, $\mathcal{S}'$:

$$\mathcal{S}'=\mathcal{S}\left[\phi\right]-\mathrm{Tr}\left[\log_e M\left[\phi\right]\right] \tag{1.70}$$

$\mathcal{S}'$ is called the effective scalar action of the model. This effective scalar model can then be treated classically, in that the allowed states of the system will be

that set of field variables $\phi(x)$ which minimises this effective action, $\mathcal{S}'$, that is the solution of the 'equations of motion':

$$\frac{\delta \mathcal{S}'}{\delta \phi(x)} = 0 \tag{1.71}$$

If interest is restricted to looking for aligned states of the model, then solutions to equations (1.71) are required of the form $\phi(x) = \Phi$, where Φ is a constant. Inserting this into equation (1.71), with $m = 0$, then:

$$0 = \left[(1 - 8\kappa) - \frac{4Y^2}{V} \sum_p \frac{1}{Y^2\Phi^2 + \sum_\mu \sin^2 p_\mu} \right] \Phi \tag{1.72}$$

Thus either $\Phi = 0$, which corresponds to a disordered phase when quantum fluctuations are taken into account, or Φ is a solution of the equation:

$$0 = (1 - 8\kappa) - \frac{4Y^2}{V} \sum_p \frac{1}{Y^2\Phi^2 + \sum_\mu \sin^2 p_\mu} \tag{1.73}$$

Where solutions to equation (1.73) exist, then these correspond to minima of the effective action, $\mathcal{S}'$, whilst $\Phi = 0$ is a maximum, except in the case where the solution to equation (1.73) is itself $\Phi = 0$. Thus Φ is continuous but its derivatives are discontinuous at the phase transition, suggesting that this transition is second order in this approximation, and the equation of the phase transition line can be found by making the substitution $\Phi = 0$ in equation (1.73), giving:

$$\kappa = \frac{1}{8} - \frac{Y^2}{2V} \sum_p \frac{1}{\left[\sum_\mu \sin^2 p_\mu \right]} \tag{1.74}$$

the disordered phase being at lower values of κ, the ordered phase being at higher values of κ.

1.6.3 Large Y Expansion

In this section, the effective scalar action derived in section 1.6.2 will be expanded as a power series in $\frac{1}{Y}$. This can be used to give information about the behaviour of the model in the large Y limit.

As used in the previous section, when the fermionic degrees of freedom are integrated out, then the result is the determinant of the fermionic matrix, M. Thus the effect of the fermions on the scalar sector can be represented by a term in the effective action equal to $-\mathrm{Tr}\left[\log_e M\right]$. This can be expanded as a power series in $\frac{1}{Y}$.

In the infinite Y limit:

$$\begin{aligned} -\mathrm{Tr}\left[\log_e M\right] &= -\mathrm{Tr}\left[\log_e \left(Y\phi\left(x\right)\delta(x,y)\right)\right] \\ &= -2\sum_x \log_e \phi\left(x\right)^2 + C(Y) \end{aligned} \tag{1.75}$$

where $C(Y)$ is independent of $\phi\left(x\right)$, and thus can be ignored.

The logarithm of the fermionic matrix, M, can then be expanded in powers of $\frac{1}{Y}$. Writing M as:

$$M\left(x_1, x_2\right) = F\left(x_1, x_2\right) + U\left(x_1, x_2\right) \tag{1.76}$$

where:

$$F\left(x_1, x_2\right) = \frac{1}{2}\sum_\mu \gamma_\mu \left[\delta\left(x_2, x_1 + \mu\right) - \delta\left(x_2, x_1 - \mu\right)\right] + m\delta\left(x_1, x_2\right) \tag{1.77}$$

and

$$U\left(x_1, x_2\right) = Y\phi\left(x_1\right)\delta\left(x_1, x_2\right) \tag{1.78}$$

then:

$$\begin{aligned} -\mathrm{Tr}\left[\log_e M\right] &= -\mathrm{Tr}\left[\log_e U\right] - \mathrm{Tr}\left[\log_e \left[1 + U^{-1}F\right]\right] \\ &= -\mathrm{Tr}\left[\log_e U\right] - \mathrm{Tr}\left[U^{-1}F - \frac{1}{2}U^{-1}FU^{-1}F + \ldots\right] \\ &= -2\sum_x \log_e \phi\left(x\right)^2 - \frac{4m}{Y}\sum_x \frac{1}{\phi\left(x\right)} + \frac{2m^2}{Y^2}\sum_x \frac{1}{\phi\left(x\right)^2} \\ &\quad -\frac{1}{2Y^2}\sum_{x\mu} \frac{1}{\phi\left(x\right)}\left[\frac{1}{\phi\left(x+\mu\right)} + \frac{1}{\phi\left(x-\mu\right)}\right] \\ &\quad +C\left(Y\right) + O\left(\frac{1}{Y^3}\right) \end{aligned} \tag{1.79}$$

1.6.4 Mean Field Theory

In this section, a simple mean field calculation will be described to find the critical value of κ in the lattice model with action given by equation (1.50) in

the case $Y = \infty$ and $m = 0$.

As has been shown in the previous sections, the effect of the fermions on the scalar sector in this model can be represented by an effective term in the scalar action. This gives rise to an effective scalar action, $\mathcal{S}'$, in the case $Y = \infty$ and $m = 0$:

$$\mathcal{S}' = -\frac{1}{2}\kappa \sum_{x_\mu} \phi(x)\left[\phi(x+\mu) + \phi(x-\mu)\right] + \frac{1}{2}\sum_{x} \phi(x)^2 - 2\sum_{x} \log_e \phi(x)^2 \quad (1.80)$$

In the mean field approximation, one site on the lattice is chosen, x, and the values of the field variables on the surrounding lattice sites, $\phi(x+\mu)$ and $\phi(x-\mu)$, are replaced by their mean value, Φ. This gives rise to a one-site partition function, $\mathcal{Z}_1(\Phi)$:

$$\begin{aligned} \mathcal{Z}_1(\Phi) &= \int \mathrm{d}\phi \exp - \left[-8\kappa\phi\Phi + \frac{1}{2}\phi^2 - 2\log_e \phi^2\right] \\ &= \int \mathrm{d}\phi\, \phi^4 \exp - \left[-8\kappa\phi\Phi + \frac{1}{2}\phi^2\right] \end{aligned} \quad (1.81)$$

For consistency, Φ must equal the expectation value of ϕ. Thus:

$$\begin{aligned} \Phi &= \frac{1}{\mathcal{Z}_1(\Phi)} \int \mathrm{d}\phi\, \phi \exp - \left[-8\kappa\phi\Phi + \frac{1}{2}\phi^2 - 2\log_e \phi^2\right] \\ &= \frac{1}{\mathcal{Z}_1(\Phi)} \int \mathrm{d}\phi\, \phi^5 \exp - \left[-8\kappa\phi\Phi + \frac{1}{2}\phi^2\right] \end{aligned} \quad (1.82)$$

This can be solved numerically to find the allowed states in this mean field approximation for $Y = \infty$ and $m = 0$. The critical value of κ, however, can be found analytically from this expression.

Figure 1.1 shows diagrammatically the solutions of equation (1.82). The curve is the right hand side of equation (1.82) as a function of $\kappa\Phi$, and the straight dashed lines are the left hand side written in the form:

$$F(\kappa\Phi) = \frac{1}{\kappa}(\kappa\Phi) \quad (1.83)$$

for differing values of κ. Thus the allowed solutions of equation (1.82) are the intersection points of the curve and the straight line for a given value of κ. It is seen that non-zero solutions of equation (1.82), corresponding to systems in

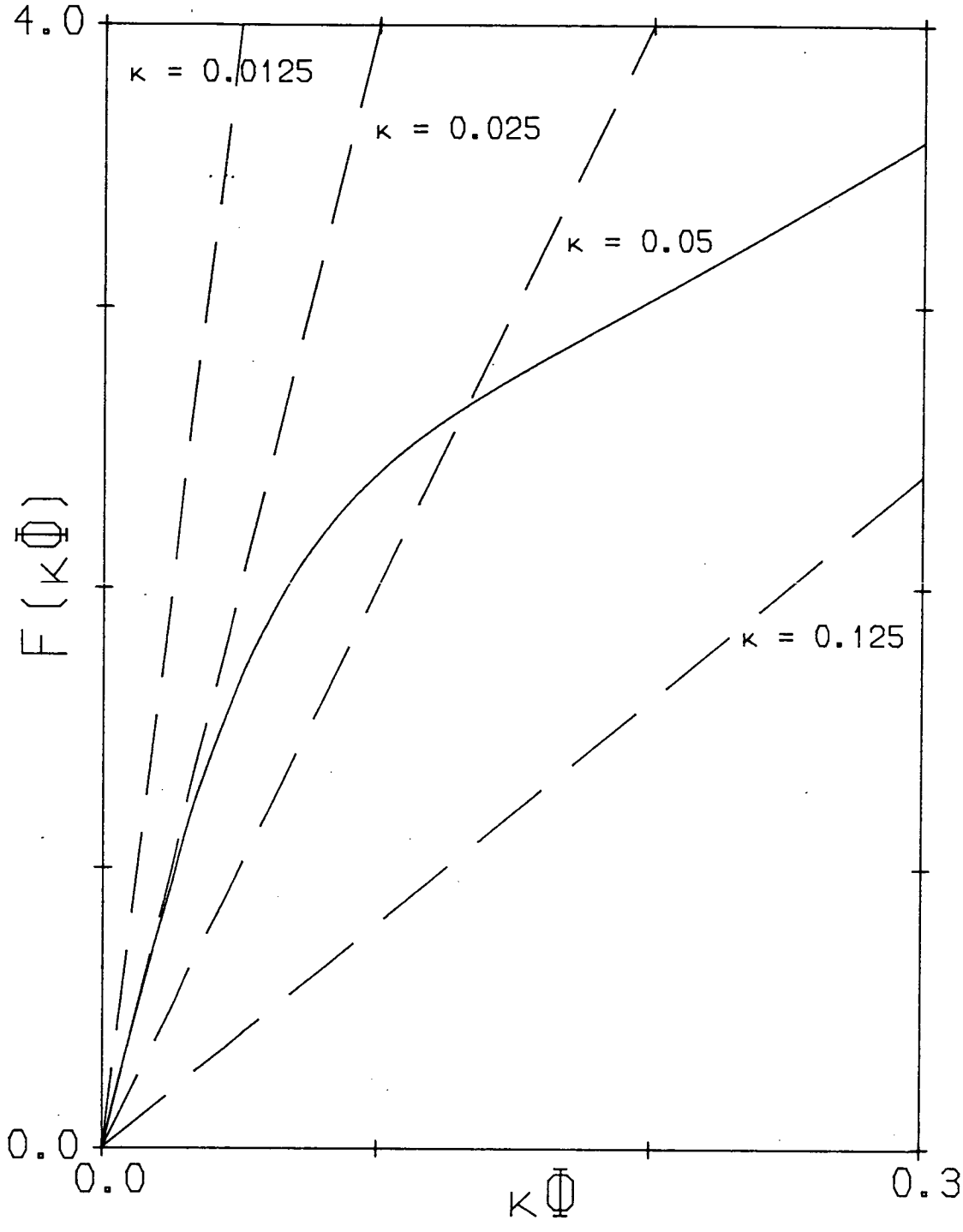

Figure 1.1: Diagram showing solutions of the mean field theory consistency equations. The allowed solutions are the intersection points of the curved and straight lines.

an aligned phase, only exist in the range $0.025 < \kappa < 0.125$. $\kappa = 0.025$ is the critical value of κ, and the model is unstable if $\kappa \geq 0.125$ as a value of $\kappa = \frac{1}{8}$ corresponds to massless scalar particles.

To find the critical value of κ analytically, the transition to look for is the one in which Φ goes from zero (in a disordered phase) to a non-zero value (in an aligned phase). Φ is continuous over this phase transition, though its derivatives are not, thus this is a second order phase transition in this approximation. To find the critical value of κ it is only necessary to look at the case of infinitesimal Φ, so the exponentials in the integrals in the above consistency equation need only be expanded to first order in Φ. Thus the consistency equation (1.82) becomes:

$$\begin{aligned} \Phi &= \frac{1}{\mathcal{Z}_1(\Phi)} \int \mathrm{d}\phi\, \phi^5 \left[1 + 8\kappa\Phi\phi + \cdots\right] e^{-\frac{1}{2}\phi^2} \\ &= \frac{1}{\mathcal{Z}_1(0)} 8\kappa\Phi \int \mathrm{d}\phi\, \phi^6 e^{-\frac{1}{2}\phi^2} + \cdots \\ &= 40\kappa\Phi + O\left(\Phi^2\right) \end{aligned} \tag{1.84}$$

Thus either $\Phi = 0$, which corresponds to a disordered phase, or if $\kappa > \frac{1}{40}$ (as alignment increases with κ) then $\Phi^2 > 0$ which corresponds to an aligned phase. Thus the critical value of κ in this approximation when $Y = \infty$ and $m = 0$ is 0.025.

Chapter 2

Lattice Higgs-Yukawa Model

2.1 Introduction

Below the Curie temperature, the local interactions between magnetic ions in a ferromagnet induce a global magnetisation in the bulk material in some direction. In a perfect crystalline structure, the local interactions have at least a discrete spatial symmetry, but the final state of the system projects out one special direction which manifestly breaks this symmetry. This occurs because the magnetised state in which the symmetry is broken has a lower free energy than any state in which the symmetry is respected. This is spontaneous symmetry breaking. If the Standard Model is to be believed, then spontaneous symmetry breaking also occurs in a quantum field theory. This means that the Higgs scalar fields, ϕ, gain a non-zero expectation value in a similar manner to the way in which a ferromagnet gains a non-zero bulk magnetisation.

It is thought that, at some energy scale, there exists a scalar potential which is of the form:

$$-m^2\phi^\star\phi + \lambda\left(\phi^\star\phi\right)^2 \tag{2.85}$$

the so-called 'Mexican Hat' potential. This potential has a global symmetry (which is U(1) if the scalar fields, ϕ, have only one component), but the field configurations with the lowest value of the action, and hence the largest contribution to the partition function, do not possess this symmetry, because the

'Mexican Hat' potential has a maximum at $\phi = 0$. The underlying symmetry of the system is hidden, or 'broken', when the system is in its ground state.

Because the Higgs bosons interact with other fields in the Standard Model, then this spontaneous symmetry breaking affects these fields. One effect is to give a mass to some of the gauge bosons - the W and Z particles recently detected in experiments using the SPS accelerator at CERN. An explicit mass term in the action for any gauge boson is not gauge invariant, but one can be generated by an interaction between the gauge bosons and a spontaneously broken scalar field. Another effect is that when the scalar fields gain a non-zero expectation value, a Yukawa interaction term in the action of the form:

$$Y\overline{\psi}\phi\psi \tag{2.86}$$

acts in a similar manner to an explicit fermion mass term:

$$m\overline{\psi}\psi \tag{2.87}$$

thus generating masses for the fermions. This is the well-known Higgs mechanism [20,21,22,23,24,25].

There are some problems with this mechanism, however. One problem is that perturbation theory tells us that the $\lambda\phi^4$ term, which is necessary to induce the spontaneous symmetry breaking, is marginally irrelevant, and thus can have no effect on the large scale properties of the model. This suggests that any $\lambda\phi^4$ term in the action could only be an effective term generated from some other interaction at some given energy scale, because if the system was studied at some energy scale lower than this, then the effective, that is renormalised, value of λ will be smaller.

Another problem with the mechanism is to do with the infra-red limit of the model in the limit in which the Yukawa coupling goes to zero. With no Yukawa coupling and no infra-red regulator, the massless fermions have an infinite correlation length, corresponding to the fermion operator having zero eigenvalues. This means that the partition function will be zero, causing singularities in the measured expectation values of observables, as these are generically derived by differentiating the logarithm of the partition function with respect to some pa-

rameter of the theory or some explicit source term in the action which is then set to zero.

With a small Yukawa coupling, the dominant scalar field configurations contributing to the path integral for the partition function will be determined by the fermionic sector. It will be these scalar configurations rather than those which just minimise the scalar contribution to the action which are important, as is assumed in the Higgs mechanism mentioned above, because of the contribution of the fermions to the scalar sector, which can be represented as a term in the effective scalar action of the form:

$$-\operatorname{Tr}[\log_e M] \tag{2.88}$$

where M is a fermionic matrix operator, as described in section 1.6. This contribution will be large if M has small eigenvalues. Thus these scalar states at small Yukawa coupling will most probably be radically different from the free scalar states when there is no Yukawa interaction. This suggests that there exists a critical point at zero Yukawa coupling.

From a purely aesthetic point of view, the Higgs mechanism is intrinsically unattractive, as the $\lambda\phi^4$ term is added 'by hand', and, for spontaneous symmetry breaking, the scalar fields, ϕ, have to be given a negative mass squared, which is counter-intuitive.

At the time of writing, no-one has observed a Higgs boson.

This chapter describes work revolving around the simulation of a very simple lattice model where naive fermions with zero bare mass interact with one-component complex scalar fields via a form of Yukawa coupling. The phase diagram of the model is discovered by performing computer simulations on small lattices. Some analytical work is also presented which helps explain some features of the phase diagram. The model studied is an extremely simplified model of a quantum field theory, when compared with the Standard Model, but some qualitative conclusions can be made about spontaneous symmetry breaking in the Standard Model from this work.

2.2 Action

The action for the model studied in this chapter is:

$$\begin{aligned} S &= -\kappa \sum_{x\mu} \phi^{\star}(x)\left[\phi(x+\mu)+\phi(x-\mu)\right] \\ &\quad + \sum_{x} \phi^{\star}(x)\,\phi(x) + \lambda \sum_{x} \left[\phi^{\star}(x)\,\phi(x)-1\right]^2 \\ &\quad + \overline{\Psi}_1 M \Psi_1 + \overline{\Psi}_2 M^{\dagger} \Psi_2 \end{aligned} \tag{2.89}$$

where:

$$\begin{aligned} \overline{\Psi} M \Psi &= \frac{1}{2} \sum_{x\mu} \overline{\psi}(x)\,\gamma_{\mu}\left[\psi(x+\mu)-\psi(x-\mu)\right] \\ &\quad + Y \sum_{x} \overline{\psi}(x)\left[\phi(x)\,R + \phi^{\star}(x)\,L\right]\psi(x) \end{aligned} \tag{2.90}$$

and:

$$\begin{aligned} R &= \frac{1}{2}(1+\gamma_5) \\ L &= \frac{1}{2}(1-\gamma_5) \end{aligned} \tag{2.91}$$

defined on a four dimensional Euclidean lattice with periodic boundary conditions for the scalar fields, ϕ. Two sets of fermions are used to facilitate the use of the Hybrid Monte-Carlo algorithm to simulate this model, as described in section 1.4. The form of the Yukawa interaction used ensures the hermiticity of the terms $\overline{\Psi}_1 M \Psi_1$ and $\overline{\Psi}_2 M^{\dagger} \Psi_2$ in the action, in that if $\overline{\psi}$ transforms under conjugation like $\psi^{\dagger} C$ where C is the Hermitian charge conjugation matrix that anticommutes with the Hermitian gamma matrix representation used (see appendix A), then these Yukawa terms are Hermitian.

The lattice provides an ultra-violet cutoff for the model, but the massless fermions, represented by the ψ fields, require an additional infra-red regulator. This is introduced by using anti-periodic boundary conditions for the fermions in the Euclidean time direction. The reason for this is explained in more detail in section 2.2.2 below.

When $\lambda = \infty$, the radial degree of freedom of the scalar fields, $\phi(x)$ and $\phi^{\star}(x)$, is fixed to unity. This is called the radially fixed case. Thus, when $\lambda = \infty$, the

degree of freedom is the phase angle, $\theta(x)$, and the following substitutions are made:

$$\begin{aligned} \phi(x) &= e^{i\theta(x)} \\ \phi^\star(x) &= e^{-i\theta(x)} \end{aligned} \tag{2.92}$$

When $\lambda = 0$, the scalar 'hopping' parameter κ is related to the bare mass, m, in inverse lattice units, of the scalar fields by the relation:

$$\kappa = \frac{1}{8 + m^2} \tag{2.93}$$

This means that for physically reasonable situations, when $\lambda = 0$, where the bare mass squared of the scalar fields is finite and non-negative, then κ varies in value between 0 and $\frac{1}{8}$. When $\lambda = 0$, the scalar sector is unstable for values of κ greater than or equal to one eighth, as the bare mass squared of the scalar fields is no longer non-negative.

When $Y = 0$, the fermionic sector is chirally invariant, as described in section 1.3.1, there being no fermionic mass term in the action, and there also exists independently a global U(1) symmetry in the scalar sector. For non-zero values of Y, the Yukawa term breaks this independence, so that the action is invariant under the set of global transformations:

$$\begin{aligned} R\psi_n(x) &\rightarrow e^{iq_n^1\alpha\gamma_5} R\psi_n(x) \\ L\psi_n(x) &\rightarrow e^{iq_n^2\alpha\gamma_5} L\psi_n(x) \\ \overline{\psi}_n(x)R &\rightarrow \overline{\psi}_n(x)Re^{iq_n^2\alpha\gamma_5} \\ \overline{\psi}_n(x)L &\rightarrow \overline{\psi}_n(x)Le^{iq_n^1\alpha\gamma_5} \\ \phi(x) &\rightarrow e^{iq\alpha}\phi(x) \\ \phi^\star(x) &\rightarrow e^{-iq\alpha}\phi^\star(x) \end{aligned} \tag{2.94}$$

for the species $n = 1, 2$ for arbitrary constant α, when:

$$\begin{aligned} q + q_1^1 + q_1^2 &= 0 \\ q - q_2^1 - q_2^2 &= 0 \end{aligned} \tag{2.95}$$

Thus the action is is invariant under certain global chiral rotations of the left and right handed projections of the fermionic fields when this is accompanied by a global rotation in phase of the scalar fields.

Note that this symmetry is strong enough to preclude the generation of an effective fermion mass term of the form:

$$m\overline{\psi}\psi \tag{2.96}$$

unless the symmetry is broken spontaneously, as a term of this form in the action explicitly breaks the above symmetry. This is of greater importance to the model studied in the next chapter than it is to the model of this chapter.

It is also possible to write down transformations mixing the two species of fermions under which the action is invariant, but these are not of interest here.

2.2.1 Phases of the Model

Looking at this model in terms of the scalar fields, an analogy with a magnetic system can be drawn. Magnetic systems, in general, can have three distinct phases: paramagnetic, ferromagnetic and anti-ferromagnetic. As in a paramagnetic phase, the scalar fields can be disordered on length scales much greater than the lattice spacing. There is the possibility of an aligned phase, where the phase of the scalar fields is almost the same throughout the system as in the ferromagnetic phase of a magnet. There is also the possibility of an anti-aligned or anti-ferromagnetic phase, where the scalar fields at neighbouring lattice sites tend to be of opposite phase. The disordered phase is often called the symmetric phase, as the ground state possesses the same symmetries as the action. In the aligned and anti-aligned phases this is not so, there is a preferred phase angle, and so these are often called broken phases. In these broken phases, the ground state of the system does not have the same symmetries as the action, and thus spontaneous symmetry breaking has occurred.

Because of the Yukawa term in the action, spontaneous symmetry breaking in the scalar sector results in the spontaneous symmetry breaking of the symmetries as stated in equations (2.94), thus effectively breaking what remains of chiral symmetry in this model.

2.2.2 $Y = 0$ Limit

As has been stated in the introduction to this chapter, there are problems with this model in the limit $Y \to 0$ due to infrared divergences in the fermionic sector. When $Y = 0$, with periodic boundary conditions for the fermions, the lowest eigenvalue of the fermionic matrix product $M^\dagger M$ is zero, and hence the partition function is zero. This is manifested in the fermionic sector by singularities in the fermionic propagator:

$$\begin{aligned} \langle \psi_1(x)\overline{\psi}_1(y)\rangle &= M^{-1}(x,y) \\ &= \frac{1}{V}\sum_p \frac{1}{i\sum_\mu \gamma_\mu \sin p_\mu} \end{aligned} \tag{2.97}$$

where V is the number of sites on the lattice and the sum over p represents the sum over the V allowed lattice momentum states (see section A.1 for the conventions used here for momentum sums). It also means that the equations 1.43 have no solution, thus the Hybrid Monte Carlo algorithm will not work in this limit.

Therefore, to simulate this model in the limit $Y \to 0$, it is necessary to introduce an infra-red regulator to remove the singularities in this propagator. One method is to add an explicit fermionic mass term to the action of the form:

$$m\overline{\psi}\psi \tag{2.98}$$

but this explicitly breaks the invariance of the action under the set of transformations (2.94). This has the effect of inducing some alignment of the scalar fields, so that there are no true disordered phases of the model. The method chosen in practice to remove these singularities is to impose anti-periodic boundary conditions on the fermionic fields in one direction, arbitrarily chosen to be the Euclidean time direction, t, so that provided there is an even number of sites in this direction, then $\sin p_t$ is never zero.

These singularities in the fermionic propagator occur not only when p is zero, but also when the components of p are all multiples of π, thus there are sixteen poles to the propagator corresponding to sixteen fermionic species. This is the fermion

doubling phenomena described in section 1.3.2. This is true whatever boundary conditions are used when the continuum limit is taken, but anti-periodic boundary conditions, provided there are an even number of lattice sites in the direction or directions in which they are imposed, ensure that these fermionic states do not manifest themselves as zero modes on finite lattices.

With the two sets of fermionic fields being used for this model, there are a total of thirty two fermionic states, thirty of which are unphysical, in this system. In this chapter, this fermionic doubling phenomenon is totally ignored. In the next chapter, however, this problem will be studied in more detail where a model related to this one will be used to induce masses for the unphysical fermionic doubles of the order of the inverse lattice spacing, so that they decouple from the theory in the continuum limit.

2.3 Observables

The expectation values of the following observables of the model are studied in this chapter:

$$\begin{aligned} Q &= \frac{1}{V}\sum_{x\mu}\phi^{\star}(x)\left[\phi(x+\mu)+\phi(x-\mu)\right] \\ CV &= \frac{\partial\langle Q\rangle}{\partial\kappa} \\ PsP &= \frac{1}{V}\sum_{x}\phi^{\star}(x)\,\phi(x) \\ R^2 &= \frac{1}{V^2}\sum_{xy}\phi^{\star}(x)\,\phi(y) \\ P2 &= \frac{1}{V}\mathrm{Tr}\left[\left(MM^{\dagger}\right)^{-1}\right] \end{aligned} \tag{2.99}$$

Q and R^2 are local and global alignment parameters respectively having expectation values around zero in a disordered phase and rising with alignment. The expectation value of Q is negative when anti-alignment occurs but R^2 has an expectation value close to zero. CV corresponds to a specific heat, by analogy with a magnetic system, and is measured from the fluctuations in Q over Monte Carlo time. The expectation value of PsP gives a measure of the amplitude of

the scalar fields and is unity, as has already been stated, when $\lambda = \infty$. $P2$ is a fermionic parameter whose expectation value gives an indication of the sum of the inverse eigenvalues of the fermionic matrix product $MM^{\dagger}$. All of these observables are invariant under the same transformations as the action (see section 2.2) and are independent of the global phase of the scalar fields if spontaneous symmetry breaking occurs.

Because of the large variation possible in the magnitude of the scalar fields, as measured by PsP, it is convenient to define a global alignment observable G:

$$G = \frac{\langle R^2 \rangle}{\langle PsP \rangle} \tag{2.100}$$

which is approximately zero in a disordered or anti-aligned phase, rising to unity in a totally aligned phase.

Perturbative expansions for the expectation values of these observables can be performed in certain parameters using techniques described in section 1.6.1. For instance, in the regime of small Y and small λ:

$$\begin{aligned}
\langle \phi^{\star}(x_1)\,\phi(x_2)\rangle = {} & \frac{1}{V}\sum_{p} \frac{e^{ip(x_2-x_1)}}{\left[1-2\lambda-2\kappa\sum_{\mu}\cos p_{\mu}\right]} \\
& + \frac{4}{V^2}\left(Y^2 \sum_{p} \frac{1}{\left[\sum_{\mu}\sin^2 p_{\mu}\right]} - \lambda \sum_{p} \frac{1}{\left[1-2\lambda-2\kappa\sum_{\mu}\cos p_{\mu}\right]} \right) \\
& \times \sum_{q} \frac{e^{iq(x_2-x_1)}}{\left[1-2\lambda-2\kappa\sum_{\mu}\cos q_{\mu}\right]^2} \\
& - 2\frac{Y^2}{V^2}\sum_{pq} \frac{\left[\sum_{\mu}[\sin p_{\mu}-\sin q_{\mu}]^2\right]\cos\left((p-q)(x_2-x_1)\right)}{\left[\sum_{\mu}\sin^2 p_{\mu}\right]\left[\sum_{\mu}\sin^2 q_{\mu}\right]\left[1-2\lambda-2\kappa\sum_{\mu}\cos(p-q)_{\mu}\right]^2} \\
& + O(\lambda^2, \lambda Y^2, Y^4)
\end{aligned} \tag{2.101}$$

Thus:

$$\langle Q \rangle = \frac{2}{V}\sum_p \frac{\sum_\mu \cos p_\mu}{\left[1-2\lambda-2\kappa\sum_\mu \cos p_\mu\right]} + \frac{8}{V^2}\sum_q \frac{\sum_\mu \cos q_\mu}{\left[1-2\lambda-2\kappa\sum_\mu \cos q_\mu\right]^2}$$
$$\times\left(Y^2\sum_p \frac{1}{\left[\sum_\mu \sin^2 p_\mu\right]} - \lambda\sum_p \frac{1}{\left[1-2\lambda-2\kappa\sum_\mu \cos p_\mu\right]}\right)$$
$$-4\frac{Y^2}{V^2}\sum_{pq} \frac{\left[\sum_\mu [\sin p_\mu - \sin q_\mu]^2\right]\sum_\mu \cos(p-q)_\mu}{\left[\sum_\mu \sin^2 p_\mu\right]\left[\sum_\mu \sin^2 q_\mu\right]\left[1-2\lambda-2\kappa\sum_\mu \cos(p-q)_\mu\right]^2} \tag{2.102}$$

$$\langle CV \rangle = \frac{4}{V}\sum_p \frac{\left[\sum_\mu \cos p_\mu\right]^2}{\left[1-2\lambda-2\kappa\sum_\mu \cos p_\mu\right]^2} + \frac{32}{V^2}\sum_q \frac{\left[\sum_\mu \cos q_\mu\right]^2}{\left[1-2\lambda-2\kappa\sum_\mu \cos q_\mu\right]^3}$$
$$\times\left(Y^2\sum_p \frac{1}{\left[\sum_\mu \sin^2 p_\mu\right]} - \lambda\sum_p \frac{1}{\left[1-2\lambda-2\kappa\sum_\mu \cos p_\mu\right]}\right)$$
$$-16\frac{\lambda}{V^2}\left[\sum_p \frac{\sum_\mu \cos p_\mu}{\left[1-2\lambda-2\kappa\sum_\mu \cos p_\mu\right]^2}\right]^2$$
$$-16\frac{Y^2}{V^2}\sum_{pq} \frac{\left[\sum_\mu [\sin p_\mu - \sin q_\mu]^2\right]\left[\sum_\mu \cos(p-q)_\mu\right]^2}{\left[\sum_\mu \sin^2 p_\mu\right]\left[\sum_\mu \sin^2 q_\mu\right]\left[1-2\lambda-2\kappa\sum_\mu \cos(p-q)_\mu\right]^3} \tag{2.103}$$

$$\langle PsP \rangle = \frac{1}{V}\sum_p \frac{1}{\left[1-2\lambda-2\kappa\sum_\mu \cos p_\mu\right]} + \frac{4}{V^2}\sum_q \frac{1}{\left[1-2\lambda-2\kappa\sum_\mu \cos q_\mu\right]^2}$$

$$\times \left(Y^2 \sum_p \frac{1}{\left[\sum_\mu \sin^2 p_\mu\right]} - \lambda \sum_p \frac{1}{\left[1 - 2\lambda - 2\kappa \sum_\mu \cos p_\mu\right]} \right)$$
$$-2\frac{Y^2}{V^2} \sum_{pq} \frac{\left[\sum_\mu [\sin p_\mu - \sin q_\mu]^2\right]}{\left[\sum_\mu \sin^2 p_\mu\right] \left[\sum_\mu \sin^2 q_\mu\right] \left[1 - 2\lambda - 2\kappa \sum_\mu \cos(p-q)_\mu\right]^2} \tag{2.104}$$

$$\left\langle R^2 \right\rangle = \frac{1}{V} \frac{1}{\left[1 - 2\lambda - 8\kappa\right]} + \frac{4}{V^2} \frac{1}{\left[1 - 2\lambda - 8\kappa\right]^2}$$
$$\times \left(Y^2 \sum_p \frac{1}{\left[\sum_\mu \sin^2 p_\mu\right]} - \lambda \sum_p \frac{1}{\left[1 - 2\lambda - 2\kappa \sum_\mu \cos p_\mu\right]} \right) \tag{2.105}$$

neglecting terms of order λ^2, λY^2 and Y^4.

With $\lambda = 0$ for small Y:

$$\langle P2 \rangle = 4 \sum_p \frac{1}{\left[\sum_\mu \sin^2 p_\mu\right]} - 4\frac{Y^2}{V^2} \sum_{pq} \frac{1}{\left[\sum_\mu \sin^2 p_\mu\right]^2 \left[1 - 2\kappa \sum_\mu \cos p - q_\mu\right]}$$
$$+4\frac{Y^2}{V^2} \sum_{pq} \frac{\sum_\mu [\sin p_\mu - \sin q_\mu]^2}{\left[\sum_\mu \sin^2 p_\mu\right]^2 \left[\sum_\mu \sin^2 q_\mu\right] \left[1 - 2\kappa \sum_\mu \cos (p-q)_\mu\right]} \tag{2.106}$$

neglecting terms of order Y^4.

When $\lambda = \infty$ in the regime of small Y and κ:

$$\langle Q \rangle = 8\kappa$$
$$-4\frac{Y^2}{V^2} \sum_{pq} \frac{\left[\sum_\mu [\sin p_\mu - \sin q_\mu]^2\right] \sum_\mu \cos(p-q)_\mu}{\left[\sum_\mu \sin^2 p_\mu\right] \left[\sum_\mu \sin^2 q_\mu\right]} \tag{2.107}$$

$$\langle P2 \rangle = 4\sum_p \frac{1}{\left[\sum_\mu \sin^2 p_\mu\right]} - 4\frac{Y^2}{V}\sum_p \frac{1}{\left[\sum_\mu \sin^2 p_\mu\right]^2} + 4\frac{Y^2}{V^2}\sum_{pq} \frac{\sum_\mu \left[\sin p_\mu - \sin q_\mu\right]^2}{\left[\sum_\mu \sin^2 p_\mu\right]^2 \left[\sum_\mu \sin^2 q_\mu\right]} \tag{2.108}$$

neglecting terms of order κ^2, κY^2 and Y^4.

See appendix A.1 for details of the conventions used for momentum sums.

In the case $Y = 0$ and $\lambda = \infty$:

$$\left\langle R^2 \right\rangle = \frac{1}{V}\left[1 + 8\kappa + O(\kappa^2)\right] \tag{2.109}$$

$$\langle CV \rangle = 8 + O(\kappa^2) \tag{2.110}$$

Values of these expressions can be calculated and compared with measurements taken from the computer simulation providing a useful check of the validity of the results of the computer program.

2.4 Simulation

A brief description is given in this section of the method by which the computer simulation of the Higgs-Yukawa model was performed. The general idea behind this simulation was to discover features of the phase diagram of the model, and to use this information to help draw some conclusions relevant to the standard model. To do this, a large number of independent simulations of the system on very small lattices with different parameter values were performed.

2.4.1 Algorithm

The models with infinite and finite λ were simulated separately using the Hybrid Monte Carlo algorithm. See section 1.4 for more details of this algorithm.

Pseudo-fermions were generated from a heatbath distribution which were kept fixed whilst the scalar configuration was evolved according to a Hybrid Monte Carlo Hamiltonian, $\mathcal{H}$, by different molecular dynamics steps for the two cases of finite and infinite λ with a final accept/reject test to remove finite time step effects.

Molecular Dynamics for $\lambda = \infty$

The N molecular dynamics steps, with time step $\delta\tau$, used to evolve the scalar degrees of freedom, $\Theta = \{\theta(x)\}$, in the radially fixed case, are as follows:

1. A scalar momentum vector, Π, is chosen from a Gaussian distribution with probability density proportional to $e^{-\Pi^2}$. Call this time 0. Note the coefficient of Π^2.

2. The value of the momentum vector, Π, at time $\frac{\delta\tau}{2}$ is calculated, along with Θ at time $\delta\tau$:

$$\Pi\left(\frac{\delta\tau}{2}\right) = \Pi(0) - \frac{\partial\mathcal{H}}{\partial\Theta}(0) \times \frac{\delta\tau}{4} \tag{2.111}$$

$$\Theta(\delta\tau) = \Theta(0) + \Pi\left(\frac{\delta\tau}{2}\right) \times \delta\tau \tag{2.112}$$

3. For the number of steps required, $n = 1, \cdots, N-1$:

$$\Pi\left(\left(n+\frac{1}{2}\right)\delta\tau\right) = \Pi\left(\left(n-\frac{1}{2}\right)\delta\tau\right) - \frac{\partial\mathcal{H}}{\partial\Theta}(n\delta\tau) \times \frac{\delta\tau}{2} \tag{2.113}$$

$$\Theta((n+1)\delta\tau) = \Theta(n\delta\tau) + \Pi\left(\left(n+\frac{1}{2}\right)\delta\tau\right) \times \delta\tau \tag{2.114}$$

4. Finally, the value of the momentum vector, Π, at the end of the molecular dynamics steps is required:

$$\Pi(N\delta\tau) = \Pi\left(\left(N-\frac{1}{2}\right)\delta\tau\right) - \frac{\partial\mathcal{H}}{\partial\Theta}(N\delta\tau) \times \frac{\delta\tau}{4} \tag{2.115}$$

Molecular Dynamics for Finite λ

The N molecular dynamics steps, with time step $\delta\tau$, used to evolve the scalar fields, $\Phi = \{\phi(x)\}$, are as follows:

1. A scalar momentum vector, Π, is chosen from a Gaussian distribution with probability density proportional to $e^{-\Pi^\dagger \Pi}$. Call this time 0.

2. The value of the momentum vector at time $\frac{\delta\tau}{2}$ is calculated, along with Φ at time $\delta\tau$:

$$\Pi\left(\frac{\delta\tau}{2}\right) = \Pi(0) - \frac{\partial\mathcal{H}}{\partial\Phi^\star}(0) \times \frac{\delta\tau}{2} \tag{2.116}$$

$$\Phi(\delta\tau) = \Phi(0) + \Pi\left(\frac{\delta\tau}{2}\right) \times \delta\tau \tag{2.117}$$

3. For the number of steps required, $n = 1, \cdots, N-1$:

$$\Pi\left(\left(n+\frac{1}{2}\right)\delta\tau\right) = \Pi\left(\left(n-\frac{1}{2}\right)\delta\tau\right) - \frac{\partial\mathcal{H}}{\partial\Phi^\star}(n\delta\tau) \times \delta\tau \tag{2.118}$$

$$\Phi((n+1)\delta\tau) = \Phi(n\delta\tau) + \Pi\left(\left(n+\frac{1}{2}\right)\delta\tau\right) \times \delta\tau \tag{2.119}$$

4. Finally, the value of the momentum vector, Π, at the end of the molecular dynamics steps is required:

$$\Pi(N\delta\tau) = \Pi\left(\left(N-\frac{1}{2}\right)\delta\tau\right) - \frac{\partial\mathcal{H}}{\partial\Phi^\star}(N\delta\tau) \times \frac{\delta\tau}{2} \tag{2.120}$$

2.4.2 Implementation

The algorithm was implemented as n copies of the system on the Edinburgh Concurrent Supercomputer, one system per Transputer plus one controlling Transputer. The program was written in **occam2** using thirty two bit arithmetic, and could be adapted to simulate the system on a four dimensional hypercube of various sizes, memory and computer time permitting. The pseudo-random number generator used was of the modulo type, with an additional shuffle stage to re-order the sequence of numbers generated.

Periodic boundary conditions were used in all directions for the scalar fields, and in the space-like directions for the pseudo-fermion fields. Anti-periodic boundary conditions were used in the Euclidean time direction for the pseudo-fermion fields. This meant that the model in the limit $Y \to 0$ was accessible to simulation as discussed in section 2.2.2.

After an initial equilibration period, and before measurements were started, the program tried to find the optimal number of molecular dynamics steps and predictor order (see section 1.5.3) that led to the maximum acceptance probability in the least computer time with the total Monte Carlo time fixed to unity in the units used.

2.4.3 Program Checks

In order to verify that the program doing the simulation was giving correct results, the following checks on the program were performed:

- The program was checked to ensure that the fermionic matrix product $M^\dagger M$ was Hermitian. This was done by generating a random pseudo-fermion vector η, and comparing the values of the expressions $|M\eta|^2$ and $\eta^\dagger \left(M^\dagger M \eta\right)$.

- Scalar observables were checked for invariance under the global transformations:

$$\begin{aligned} \phi(x) &\rightarrow e^{i\alpha}\phi(x) \\ \phi^\star(x) &\rightarrow e^{-i\alpha}\phi^\star(x) \end{aligned} \tag{2.121}$$

  for arbitrary constant α.

- The Molecular Dynamics steps were checked for reversibility to a degree of accuracy determined by how accurately the sets of linear equations were solved. This was done by evolving a scalar configuration with fixed pseudo-fermions for a number of steps with step size $\delta\tau$, and then evolving it for the same number of steps with step size $-\delta\tau$, using the final momentum vector for the forward pass as the initial momentum vector for the reverse pass. The change in the value of the Hybrid Monte Carlo Hamiltonian over this process was measured. As the initial guess for the solution to the sets of linear equations to be solved were different in the two passes, then reversibility of the Molecular Dynamics steps could be verified. This procedure also verified that thirty two bit arithmetic was accurate enough for the purposes of the simulation.

	$\delta\tau = 0.1$	$\delta\tau = 0.5$
Acceptance	~ 0.95	~ 0.3
Q	2.328(21)	2.293(26)
CV	115(3)	118(3)
R^2	0.209(3)	0.203(4)
$P2$	3.048(6)	3.059(8)

Table 2.1: Measured expectation values of observables of the Higgs-Yukawa model at $Y = 0.64$, $\kappa = 0.02$ and $\lambda = \infty$ on a 4^4 lattice as a function of the time step $\delta\tau$ with total Monte Carlo time per step fixed at 1.0.

	$\delta\tau = 0.1$	$\delta\tau = 0.2$	$\delta\tau = 0.3333$
Acceptance	0.94	0.77	0.39
Q	24.627(6)	24.629(2)	24.634(5)
CV	190.7(14)	191.3(6)	193.5(15)
PsP	3.6944(6)	3.6944(2)	3.6945(6)
R^2	2.9926(8)	2.9929(3)	2.9940(7)
$P2$	0.85431(15)	0.85442(7)	0.85422(14)

Table 2.2: Measured expectation values of observables of the Higgs-Yukawa model at $Y = 1$, $\kappa = 0.1$ and $\lambda = 0.1$ on a 4^4 lattice as a function of the time step $\delta\tau$ with total Monte Carlo time per step fixed at 1.0.

- Independence of the measured expectation values of observables from the value of the time step, $\delta\tau$, and hence the acceptance probability, was verified. See tables 2.1 and 2.2.

- Comparisons were made between the measured expectation values of observables gained from the computer simulation of the model and the values of the perturbative expressions listed in section 2.3. See figures 2.1, 2.2, 2.3 and 2.4.

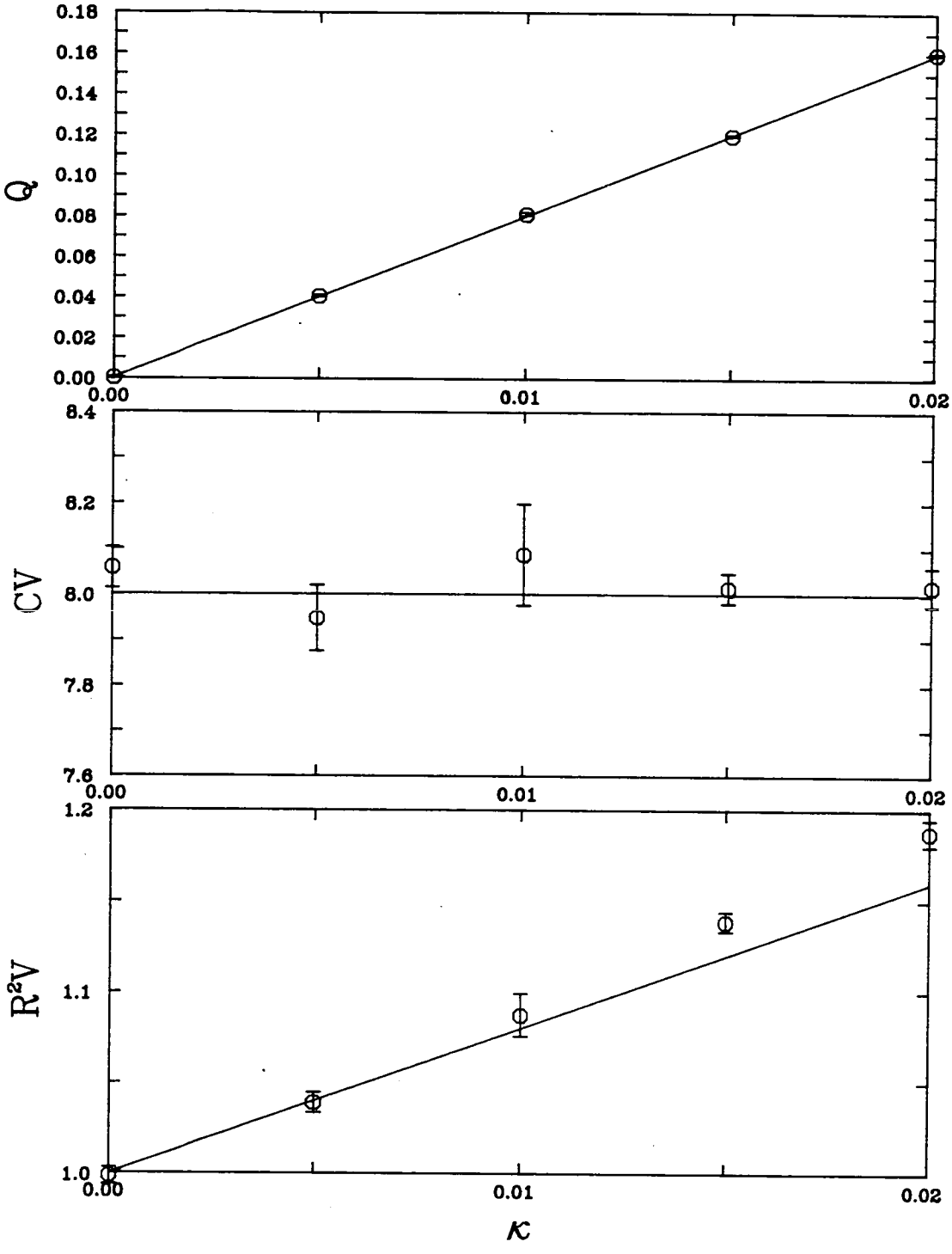

Figure 2.1: Comparison of measured expectation values with perturbative expressions for Q, CV and R^2 when $Y = 0$ and $\lambda = \infty$ for small κ on a 6^4 lattice for the radially fixed Higgs-Yukawa model. The points are measured data, the lines are the values of the perturbative expressions.

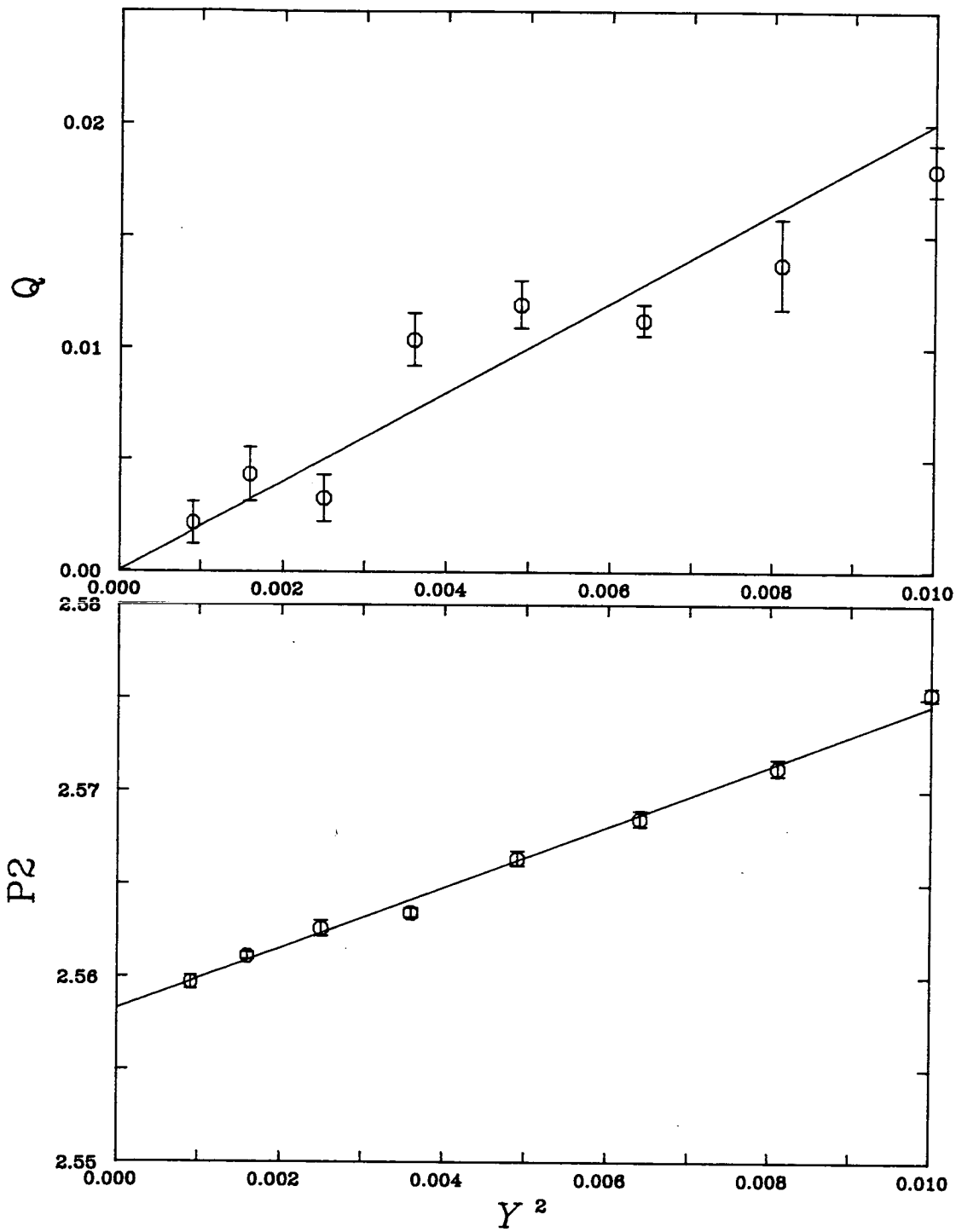

Figure 2.2: Comparison of measured expectation values with perturbative expressions for Q and $P2$ when $\kappa = 0$ and $\lambda = \infty$ for small Y on a 6^4 lattice. The points are results of the simulation of the radially fixed Higgs-Yukawa model, the lines are the values of the perturbative expressions.

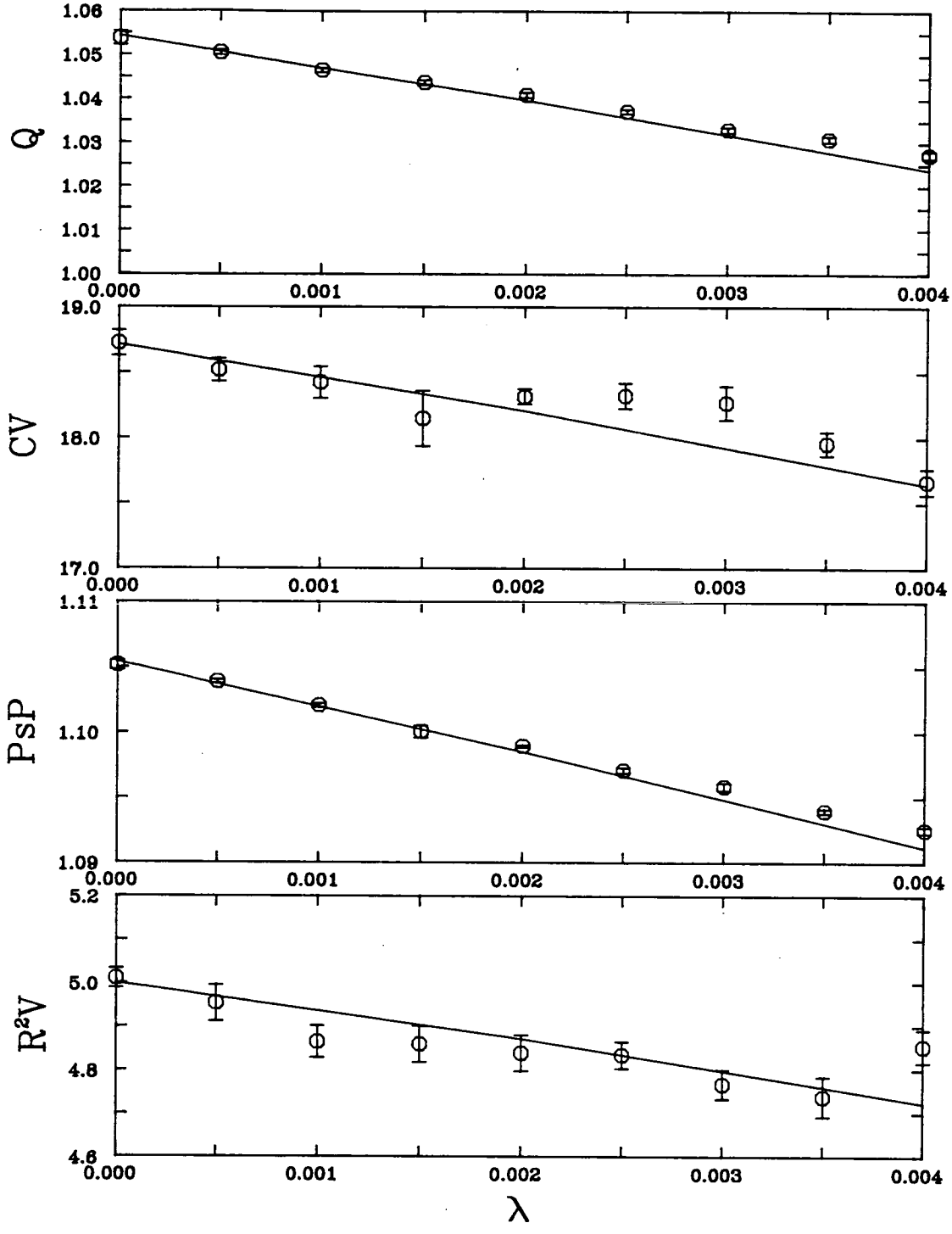

Figure 2.3: Comparison of measured expectation values with perturbative expressions for Q, CV, PsP and R^2 when $\kappa = 0.1$ and $Y = 0$ for small λ on a 6^4 lattice for the Higgs-Yukawa model. The points are measurements, the lines are values of the perturbative expressions.

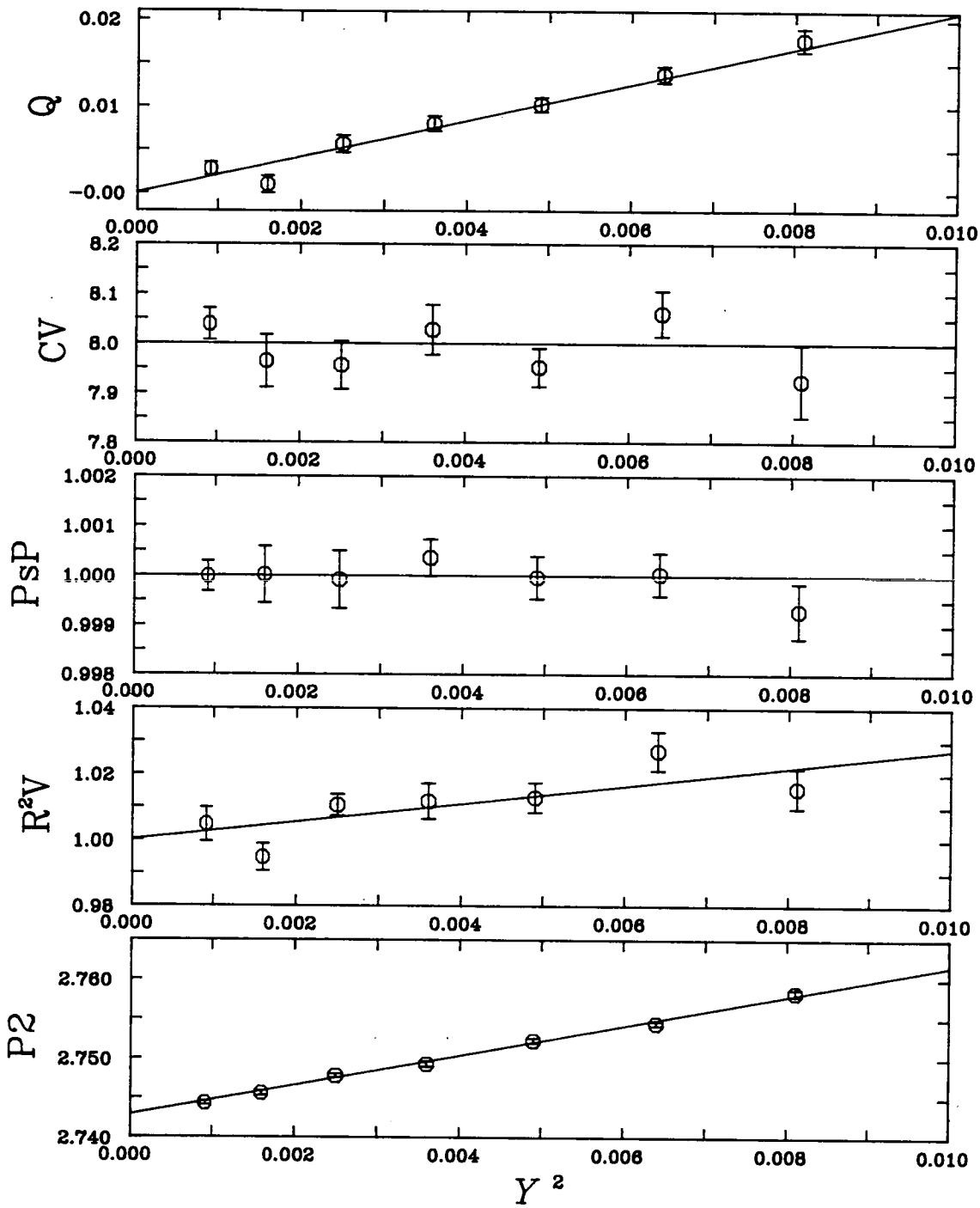

Figure 2.4: Comparison of measured expectation values with perturbative expressions for Q, CV, PsP, R^2 and $P2$ when $\kappa = 0$ and $\lambda = 0$ for small Y on a 4^4 lattice. The points are measurements taken from the simulation of the radially free Higgs-Yukawa model, the lines are the values of the perturbative expressions.

2.5 Results

To discover features of the phase diagram, a large number of independent simulations of the model were performed with different sets of parameters. This was done in planes of parameter space, from which contour plots of the measured expectation value of observables could be made, giving a good overview of the general phase structure of the model. Lines in parameter space were also studied showing features of parts of the phase diagram to a higher resolution than that achieved in the contour plots.

Contour plots of the measured value of the global alignment parameter, G, as defined in section 2.3, measured on a 4^4 lattice, as a function of the coefficients λ, κ, and Y of terms in the action stated in equation (2.89), are shown in figures 2.5, 2.6, 2.7, 2.8, 2.9, 2.10 and 2.11, where measurements are taken in the planes $\lambda = 0$, $\lambda = 1$, $\lambda = \infty$, $Y = 0$, $Y = 3$, $\kappa = 0$ and $\kappa = 0.1$ respectively. Values of G close to zero correspond to disordered and anti-aligned phases of the model. A value of G equal to unity corresponds to a totally aligned phase. Phase transition lines are seen and are characterised by regions in the plane where the contours are closely spaced showing that the value of G changes rapidly with a small change in the value of parameters of the model. A schematic phase diagram of the model on a 4^4 lattice with these boundary conditions for non-negative values of κ is shown in figure 2.12.

The measured expectation values along the line $\kappa = 0$ in parameter space on 6^4 lattices in the cases $\lambda = 0$ and $\lambda = \infty$ are shown in figures 2.13 and 2.14. No error estimates are given in these figures. For most of the observables, the errors can be estimated from the scatter of the points, though for CV this is unreliable close to a phase transition, as it is measured from the fluctuations of Q over Monte Carlo time, and thus is subject to phenomena such as critical slowing down. From this, and from similar results taken from simulations on 4^4 lattices, the critical values of Y when $\kappa = 0$ are measured to be 0.62(5) and 1.23(10) on the 4^4 lattice and 0.65(5) and 1.28(10) on the 6^4 lattice when $\lambda = 0$. With $\lambda = \infty$, the measured critical values of Y are found to be 0.64(10) and 2.44(10) on the 4^4 lattice, and 0.68(10) and 2.48(10) on the 6^4 lattice when $\kappa = 0$.

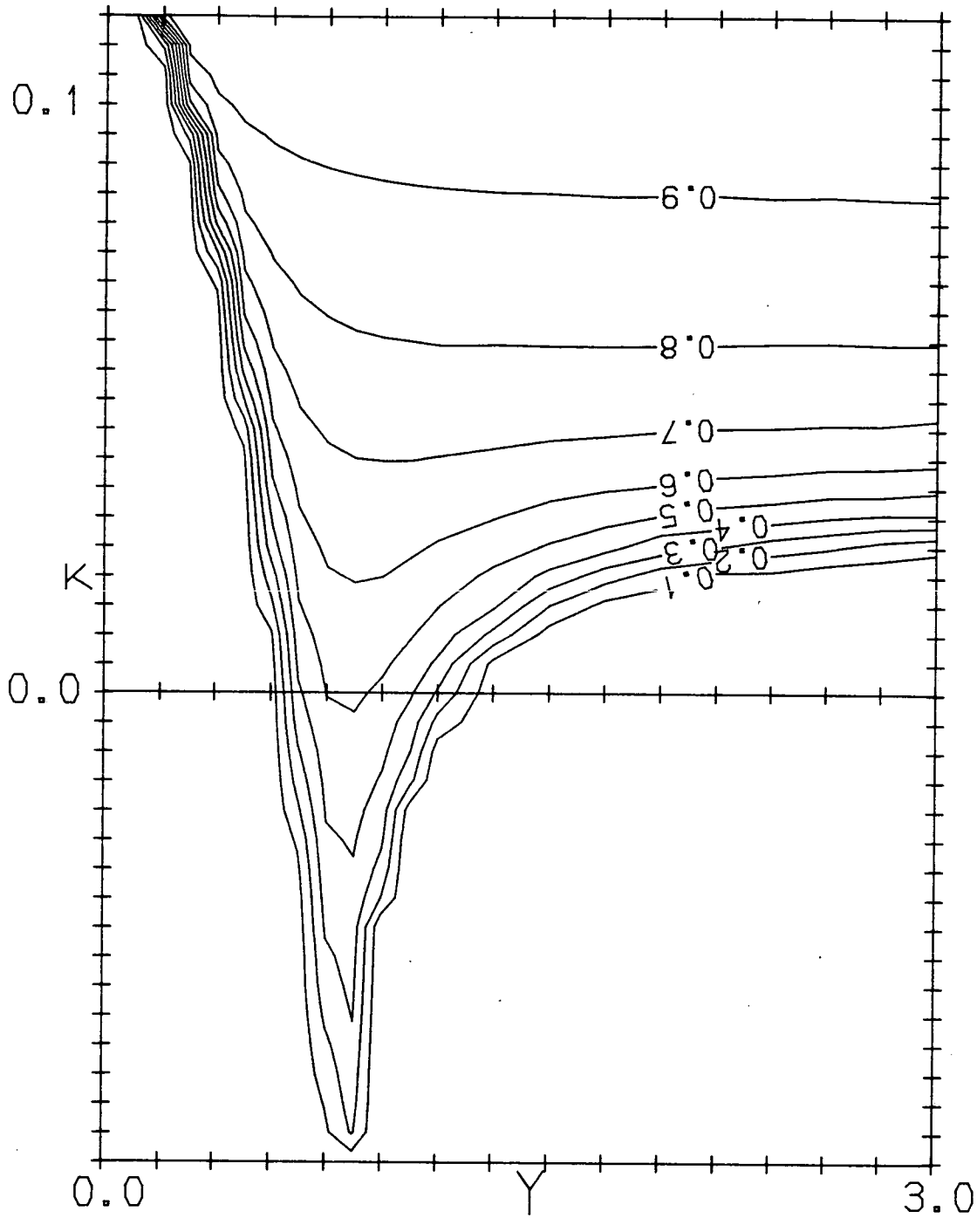

Figure 2.5: Contour plot of G in the $\lambda = 0$ plane measured on a 4^4 lattice for the radially free Higgs-Yukawa model.

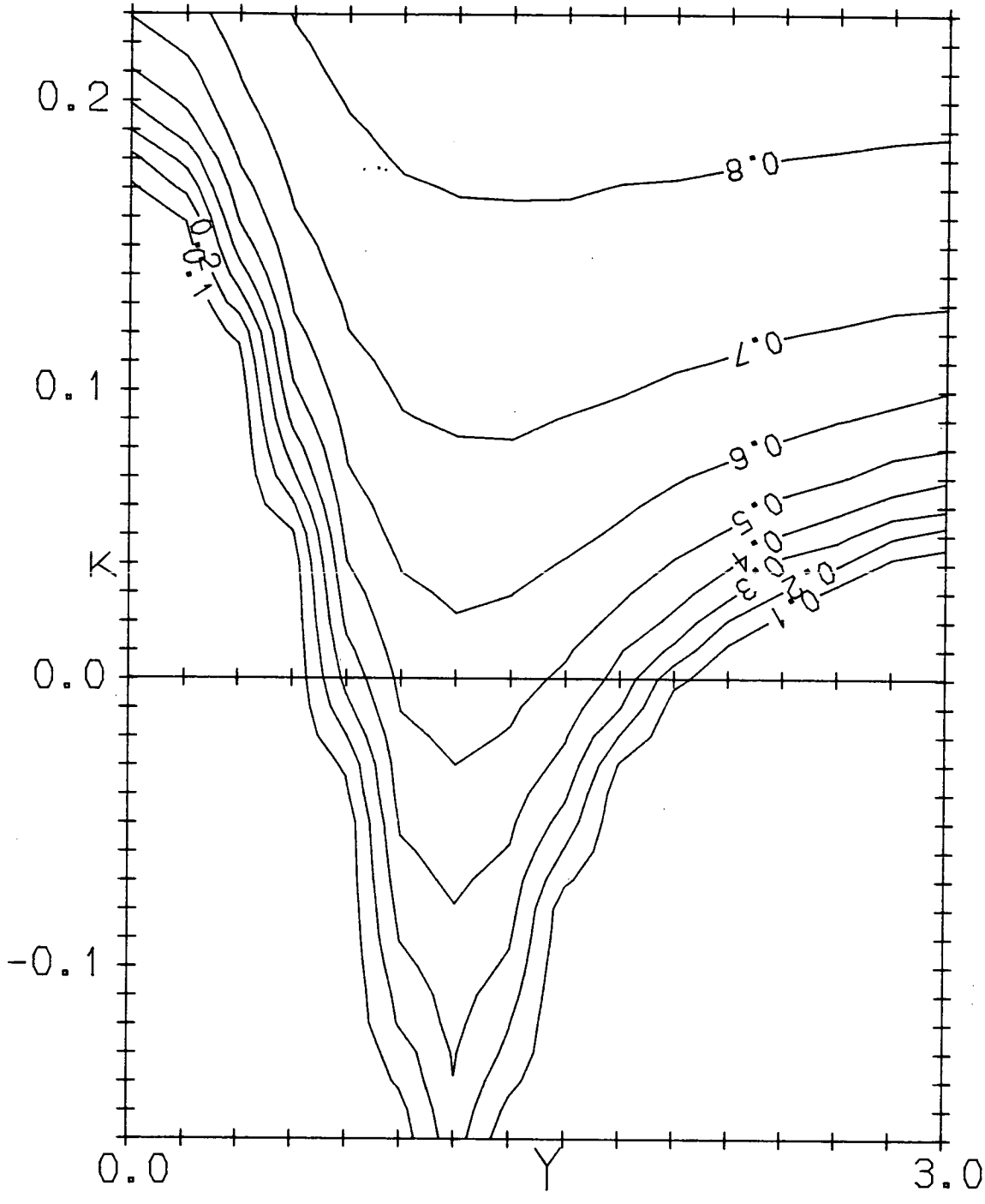

Figure 2.6: Contour plot of G in the $\lambda = 1$ plane measured on a 4^4 lattice from simulations of the Higgs-Yukawa model.

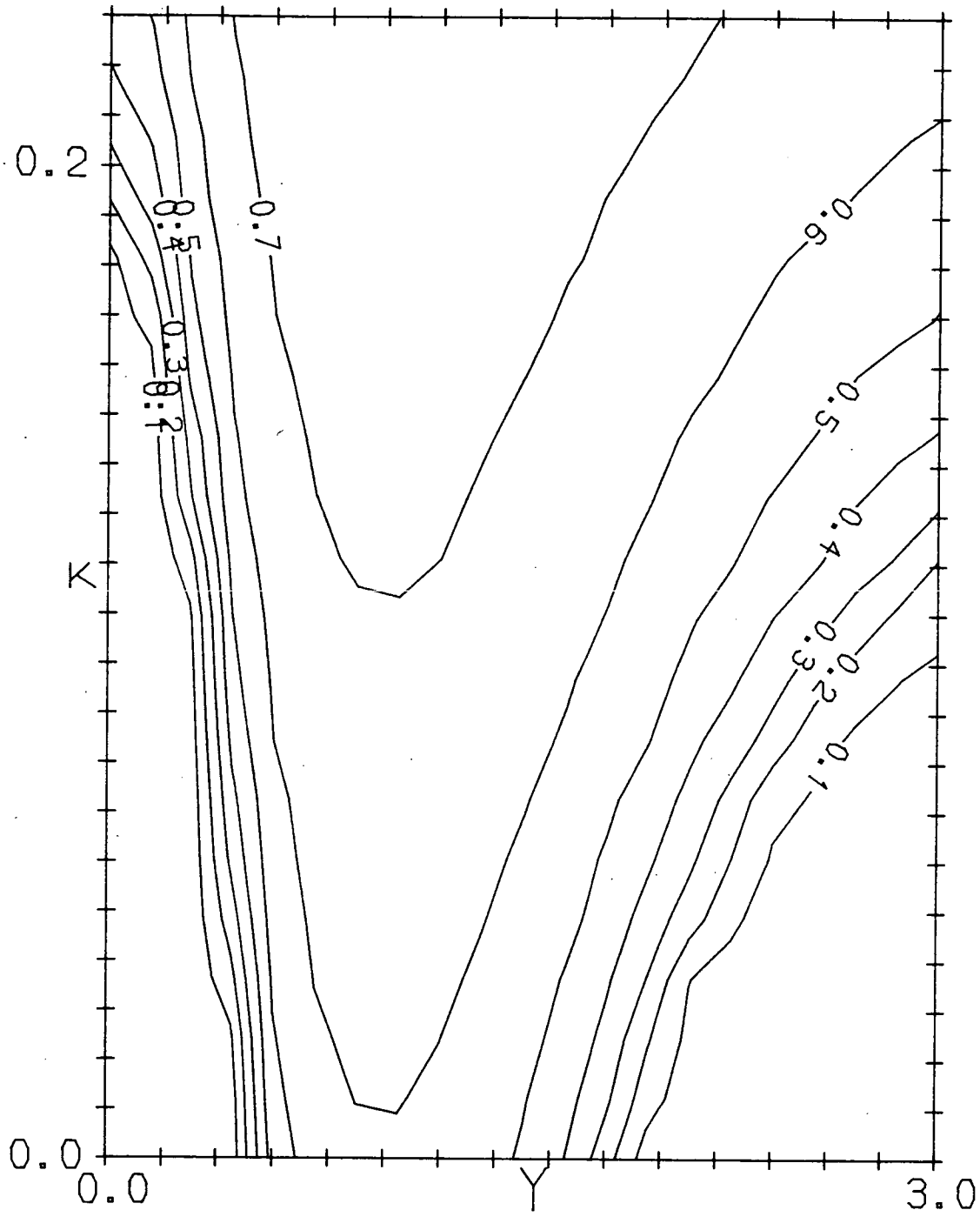

Figure 2.7: Contour plot of G in the $\lambda = \infty$ plane measured on a 4^4 lattice measured from simulations of the radially fixed Higgs-Yukawa model.

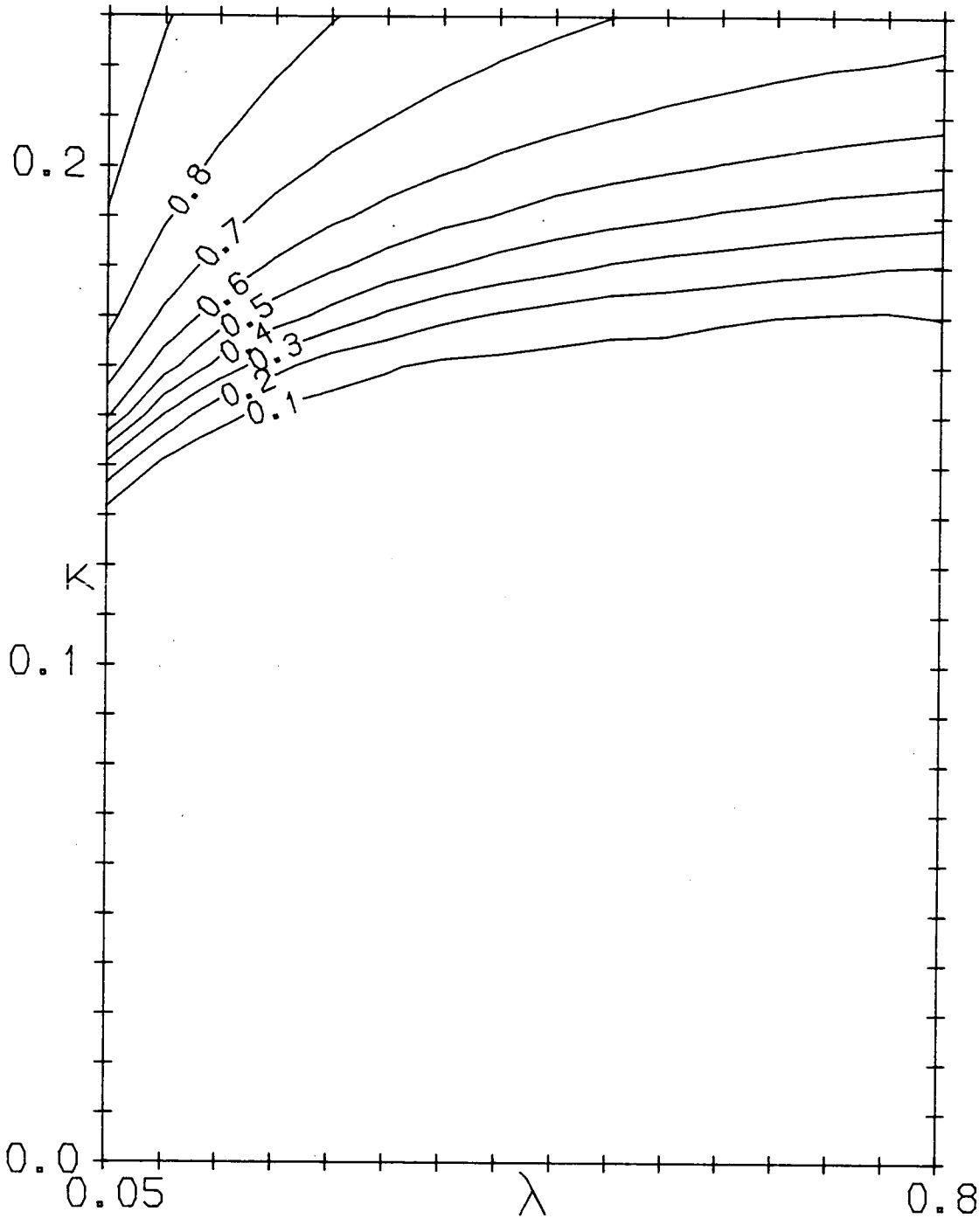

Figure 2.8: Contour plot of G measured in the $Y = 0$ plane on a 4^4 lattice for the Higgs-Yukawa model.

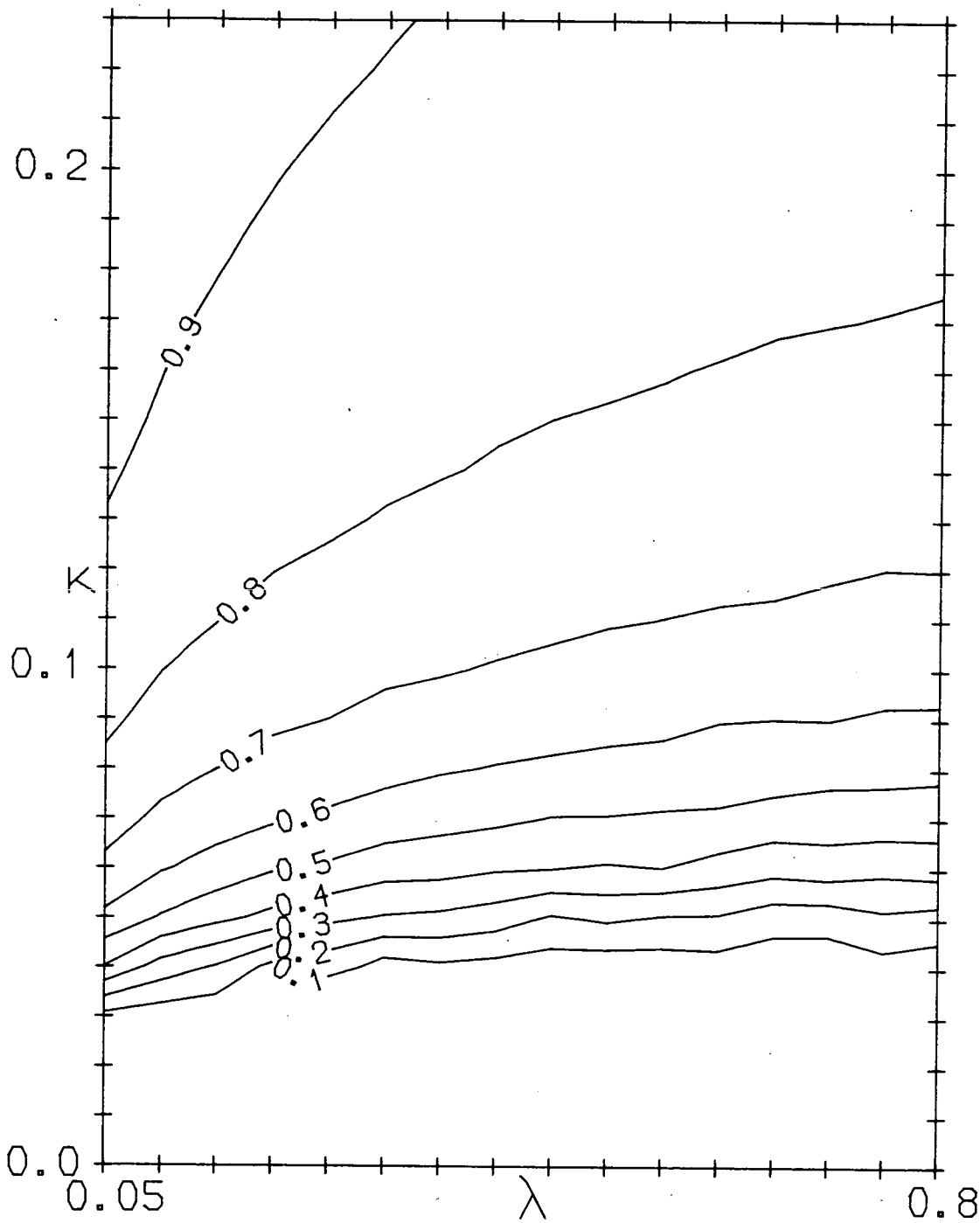

Figure 2.9: Contour plot of G in the $Y = 3$ plane measured on a 4^4 lattice from simulations of the Higgs-Yukawa model.

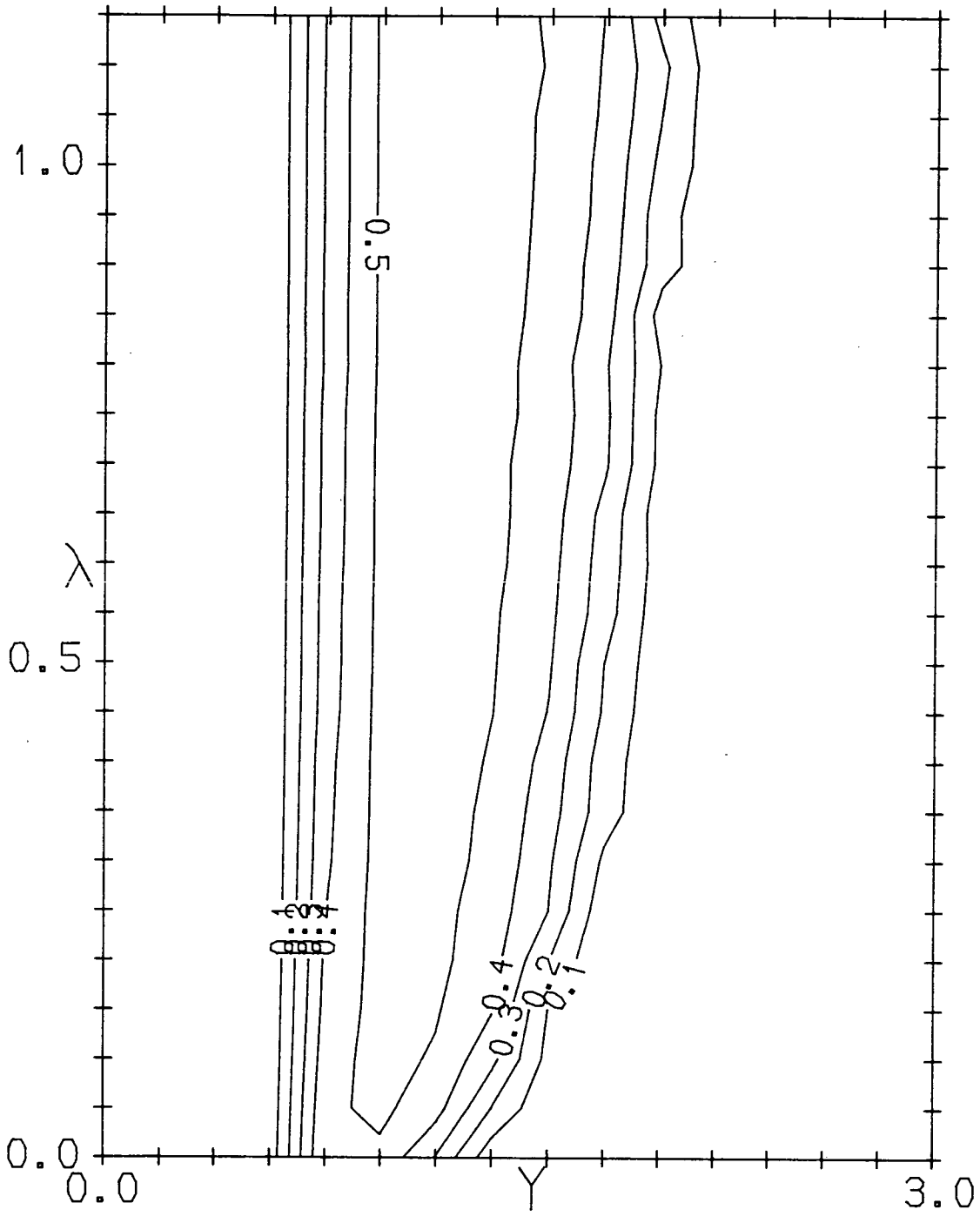

Figure 2.10: Contour plot of the global alignment parameter G in the $\kappa = 0$ plane measured on a 4^4 lattice taken from simulations of the Higgs-Yukawa model.

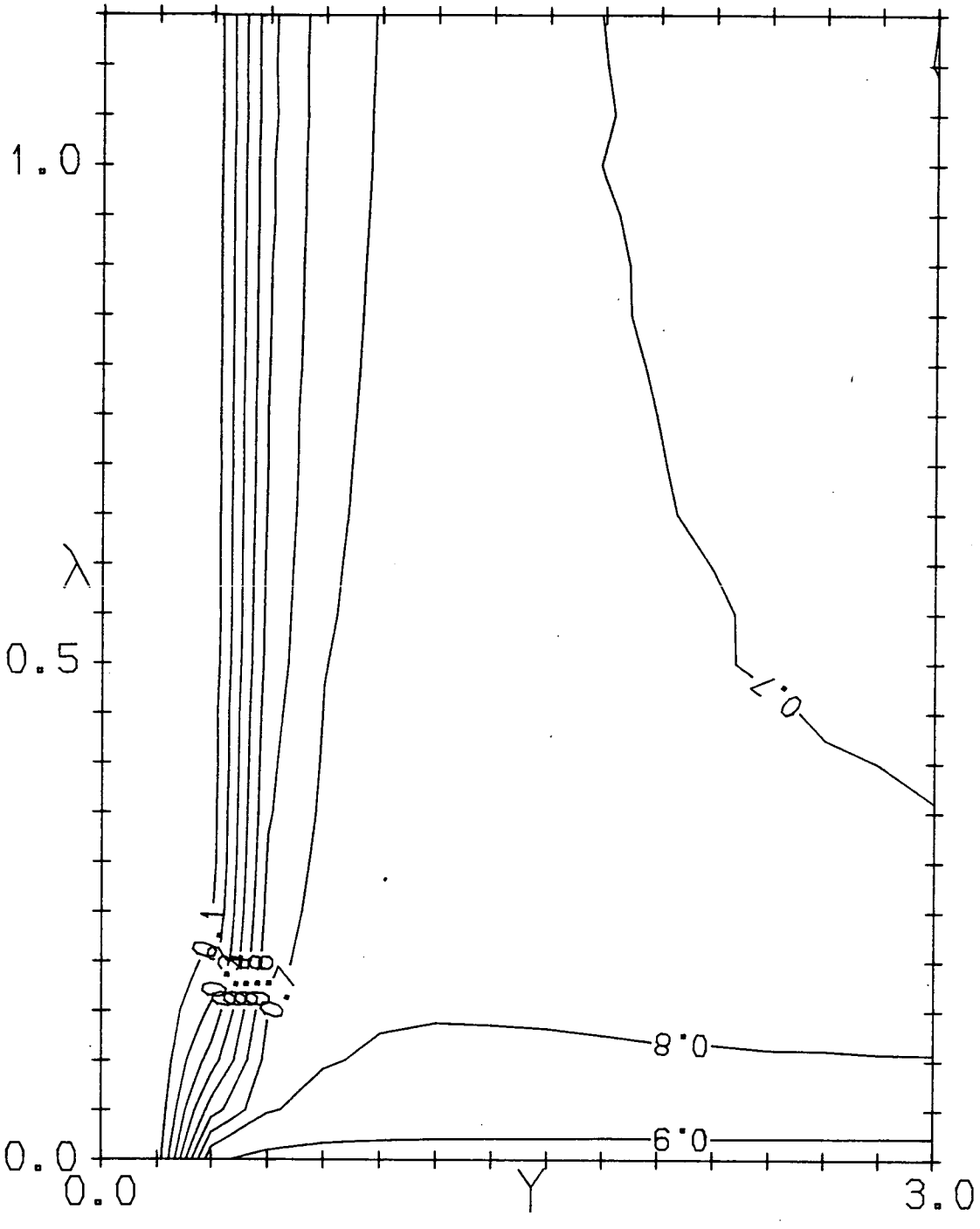

Figure 2.11: Contour plot of G in the $\kappa = 0.1$ plane measured on a 4^4 lattice in simulations of the Higgs-Yukawa model.

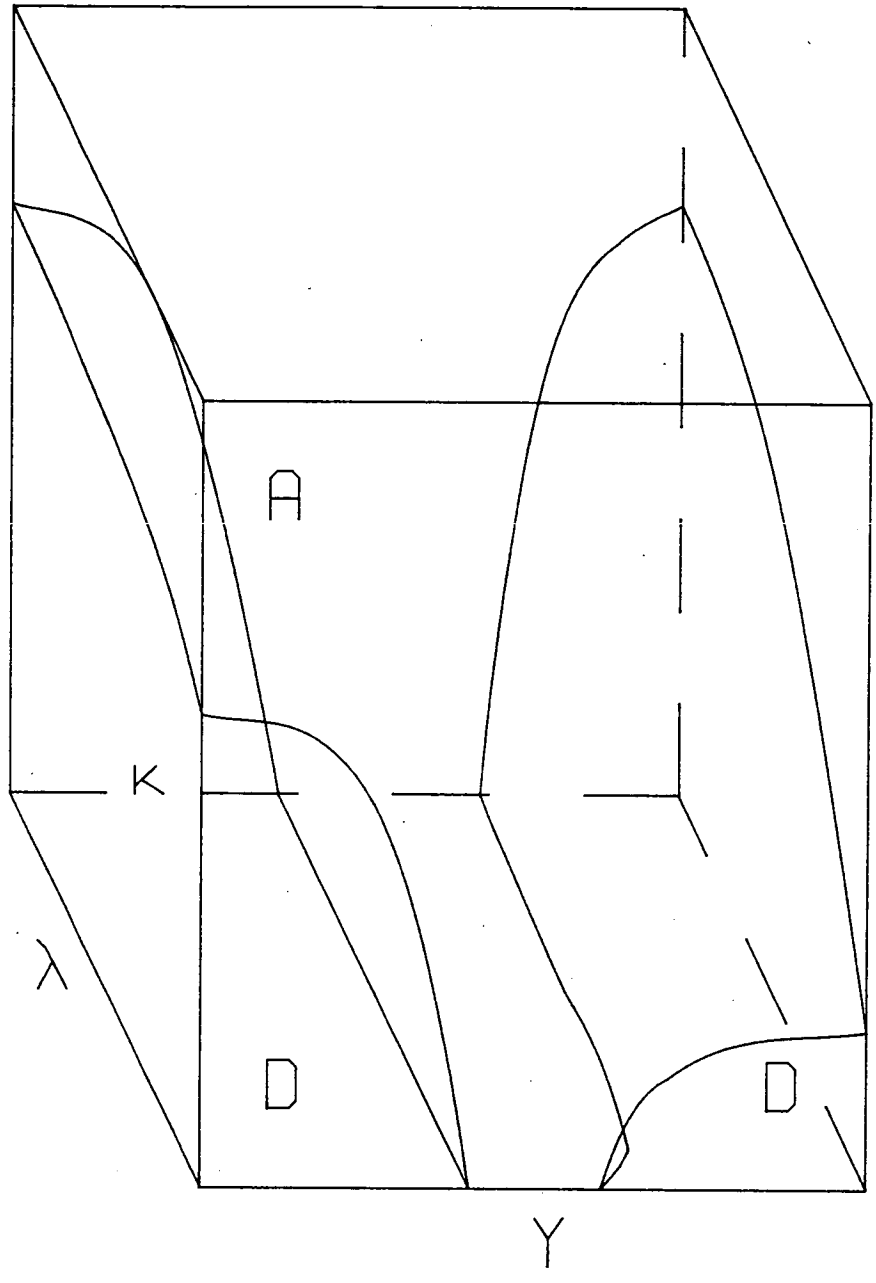

Figure 2.12: Schematic phase diagram, as observed by simulation, of the Higgs-Yukawa model for non-negative values of κ. The aligned and disordered phases are denoted by the letters A and D respectively.

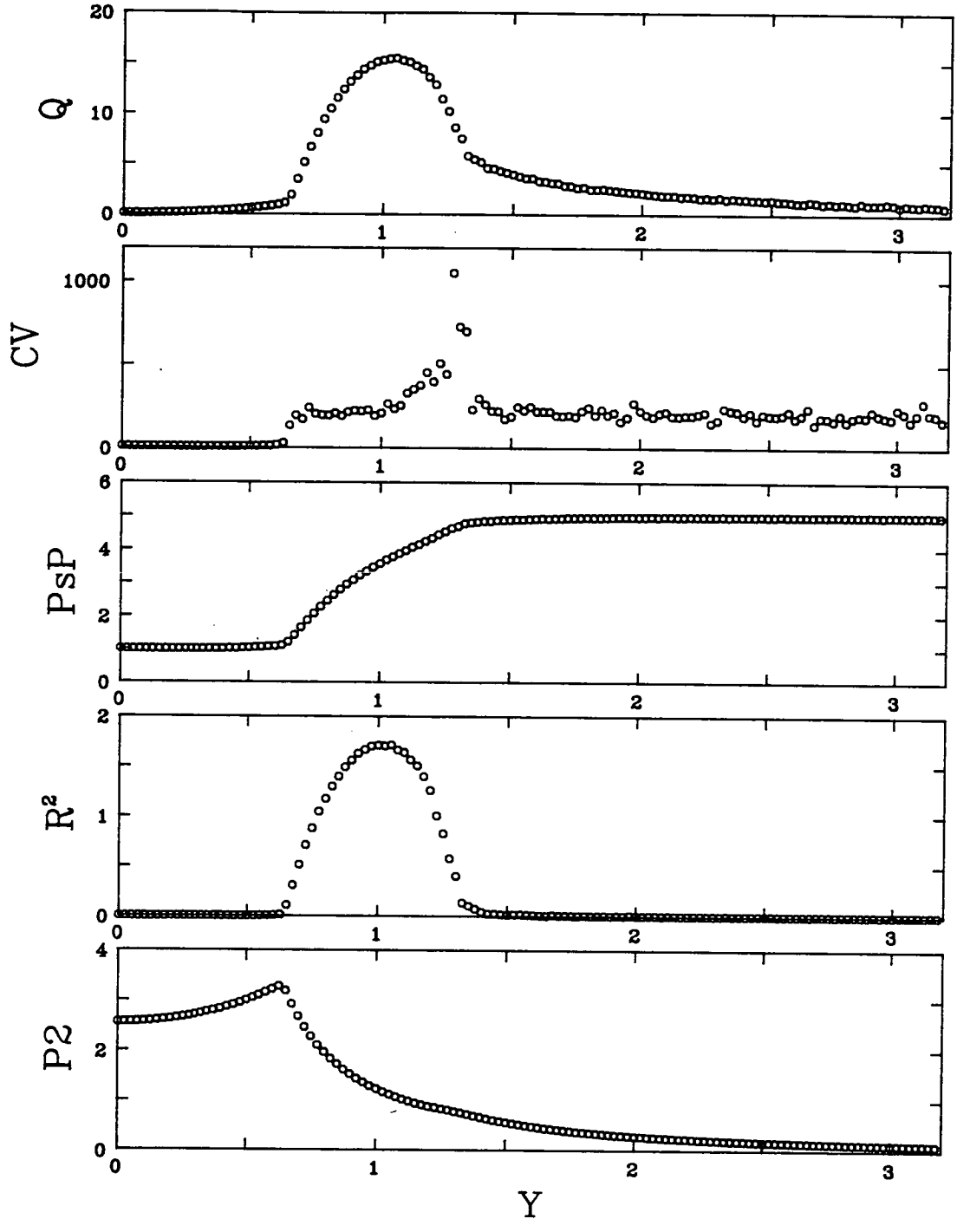

Figure 2.13: Measured expectation values of observables along the line $\kappa = 0$, $\lambda = 0$ on a 6^4 lattice for the Higgs-Yukawa model. No error bars are given.

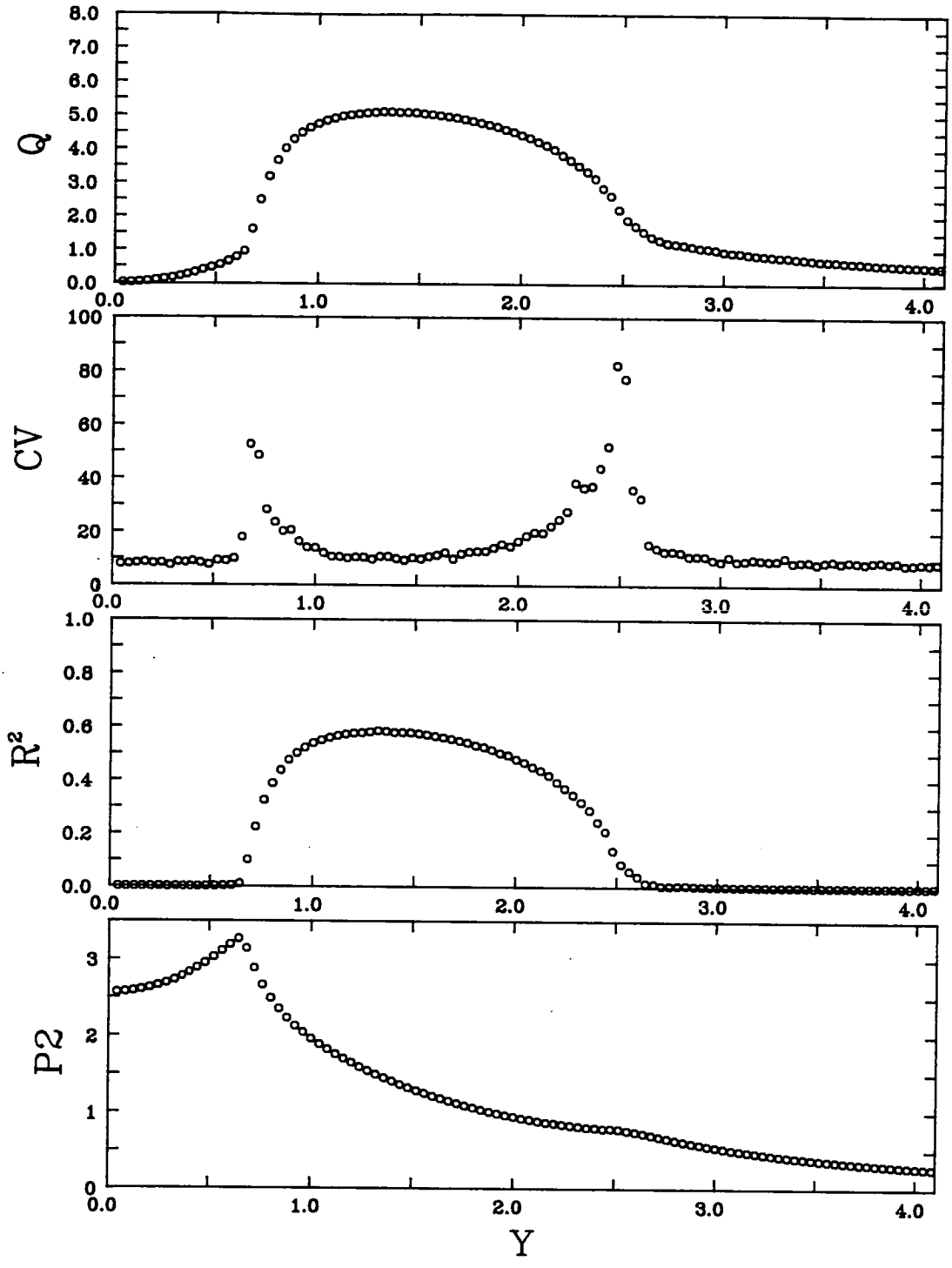

Figure 2.14: Measured expectation values of observables along the line $\kappa = 0$, $\lambda = \infty$ on a 6^4 lattice taken from simulations of the radially fixed Higgs-Yukawa model. No error bars are given.

For non-negative values of κ three phases are seen, two in which the scalar fields are disordered, and one in which the scalar fields are aligned. This latter phase is the broken phase. As the value of κ is increased, then the degree of alignment in the scalar sector increases. Thus the aligned phase occurs at the larger values of κ and the disordered phases occur at the smaller or more negative values of κ.

The action of the fermions on the scalar fields is always to correlate them, so that for a given value of κ, the minimum value of the global alignment parameter, G, occurs when $Y = 0$. This is because the infra-red regulator (the anti-periodic boundary conditions imposed on the fermionic fields in the lattice Euclidean time direction) ensures that the fermions decouple from the scalar sector in the limit $Y \to 0$, so that when $Y = 0$, the fermions have no effect on the scalar sector.

It is seen that the phase structure of the model is very similar for all values of λ, in that for all values of λ between 0 and ∞ there are two phase transition points when $\kappa = 0$, the one at the smaller values of Y occurring at almost the same value of Y for all values of λ. There seems to be no critical value of λ which separates regions of parameter space where different phase structures exist.

There is seen to be a well defined model in the limit $Y \to \infty$ in that for large Y, the measured expectation values of the observables become practically independent of Y. In the radially fixed case, that is when $\lambda = \infty$, this limiting model is the same as the model when $Y = 0$, that is a classical X-Y model, so that it is seen that in this case the fermions decouple from the scalar sector in the infinite Y limit. For finite values of λ a limiting model is also seen for $Y \to \infty$, but this limiting model is not the same as when $Y = 0$.

At negative values of κ, there also exists an anti-aligned phase, but G does not show this because of cancellations between the values of the variables representing the scalar fields at neighbouring sites. It is difficult to find any physical interpretation of this behaviour in a quantum field theory, because it is unclear how a meaningful continuum limit could be seen when the lattice spacing is taken to zero.

2.6 Analytical Study

It is possible to do some analytical work to study some aspects of the phase structure of this model using the techniques described in section 1.6. In this section, three such calculations are discussed. In the first, an approximate equation of the phase transition line seen at the smaller values of Y in the case $\lambda = 0$ is derived by looking semi-classically at the model. In the second, the critical value of κ is calculated using naive mean field theory arguments in the case $\lambda = 0$ and $Y = \infty$. In the third, the effective scalar potential for large Y is derived as an expansion in $\frac{1}{Y^2}$.

2.6.1 Semi-Classical Study

In this study, the scalar fields in the radially free ($\lambda = 0$) case are treated classically by finding the equations of motion of the effective scalar action after the fermionic degrees of freedom have been integrated out.

Following the example calculation described in section 1.6.2, the fermionic degrees of freedom of the model can be integrated out analytically, giving the determinant of the fermionic matrix product $M^\dagger M$. This leaves an effective scalar model with effective action, $\mathcal{S}'$:

$$\begin{aligned} \mathcal{S}' &= -\kappa \sum_{x\mu} \phi^*(x) \left[\phi(x+\mu) + \phi(x-\mu)\right] \\ &\quad + \sum_x \phi^*(x)\phi(x) + \lambda \sum_x \left[\phi^*(x)\phi(x) - 1\right]^2 \\ &\quad - \mathrm{Tr}\left[\log_e\left(M^\dagger M\right)\right] \end{aligned} \tag{2.122}$$

Treating the resulting effective scalar field theory classically, the allowed stable states of the system correspond to minima of $\mathcal{S}'$, that is they are solutions of the equations:

$$\begin{aligned} \frac{\delta \mathcal{S}'}{\delta \phi(x)} &= 0 \\ \frac{\delta \mathcal{S}'}{\delta \phi^*(x)} &= 0 \end{aligned} \tag{2.123}$$

Restricting attention to the case $\lambda = 0$, then it is possible to look for such semi-classical scalar states which are aligned states. To do this then it is necessary to look for solutions of equations (2.123) of the form:

$$\begin{aligned} \phi(x) &= \Phi \\ \phi^\star(x) &= \Phi^\star \end{aligned} \tag{2.124}$$

for constant values of Φ and its complex conjugate $\Phi^\star$.

Solutions of this form of equations (2.123) do exist if either

$$\Phi = \Phi^\star = 0 \tag{2.125}$$

or:

$$1 - 8\kappa - 4\frac{Y^2}{V}\sum_p \frac{1}{Y^2\left|\Phi\right|^2 + \sum_\mu \sin^2 p_\mu} = 0 \tag{2.126}$$

Where solutions to equation (2.126) exist, these solutions have a smaller value of the effective action than the solutions with zero scalar fields. This suggests that there may be two phases, one symmetric phase in which $\Phi^\star\Phi = 0$, which becomes disordered when quantum fluctuations are taken into account, and one where $\Phi^\star\Phi > 0$, which is an aligned phase. To find the equation of the phase transition line separating these two phases, then the substitution $\Phi^\star\Phi = 0$ is made in equation (2.126).

This procedure suggests that there is a phase transition line between disordered and ordered phases obeying the equation:

$$\kappa = \frac{1}{8} - \frac{Y^2}{2V}\sum_p \frac{1}{\left[\sum_\mu \sin^2 p_\mu\right]} \tag{2.127}$$

For a given value of Y, the ordered phase occurs at higher values of κ than this, the disordered phase occurring at lower values of κ, as would be expected by naively looking at the action. This transition is second order in this approximation, as the expectation value of the scalar observables (apart from CV) are continuous, but have discontinuous derivatives at the phase transition line.

This suggests that when $\kappa = 0$ and $\lambda = 0$, there is a phase transition at $Y = 0.6038$ on a 4^4 lattice, and at $Y = 0.6252$ on a 6^4 lattice. These predictions

are compatible with the measured values of the smaller critical values of Y of 0.62(5) and 0.65(5) on the 4^4 and 6^4 lattices respectively in the case $\kappa = 0$ and $\lambda = 0$ given in the previous section. It is clear from this, and from the form of equation (2.127), that the phase transition line predicted by this semi-classical treatment corresponds to the observed phase transition at the smaller values of Y.

If, instead of using anti-periodic boundary conditions in the Euclidean time direction, as used in the simulation, periodic boundary conditions were used in all directions for the fermionic fields, then equation (2.127) suggests that $Y = 0$ would be a critical point when $\kappa = 0$ and $\lambda = 0$. This assertion is supported by the observation that the partition function of the model is zero at these values of the parameters. This shows that this phase transition, and hence the disordered phase that occurs at small values of Y, is dependent on the method by which the infra-red regulator is imposed.

To make the calculation of this section more rigorous, both the stability of this semi-classical vacuum state and the effects of quantum fluctuations need to be studied in detail. It would be necessary to look at minima of the free energy of the effective scalar model, rather than to look just at minima of the effective action.

2.6.2 $Y = \infty$

In this study, the mean field theory technique described in section 1.6.4 is used to calculate an approximate critical value of κ when $\lambda = 0$ and $Y = \infty$.

In the $Y = \infty$ limit, that is neglecting the Dirac terms in the action (equation (2.89)), the fermionic degrees of freedom can be integrated out:

$$\begin{aligned} &\int \mathcal{D}\overline{\Psi}_1 \mathcal{D}\Psi_1 \mathcal{D}\overline{\Psi}_2 \mathcal{D}\Psi_2 \exp - \left[\overline{\Psi}_1 M \Psi_1 + \overline{\Psi}_2 M^\dagger \Psi_2\right] \\ &\quad \sim \ \mathrm{Det}\left[M^\dagger M\right] \\ &\quad \sim \ \prod_x \left(\phi^\star(x)\,\phi(x)\right)^4 \end{aligned} \tag{2.128}$$

This is just a constant in the radially fixed case when $\lambda = \infty$.

In the case $\lambda = 0$, a naive mean field theory calculation can then be performed to find the critical value of κ. Choosing just one site, and replacing the scalar fields on neighbouring sites by average values Φ and $\Phi^\star$, which are conjugate to each other, the one-site partition function, $\mathcal{Z}_1$, is:

$$\begin{aligned} \mathcal{Z}_1 &= \int \mathrm{d}\phi^\star \mathrm{d}\phi \, (\phi^\star \phi)^4 \exp - \left[-8\kappa \left[\Phi^\star \phi + \phi^\star \Phi \right] + \phi^\star \phi \right] \\ &\sim \int \mathrm{d}r \mathrm{d}\theta \, r^9 \exp - \left[r^2 - 16 r R \kappa \cos\left(\theta - \Theta\right) \right] \end{aligned} \tag{2.129}$$

where:

$$\begin{aligned} \phi &= r e^{i\theta} \\ \phi^\star &= r e^{-i\theta} \\ \Phi &= R e^{i\Theta} \\ \Phi^\star &= R e^{-i\Theta} \end{aligned} \tag{2.130}$$

For consistency, it is required that Φ equals the expectation value of ϕ. Thus:

$$\begin{aligned} R e^{i\Theta} &= \frac{1}{\mathcal{Z}_1} \int \mathrm{d}r \mathrm{d}\theta \, r^{10} e^{i\theta} \exp - \left[r^2 - 16 r R \kappa \cos\left(\theta - \Theta\right) \right] \\ &= \frac{1}{\mathcal{Z}_1} e^{i\Theta} \int \mathrm{d}r \mathrm{d}\theta \, r^{10} \cos\theta \exp - \left[r^2 - 16 r R \kappa \cos\theta \right] \end{aligned} \tag{2.131}$$

and similarly for $\Phi^\star$. Solutions of this self-consistency equation are the allowed states of the system, in this approximation, and can be found numerically.

The integral increases as the value of $R\kappa$ increases, so to find the critical value of κ at which a non-trivial solution exists to the above consistency equation, it is only necessary to expand the integrand to first order in R, as R varies continuously from zero (in this approximation) across the phase transition. Thus:

$$\begin{aligned} R &= \frac{1}{\mathcal{Z}_1} 16 R \kappa \int \mathrm{d}r \mathrm{d}\theta \cos^2\theta \, r^{11} e^{-r^2} + \cdots \\ &= 8 R \kappa \frac{5!}{4!} + \cdots \\ &= 40 R \kappa + \cdots \end{aligned} \tag{2.132}$$

Thus for non-trivial values of R, $\kappa > \kappa_C$ where:

$$\kappa_C = \frac{1}{40} \tag{2.133}$$

R is continuous at the transition, but with discontinuous derivatives, suggesting that when $Y = \infty$ and $\lambda = 0$, there is a second order phase transition between

a disordered phase (at lower values of κ), where $R = 0$ in this approximation, and an ordered phase (at higher values of κ), where $R > 0$, at a critical value of $\kappa = \kappa_C = 0.025$.

A value of $\kappa_C = 0.025$ when $\lambda = 0$ and $Y = \infty$ is not incompatible with the results of the simulation, as shown in figure 2.5.

A similar analysis can be performed to study the transition between a disordered and an anti-aligned phase when $Y = \infty$ and $\lambda = 0$. This is done by replacing the scalar fields ϕ and $\phi^\star$ at the neighbouring sites by $-\Phi$ and $-\Phi^\star$. This indicates an anti-aligned phase when κ is less that -0.025 in the case $\lambda = 0$ and $Y = \infty$.

2.6.3 Effective Scalar Potential

In this section, the effective scalar potential induced by the fermions at large values of Y is calculated as an expansion in $\frac{1}{Y^2}$ in a similar manner to the example $\frac{1}{Y}$ expansion derived in section 1.6.3. In this case, the terms in odd inverse powers of Y are zero because the bare mass of the fermions is zero.

As in the previous section, the fermionic degrees of freedom can be integrated out analytically:

$$\begin{aligned} &\int \mathcal{D}\overline{\Psi}_1 \mathcal{D}\Psi_1 \mathcal{D}\overline{\Psi}_2 \mathcal{D}\Psi_2 \exp - \left[\overline{\Psi}_1 M \Psi_1 + \overline{\Psi}_2 M^\dagger \Psi_2\right] \\ &\sim \ \mathrm{Det}\left[M^\dagger M\right] \\ &\sim \ \exp \mathrm{Tr}\left[\log_e\left(M^\dagger M\right)\right] \end{aligned} \tag{2.134}$$

Thus the effect of the fermions on the scalar sector can be represented by a contribution to the scalar potential, which can be written as an expansion in powers of $\frac{1}{Y^2}$:

$$\begin{aligned} -\mathrm{Tr}\left[\log_e\left(M^\dagger M\right)\right] \ = \ & -4\sum_x \log_e\left(Y^2 \phi^\star(x)\,\phi(x)\right) \\ & -\frac{1}{Y^2}\sum_{x\mu}\frac{1}{\phi(x)}\left[\frac{1}{\phi^\star(x+\mu)} + \frac{1}{\phi^\star(x-\mu)}\right] \\ & +O\left(\frac{1}{Y^4}\right) \end{aligned} \tag{2.135}$$

In the radially fixed case, that is when $\lambda = \infty$, the $O\left(\frac{1}{Y^2}\right)$ term in equation (2.135) simplifies to:

$$-\frac{2}{Y^2}\sum_{x\mu}\cos\left(\theta(x)-\theta(x+\mu)\right) \tag{2.136}$$

which is of the same form as the κ term in the scalar part of the action. Thus the effect of the fermions on the scalar sector in the radially fixed case at large Y is to generate an effective value of the scalar hopping parameter, κ:

$$\kappa_{\text{eff}} = \kappa + \frac{1}{Y^2} \tag{2.137}$$

plus corrections of order $\frac{1}{Y^4}$. This gives some indication of the form of the phase transition line that occurs at large values of Y in the radially fixed version of the model.

2.7 Discussion

The results of simulating the Higgs-Yukawa model with action stated in equation (2.89) show clearly that its phase structure is basically the same for all values of λ between 0 and ∞. It is seen that spontaneous symmetry breaking in the scalar sector, characterised by an aligned phase, can occur as easily at $\lambda = 0$ as it does at $\lambda = \infty$. Thus it is manifestly clear that the $\lambda\phi^4$ term in the action cannot be the term which is most responsible for symmetry breaking in this model.

If this $\lambda\phi^4$ term is to be discounted as being irrelevant, then it is necessary to understand the dominant process by which symmetry breaking does occur in this model. By looking at the dependence of the phase of the model on the value of Y, it is clear that the fermions can and do induce symmetry breaking in the scalar sector.

Equation (2.128), in section 2.6, is an explicit expression for the fermionic contribution, inside the scalar functional integral, to the partition function in the infinite Y limit. This contribution can thus be represented by an effective po-

tential term in the scalar action in this limit:

$$-4\sum_{x}\log_e\left[\phi^\star(x)\,\phi(x)\right] \tag{2.138}$$

This is a constant in the $\lambda = \infty$ case, which explains why the fermions are seen to decouple from the scalar sector for large values of Y, causing the $Y = \infty$ model to be the same as that at $Y = 0$ in the radially fixed model. Looking at the case $\lambda = 0$ and $Y = \infty$, then the total effective potential in the scalar sector is of the form of a 'ring mould' [26]:

$$\phi^\star\phi - \log_e\left[\phi^\star\phi\right] \tag{2.139}$$

which is infinite when the scalar fields are in the only symmetric semi-classical state, which is $\phi^\star\phi = 0$, so that when there is a suitable correlating term in the action, such as at large enough κ (of order 0.025), or when the corrections to the effective action for finite Y are significant, then symmetry breaking can be induced in the scalar sector.

Note that an effective potential of this form is not restricted to the form of Yukawa coupling used in the model studied in this chapter. See, for instance, the example model studied in section (1.6). Thus this fermion induced spontaneous symmetry breaking can occur in models other than the one studied in this chapter.

Thus the fermions induce in the scalar sector a potential, not unlike the 'Mexican Hat' potential in the Standard Model, which makes it energetically unfavourable for the scalar states to be dominated by configurations where the scalar fields are zero. This 'ring mould' potential comes naturally out of the interactions between the fermions and the scalar fields in the model and thus does not suffer from the same limitation as the 'Mexican Hat' potential which has to be added to the scalar sector 'by hand'. The Yukawa interaction is required anyway in the Higgs mechanism so that the spontaneous symmetry breaking in the scalar sector gives masses to the fermions.

Looking in the region of negative κ, as shown in figures 2.5 and 2.6, the fact that the two critical surfaces separating aligned from disordered phases do not seem to be trivially the same surface suggests that the critical phenomena associated

with them may well be different, so that continuum models (if any exist) built around these critical surfaces need not be the same. The coefficient of the logarithmic term in the effective scalar action is not a parameter, it is, in fact, related to the number of species of fermions being simulated and the number of lattice dimensions, thus it cannot be affected by renormalisation in the way that the λ parameter in the Higgs mechanism is.

The analytical work outlined in section 2.6 suggests that the disordered phase at the smaller values of Y is in fact different from that at the larger values of Y. In the case $\lambda = 0$, at the smaller values of Y, the scalar fields ϕ fluctuate about zero, the pseudo-classical vacuum state. At the larger values of Y, this is not so, as the 'ring mould' potential makes a zero value of ϕ energetically unfavourable. Instead, the disorder comes from the phase of the scalar fields fluctuating from site to site, similar to the way in which the scalar fields in the radially fixed model can be disordered, even though their modulus is fixed, because of the fluctuations in phase that can occur.

It is noted that in the conventional treatment of the Standard Model (see for instance Bailin and Love [27]), the classical scalar vacuum state, about which quantum fluctuations are taken into account by perturbation theory, is taken to be that scalar state which minimises the scalar action *without* taking into account the effect of the fermions on the scalar sector. This is why the $\lambda\phi^4$ term has to be added 'by hand', and why the bare mass squared of the scalar fields has to be unphysically negative. The work performed on the greatly simplified model studied in this chapter tends to suggest that this procedure may well be mistaken. In this Higgs-Yukawa model, it is necessary to take account of the fermions *before* finding the classical vacuum state.

To do analytical calculations involving massless fermions, it is usually necessary to introduce an infra-red regulator for the fermionic fields. In the Standard Model, it is the generation of fermion masses by the Higgs mechanism which is the fermionic infra-red regulator. The study of the Higgs-Yukawa model described in this chapter tends to suggest that the need for a fermionic infra-red regulator is the cause of the symmetry breaking in the scalar sector.

It can be suggested that it may be possible to formulate an alternative to the Standard Model in which no 'Mexican Hat' potential has to be added to the Higgs sector, the Yukawa interaction may well be sufficient to induce the required spontaneous symmetry breaking so that the fermions and the gauge bosons can gain a mass as required. Thus there are many unanswered questions about the Standard Model in general, and on the role of the Higgs field in particular. Observations (or lack of observations) of a Higgs boson must shed light on this.

It is clear that there is also a need for the simulation of more physically realistic models on physically realistic lattice sizes to try and understand the phenomena which occur at these energies just beyond our experimental reach at present. To do this, then it is first necessary to find a satisfactory way to remove the unphysical doubled fermion species from lattice simulations. A possible method by which this may be achieved is discussed in the next chapter, where a model, not unlike the model of this chapter, is studied.

Chapter 3

Lattice Yukawa-Wilson Model

3.1 Introduction

In this chapter, a lattice model is studied which may be useful in understanding a method by which the doubled fermionic species that occur on the lattice can be removed.

As explained in section 1.3.2, extra unphysical species of fermions are generated when fermionic fields are discretised on the lattice. These occur at non-zero values of the lattice momentum, so schemes for their removal use an extra momentum dependent term in the action which couples to these doubled fermions effectively generating masses for them of order one in inverse lattice units. In physical units, this means that these masses go to infinity as the lattice spacing is taken to zero, thus effectively removing them from the model in the continuum limit.

Unfortunately, these momentum dependent terms break the chiral symmetry of the fermionic sector, thus there is nothing to stop effective fermionic mass terms of the form:

$$m\overline{\Psi}\Psi \tag{3.140}$$

being generated when interactions with gauge fields, for instance, are included. This means that the bare fermion mass in the action has to be tuned if massless

fermions are to be simulated when interactions are included to cancel out these effective fermion mass terms.

In the Higgs-Yukawa model studied in the previous chapter, the Yukawa term couples the chiral symmetry of the fermionic sector to the U(1) symmetry of the scalar sector which exist independently when $Y = 0$. Provided this remnant of chiral symmetry that exists when Y is non-zero is not broken spontaneously, then effective fermionic mass terms cannot be generated.

Thus it has been suggested [28,29,30] that fermion doubles may be removed without the necessity of tuning bare fermion masses if auxiliary scalar fields are added to an interacting lattice model which couple to the fermions via a point-split Wilson-like Yukawa term in the action. When the bare fermion mass is set to zero, this Yukawa-Wilson term in the action is invariant under the same set of transformations (2.94) as the Higgs-Yukawa model studied in the previous chapter, where the identification is made between the Higgs scalar fields of the Higgs-Yukawa model and the auxiliary scalar fields which couple to the fermions in the Yukawa-Wilson term. Under what circumstances this symmetry may be enough to prevent the generation of effective fermion mass terms is the subject of the work described in this chapter.

In this chapter, the results of two simulations of a Yukawa-Wilson model are given. The model includes the fermionic fields and the auxiliary scalar fields, but does not include any other field interacting with the fermions. The first simulation finds features of the phase diagram of the model on a small lattice with zero bare fermion mass, in a similar way to the model in the previous chapter, to see if there is a disordered scalar phase in which the chiral symmetries of the action are preserved in the ground state, which will be a candidate phase for effective fermion mass terms to be prohibited when interactions with other fields are included. The second simulation looks at fermionic propagators on lattices extended in the Euclidean time direction to observe the behaviour of the masses of the physical fermion state and one of its doubles as a function of the bare fermion mass in two different phases of the model.

3.2 Action

The action for the model studied in this chapter is similar to that studied in the previous chapter, except that the simple one site Yukawa term is replaced by a point-split one, and that the radial degree of freedom of the scalar fields is set to unity, like the $\lambda = \infty$ version of the previous model. An explicit fermion mass term is also included:

$$\begin{aligned} \mathcal{S} &= -\kappa \sum_{x\mu} \phi^{\star}(x) \left[\phi(x+\mu) + \phi(x-\mu)\right] \\ &\quad + \overline{\Psi}_1 M \Psi_1 + \overline{\Psi}_2 M^{\dagger} \Psi_2 \end{aligned} \tag{3.141}$$

where:

$$\begin{aligned} \phi(x) &= e^{i\theta(x)} \\ \phi^{\star}(x) &= e^{-i\theta(x)} \end{aligned} \tag{3.142}$$

and:

$$\begin{aligned} \overline{\Psi} M \Psi = \frac{1}{2} \sum_{x\mu} \overline{\psi}(x) \gamma_{\mu} \left[\psi(x+\mu) - \psi(x-\mu)\right] + m \sum_{x} \overline{\psi}(x) \psi(x) \\ + Y \sum_{xy\mu} \overline{\psi}(x) \left[\delta(y, x+\mu) + \delta(y, x-\mu) - 2\delta(y,x)\right] \left[\phi(x) R + \phi^{\star}(y) L\right] \psi(y) \end{aligned} \tag{3.143}$$

with:

$$\begin{aligned} R &= \frac{1}{2}(1+\gamma_5) \\ L &= \frac{1}{2}(1-\gamma_5) \end{aligned} \tag{3.144}$$

defined on a regular four dimensional Euclidean lattice.

In this model, explicit dynamics are added to the auxiliary scalar fields, ϕ, hence the term in the action with coefficient κ, so as to help the study of the phase diagram, and also to permit comparisons to be made with the results of the previous chapter, as then this model is a direct extension of the radially fixed Higgs-Yukawa model studied there. When the explicit fermion mass, m, is set to zero, then this action is invariant under the same set of transformations as the

Higgs-Yukawa model as stated in equations (2.94). The explicit fermion mass term breaks this symmetry.

The action of the point-split Yukawa-Wilson term on the fermion doubled states can be understood by a simple mean field argument. Suppose the scalar fields are aligned to some degree, so that there is a non-zero expectation value of $\phi(x)$, denoted by Φ. In a mean field approximation, the scalar field variables $\phi(x)$ and $\phi^\star(x)$ can be replaced in the action by their expectation values Φ and $\Phi^\star$, which are complex conjugates. In this approximation the fermion propagator is:

$$\begin{aligned}\left\langle \psi_1(x_1)\,\overline{\psi}_1(x_2)\right\rangle &= M^{-1}(x_1,x_2) \\ &= \frac{1}{V}\sum_p \frac{e^{ip(x_1-x_2)}}{\left[m + i\sum_\mu \gamma_\mu \sin p_\mu + 2Y\left[\sum_\mu \cos p_\mu - 4\right]\left[\Phi R + \Phi^\star L\right]\right]}\end{aligned} \tag{3.145}$$

which has only one pole for $m = 0$ at $p = 0$, as required, provided $\Phi^\star\Phi > 0$, because the term:

$$\left[\sum_\mu \cos p_\mu - 4\right] \tag{3.146}$$

is zero only if $p = 0$. Thus, when the lattice spacing is taken to zero, only the physical fermion state remains if the scalar fields are aligned.

There seems to be a contradiction in purposes here. To remove the doubled fermion states an aligned scalar state is required, whilst for there to be no necessity to tune bare fermion masses, a disordered scalar state is required. This is a manifestation of the no-go theorem mentioned in section 1.3.2, which this model must circumvent if it is to be useful in removing the unphysical fermion doubles from lattice simulations without the necessity for tuning the bare fermion mass to obtain massless fermions when other interactions are included.

Note that if the auxiliary scalar fields are set to -1, and $Y = \frac{1}{2}$, then the action is equivalent to that for Wilson fermions, as specified in section 1.3.2.

3.3 Observables

The expectation values of certain observables of this model are studied. These are basically the same as those of the Higgs-Yukawa model as stated in section 2.3, with the additional observable $P1$, defined below:

$$\begin{aligned} Q &= \frac{1}{V}\sum_{x\mu}\phi^{\star}(x)\left[\phi(x+\mu)+\phi(x-\mu)\right] \\ CV &= \frac{\partial\langle Q\rangle}{\partial\kappa} \\ R^2 &= \frac{1}{V^2}\sum_{xy}\phi^{\star}(x)\,\phi(y) \\ P1 &= \frac{1}{V}\mathrm{Tr}\left[M^{-1}\right] \\ P2 &= \frac{1}{V}\mathrm{Tr}\left[\left(MM^{\dagger}\right)^{-1}\right] \end{aligned} \tag{3.147}$$

where V is the number of sites on the lattice. The expectation value of $P1$ is zero in a chirally symmetric phase, and is non-zero in a chirally broken phase. All of these observables, except for $P1$, are invariant under the same sets of transformations as the action when $m = 0$ as stated in equations (2.94). In principle, on a finite lattice, these symmetries should ensure that the expectation value of $P1$ is zero when $m = 0$.

Perturbative expansions can be performed in certain parameters using techniques described in section 1.6.1. For instance, in the regime of small Y and small κ, then:

$$\begin{aligned} \langle Q\rangle = 8\kappa &+ \frac{512m^2Y^2}{V^2}\sum_{pq}\frac{\left[\sum_{\mu}\cos p_{\mu}-4\right]\left[\sum_{\mu}\cos q_{\mu}-4\right]}{\left[m^2+\sum_{\mu}\sin^2 p_{\mu}\right]\left[m^2+\sum_{\mu}\sin^2 q_{\mu}\right]} \\ &+ \frac{32Y^2}{V^2}\sum_{pq}\frac{\left[\sum_{\mu}\cos p_{\mu}-4\right]^2\sum_{\mu}\sin p_{\mu}\sin q_{\mu}\sum_{\mu}\cos(p-q)_{\mu}}{\left[m^2+\sum_{\mu}\sin^2 p_{\mu}\right]\left[m^2+\sum_{\mu}\sin^2 q_{\mu}\right]} \end{aligned} \tag{3.148}$$

$$\langle P1\rangle = \frac{4m}{V}\sum_{p}\frac{1}{\left[m^2+\sum_{\mu}\sin^2 p_{\mu}\right]}$$

$$-\frac{16mY^2}{V^2}\sum_{pq}\frac{\left[\left[\sum_\mu \cos p_\mu - 4\right]^2 + \left[\sum_\mu \cos q_\mu - 4\right]^2\right]\sum_\mu \sin p_\mu \sin q_\mu}{\left[m^2 + \sum_\mu \sin^2 p_\mu\right]^2\left[m^2 + \sum_\mu \sin^2 q_\mu\right]}$$

$$-\frac{64mY^2}{V^2}\sum_{pq}\frac{\left[m^2 - \sum_\mu \sin^2 p_\mu\right]\left[\sum_\mu \cos p_\mu - 4\right]\left[\sum_\mu \cos q_\mu - 4\right]}{\left[m^2 + \sum_\mu \sin^2 p_\mu\right]^2\left[m^2 + \sum_\mu \sin^2 q_\mu\right]} \tag{3.149}$$

$$\begin{aligned}\langle P2\rangle \;=\; & \frac{4}{V}\sum_p \frac{1}{\left[m^2 + \sum_\mu \sin^2 p_\mu\right]} \\ & + \frac{8Y^2}{V^2}\sum_{pq}\frac{\left[\left[\sum_\mu \cos p_\mu - 4\right]^2 + \left[\sum_\mu \cos q_\mu - 4\right]^2\right]}{\left[m^2 + \sum_\mu \sin^2 p_\mu\right]\left[m^2 + \sum_\mu \sin^2 q_\mu\right]} \\ & - \frac{16Y^2}{V^2}\sum_{pq}\frac{\left[\left[\sum_\mu \cos p_\mu - 4\right]^2 + \left[\sum_\mu \cos q_\mu - 4\right]^2\right]\sum_\mu \sin p_\mu \sin q_\mu}{\left[m^2 + \sum_\mu \sin^2 p_\mu\right]^2\left[m^2 + \sum_\mu \sin^2 q_\mu\right]} \\ & - \frac{128m^2Y^2}{V^2}\sum_{pq}\frac{\left[\sum_\mu \cos p_\mu - 4\right]\left[\sum_\mu \cos q_\mu - 4\right]}{\left[m^2 + \sum_\mu \sin^2 p_\mu\right]^2\left[m^2 + \sum_\mu \sin^2 q_\mu\right]}\end{aligned} \tag{3.150}$$

neglecting terms of order κ^2, κY^2 and Y^4. See appendix A.1 for details of the conventions used for momentum sums.

In the case $m = 0$ and $Y = 0$:

$$\left\langle R^2\right\rangle = \frac{1}{V}\left[1 + 8\kappa + O(\kappa^2)\right] \tag{3.151}$$

$$\langle CV\rangle = 8 + O(\kappa^2) \tag{3.152}$$

From these expressions, the expectation values of the observables can be calculated and compared with values measured from the computer simulation, which forms a useful check on the validity of the results of the computer simulation.

3.4 Phase Diagram

In this section, results are given of a simulation of the Yukawa-Wilson model whose action is defined in equation (3.141) on a 4^4 lattice to discover features of its phase diagram in the case $m = 0$. It is necessary to know in what regions of parameter space the model is in a chirally symmetric phase, corresponding to disordered phases of the auxiliary scalar fields, and in what regions it is in a chirally broken phase, corresponding to an ordered phase, because this may well determine whether or not bare fermion mass tuning will be required to obtain massless fermions when interactions between the fermions and other bosonic fields are included.

Anti-periodic boundary conditions are used for the fermionic fields in the Euclidean time direction, periodic boundary conditions are used everywhere else. These boundary conditions are used here to act as an infra-red regulator for the fermions in the same way in which they were used for the one site Yukawa model studied in the previous chapter (see section 2.2.2) so that the model is, in principle, accessible to simulation in the limit $Y \to 0$ with $m = 0$.

The method by which the model was simulated in this case is very similar to that used for the radially fixed version of the one site model studied in the previous chapter. Many of the details mentioned there also apply to this model, so they will not be repeated here. One difference between this simulation and that for the radially fixed model of the previous chapter is that sixty four bit arithmetic was used rather than thirty two bit for reasons given below.

3.4.1 Program Checks

The program checks used for the one-site Yukawa model, as described in section 2.4.3, were also applied to this model.

- Independence of the measured expectation values of observables from the value of the time step, $\delta\tau$, was verified. See table 3.1.

	$\delta\tau = 0.1$	$\delta\tau = 0.5$
Acceptance	0.96	0.13
Q	4.859(2)	4.859(3)
CV	14.93(14)	14.67(18)
R^2	0.5555(4)	0.5550(5)
PbP	2.2858(9)	2.2865(9)

Table 3.1: Measured expectation values of observables of the Yukawa-Wilson model with $m = 0$, $Y = 0.1$, and $\kappa = 0.05$ on a 4^4 lattice, as a function of $\delta\tau$ with total Monte Carlo time per step fixed at 1.0.

- Comparisons were made between measured expectation values of observables and the values of perturbative expressions. See figures 3.1 and 3.2.

- The molecular dynamics steps were seen to be reversible to the accuracy with which the sets of linear equations were solved. The process by which this was done is the same as was used for the Higgs-Yukawa model of the previous chapter. It was seen that to solve the sets of linear equations accurately enough for the purposes of this simulation in the disordered phase of the model, then it was necessary to use sixty four bit arithmetic.

3.4.2 Results

A contour plot of the measured expectation value of the observable R^2 in the plane $m = 0$ is shown in figure 3.3. Because the radius of the auxiliary scalar fields is set to unity, then R^2 is equivalent to the global alignment parameter G used in the previous chapter, so that disordered (and hence chirally symmetric) phases are characterised by expectation values of R^2 close to zero, and an ordered (chirally broken) phase by expectation values of R^2 of order unity for non-negative values of κ. The measured expectation values of some of the observables along the line $\kappa = 0$ are shown in figure 3.4. No error estimates are

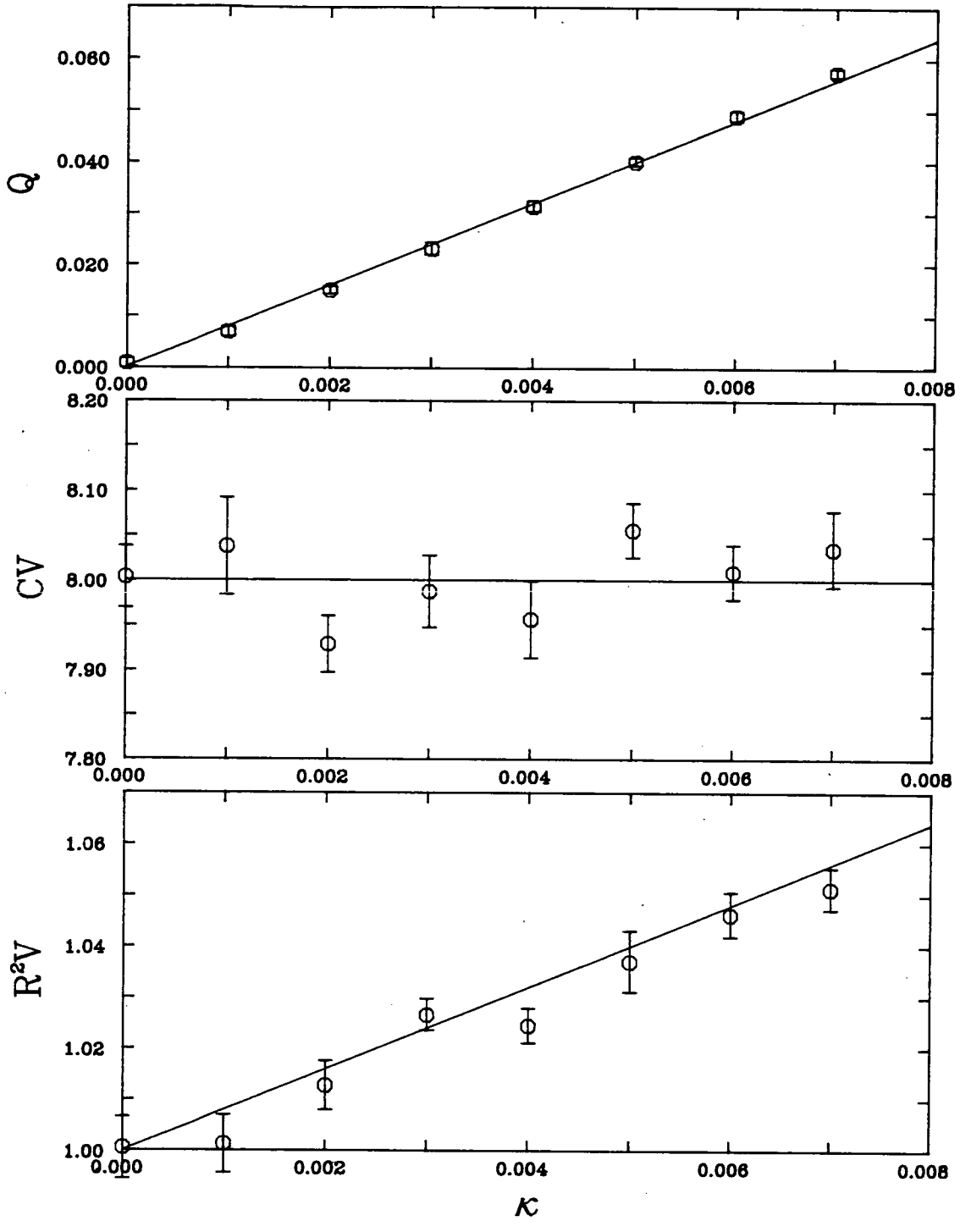

Figure 3.1: Comparison of measured expectation values with perturbative expressions for Q, CV and R^2 when $m = 0$ at $Y = 0$ for small κ for the Yukawa-Wilson model on a 4^4 lattice.

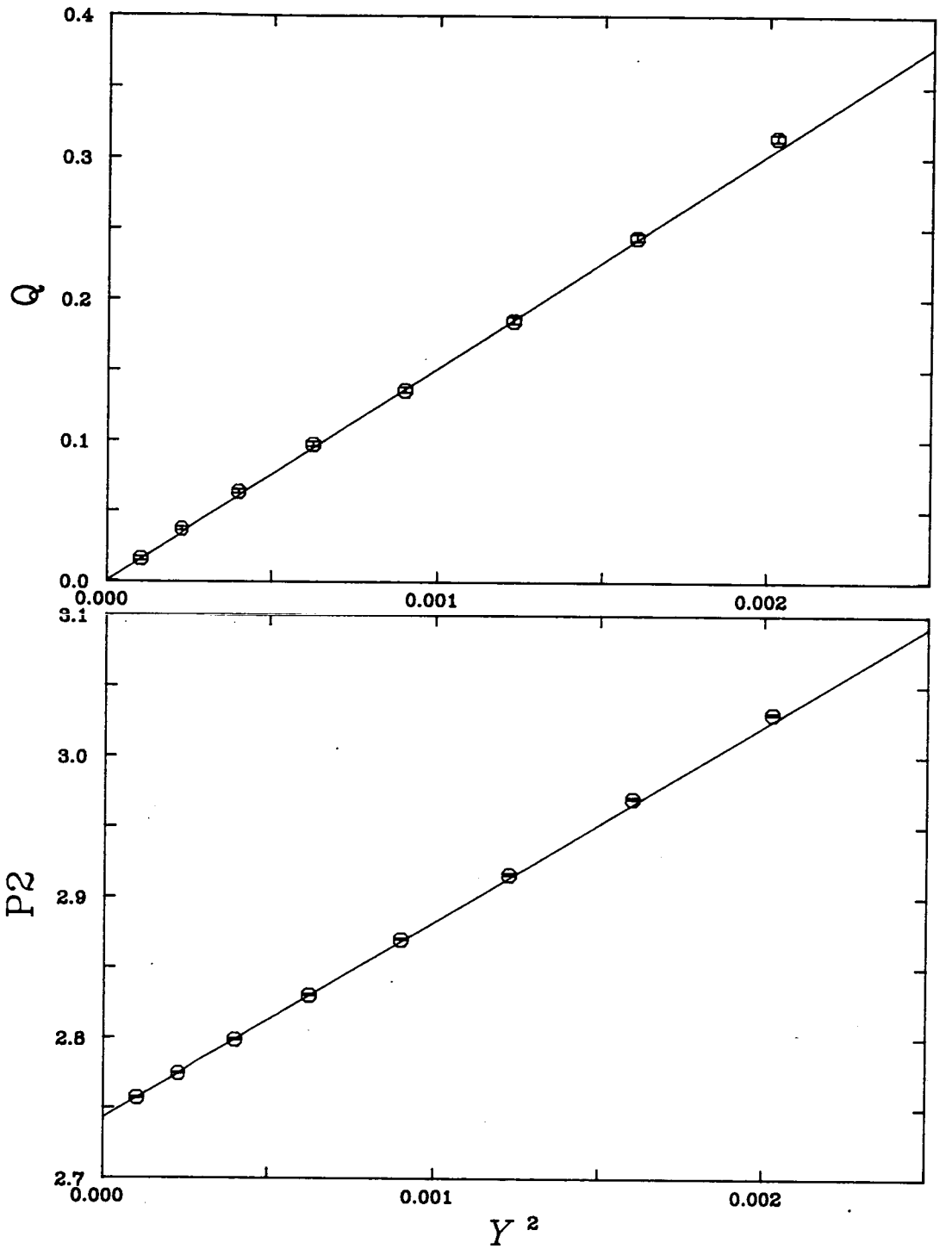

Figure 3.2: Comparison of measured expectation values with perturbative expressions for Q and $P2$ when $m = 0$ and $\kappa = 0$ for small Y on a 4^4 lattice for the Yukawa-Wilson model.

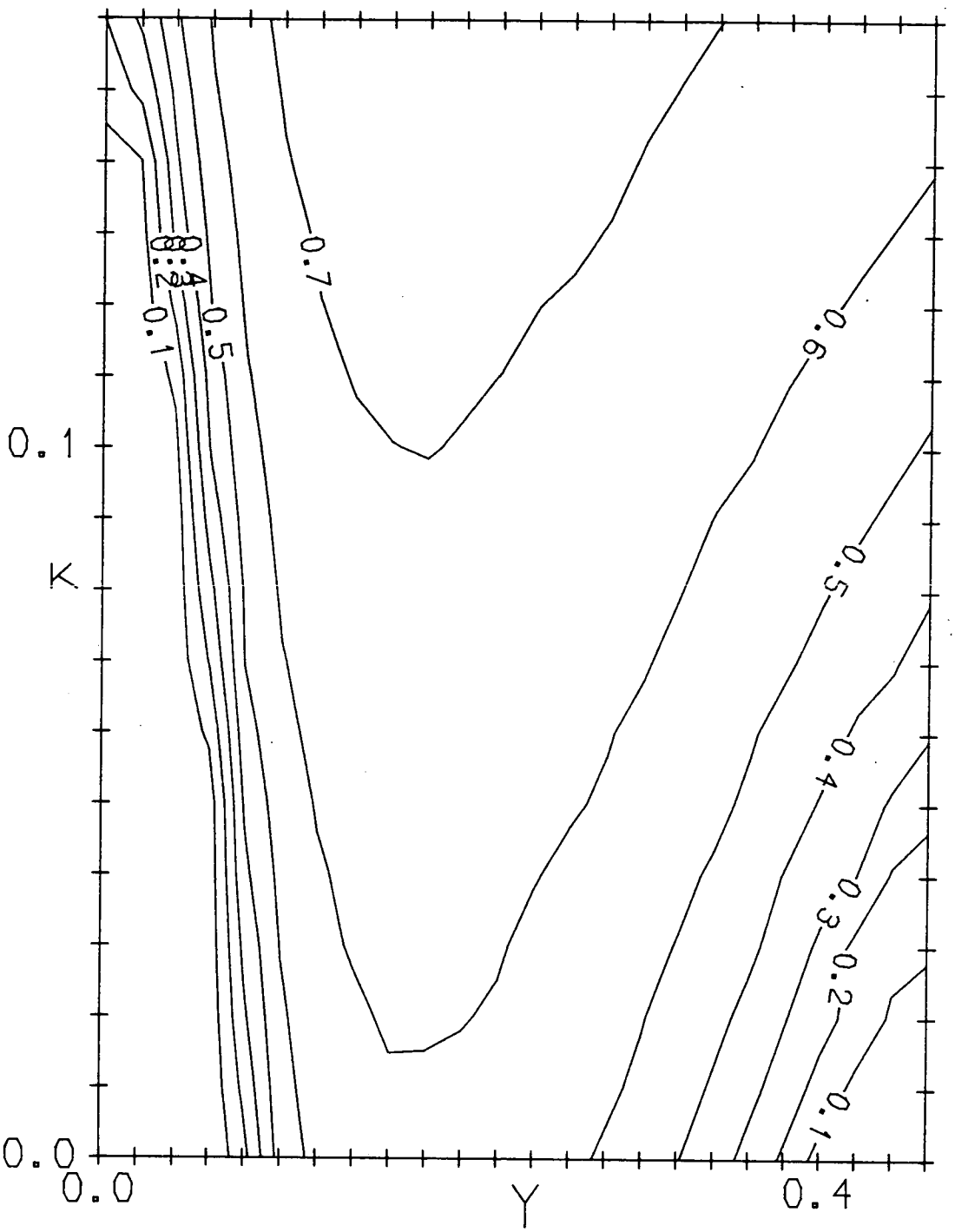

Figure 3.3: Contour plot of the measured expectation value of R^2 for the Yukawa-Wilson model on a 4^4 lattice interpolated from 408 data points in the Y - κ plane with $m = 0$.

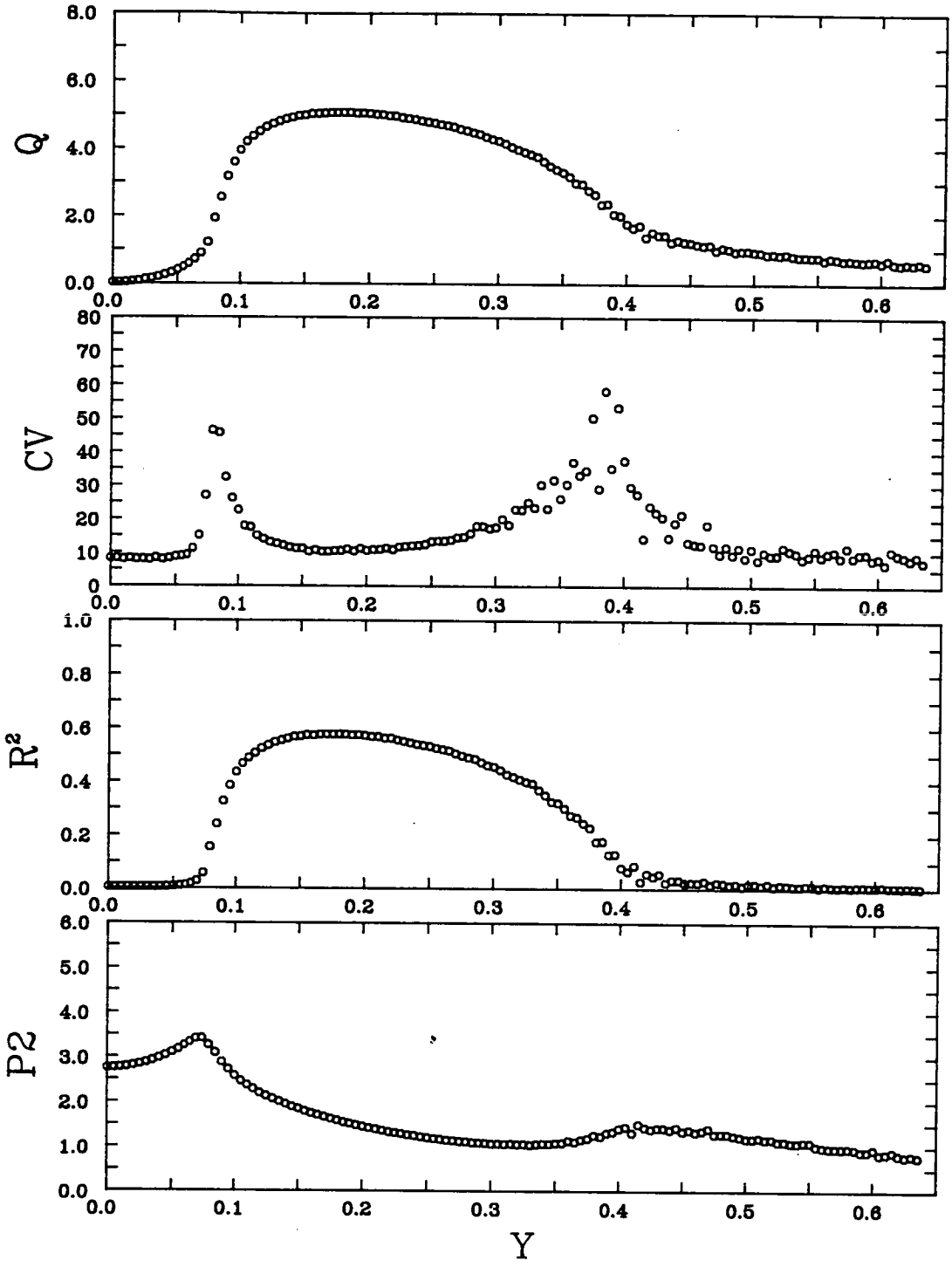

Figure 3.4: Measured expectation values of the observables Q, CV, R^2 and $P2$ along the line $m = 0$, $\kappa = 0$ on a 4^4 lattice. No error estimates are given.

given, but some indication as to the errors in the points given can be gauged from their scatter.

It is seen that the phase diagram of this Yukawa-Wilson model has basically the same structure as the phase diagram of the radially fixed version of the one-site model discussed in the previous chapter, although the critical values of Y for a given value of κ are different in the two models. Along the line $\kappa = 0$, as seen in figure 3.4, the critical values of Y are $Y = 0.08(2)$ and $Y = 0.38(4)$ for the 4^4 lattice.

3.4.3 Analytical Study

It is possible to use the semi-classical technique as described in section 1.6.2 on the radially free version of this model to discover some information about one of the phase transition lines seen in the case $m = 0$. This radially free version of the model has an additional term in the action as given in equation (3.141) which is:

$$+\sum_x \phi^*(x)\,\phi(x) \tag{3.153}$$

and the constraint on the radial degree of freedom is relaxed. Experience of the one-site Yukawa model studied in the previous chapter suggests that this phase transition line will be in almost the same position in the radially free case as it is for the radially fixed case, the latter being the model simulated here. The phase transition in question is the one that occurs at the smaller values of Y as seen in figures 3.3 and 3.4.

Proceeding as in the calculation described in section 2.6.1, the semi-classical treatment suggests that, for the radially free version of the model, there is a second order phase transition between a disordered phase (at lower values of κ) and an aligned phase (at higher values of κ) obeying the equation:

$$\kappa = \frac{1}{8} - \frac{2Y^2}{V}\sum_p \frac{\left[\sum_\mu \cos p_\mu - 4\right]^2}{\left[\sum_\mu \sin^2 p_\mu\right]} \tag{3.154}$$

(see section A.1 for details of the conventions used for lattice momentum sums).

This suggests that in the radially free case, there is a phase transition at $Y = 0.0701$ when $\kappa = 0$ on a 4^4 lattice when periodic boundary conditions are used for the fermions except in the lattice Euclidean time direction, where anti-periodic boundary conditions are used, as is used in the computer simulation. This is to be compared with the measured critical value for the radially fixed model, which is $Y = 0.08(2)$. As in the Higgs-Yukawa model studied in the previous chapter, if periodic boundary conditions are used for the fermions in all lattice directions, then this semi-classical calculation suggests that when $\kappa = 0$ there is a critical value of Y at $Y = 0$. Again this is supported by the observation that the partition function of the model is zero at $Y = 0$ with these boundary conditions.

3.4.4 Discussion

Thus it is seen that there are three phases of this model when $m = 0$, for non-negative values of κ, as was seen in the Higgs-Yukawa model of the previous chapter. Along the line $\kappa = 0$, the auxiliary fields are disordered at small values of Y, meaning that this is a chirally symmetric phase. Then, at medium values of Y, the auxiliary fields are aligned, meaning that this is a chirally broken phase, the critical value of Y between these two phases being dependent on the method by which the infra-red regulator is imposed in the fermionic sector. At large values of Y, the auxiliary fields are disordered, meaning that this phase is chirally symmetric.

So the candidate phase in which bare fermion mass tuning may not be required for massless fermions, when the fermions interact with other bosonic fields, is the disordered phase that occurs at large values of Y when $\kappa = 0$ and $m = 0$, the disordered phase at the small values of Y being discounted because of its dependence on the infra-red regulator. In the aligned phase that occurs at medium values of Y, the chiral symmetry is spontaneously broken, and thus it seems likely that bare fermion mass tuning will be needed in this phase when other interactions are included, as is required when using Wilson fermions.

3.5 Fermion Propagators

In this section, a study is made of fermion propagators measured from simulations of the Yukawa-Wilson model on a $4^3 \times 16$ lattice in the case $\kappa = 0$. Fermion masses are obtained by fitting decaying exponentials to the measured propagators for the physical fermion that occurs at zero momentum, and for one of the doubled species that occur on the lattice at a non-zero momentum value.

The fermionic propagator:

$$\left\langle \psi_1(y_1)\,\overline{\psi}_1(y_2) \right\rangle \tag{3.155}$$

measured from a computer simulation, is not useful in this raw form, because of the large number of degrees of freedom involved. So the propagators studied in this section are so-called 'timesliced propagators' in which y_1 is set at the lattice origin, and all other degrees of freedom, except the lattice Euclidean time component of y_2, are summed over.

The two timesliced propagators studied in this section, $G_0(t)$ and $G_\pi(t)$, are defined as:

$$\begin{aligned} G_0(t) &= \sum_{\mathbf{x}\alpha\beta} \left\langle \psi_1^\alpha(0)\,\overline{\psi}_1^\beta(x) \right\rangle \\ &= \sum_{\mathbf{x}\alpha\beta} \left\langle M^{-1}_{\alpha\beta}(0,x) \right\rangle \\ G_\pi(t) &= \sum_{\mathbf{x}\alpha\beta} e^{i\pi x_1} \left\langle \psi_1^\alpha(0)\,\overline{\psi}_1^\beta(x) \right\rangle \\ &= \sum_{\mathbf{x}\alpha\beta} e^{i\pi x_1} \left\langle M^{-1}_{\alpha\beta}(0,x) \right\rangle \end{aligned} \tag{3.156}$$

where the sum over $\mathbf{x}$ represents the sum over the spatial components of the site coordinate, x, of which x_1 is the lattice x coordinate. The free parameter t is the lattice Euclidean time coordinate. The spinor degrees of freedom are also summed over. The action of the weighted spatial sum is to project out contributions to the full propagator with a given spatial momentum. Thus for naive fermions, when $Y = 0$, $G_0(t)$ and $G_\pi(t)$ project out the physical fermionic state and the doubled state with spatial momentum of π in the lattice x direction, plus their doubles in the Euclidean time direction.

Perturbation theory has been used to obtain an expression for the timesliced propagators in the limit of small Y in the case $\kappa = 0$ using techniques described in section 1.6.1:

$$G_0(t) = \frac{4m}{N_t} \sum_{p_t} \frac{e^{-ip_t t}}{\left[m^2 + \sin^2 p_t\right]}$$
$$- \frac{16mY^2}{VN_t} \sum_{p_t q} \frac{\left[\left[\cos p_t - 1\right]^2 + \left[\sum_\mu \cos q_\mu - 4\right]^2\right] \sin p_t \sin q_t e^{-ip_t t}}{\left[m^2 + \sin^2 p_t\right]^2 \left[m^2 + \sum_\mu \sin^2 q_\mu\right]}$$
$$- \frac{64mY^2}{VN_t} \sum_{p_t q} \frac{\left[m^2 - \sin^2 p_t\right] \left[\cos p_t - 1\right] \left[\sum_\mu \cos q_\mu - 4\right] e^{-ip_t t}}{\left[m^2 + \sin^2 p_t\right]^2 \left[m^2 + \sum_\mu \sin^2 q_\mu\right]} \qquad (3.157)$$

$$G_\pi(t) = \frac{4m}{N_t} \sum_{p_t} \frac{e^{-ip_t t}}{\left[m^2 + \sin^2 p_t\right]}$$
$$- \frac{16mY^2}{VN_t} \sum_{p_t q} \frac{\left[\left[\cos p_t - 3\right]^2 + \left[\sum_\mu \cos q_\mu - 4\right]^2\right] \sin p_t \sin q_t e^{-ip_t t}}{\left[m^2 + \sin^2 p_t\right]^2 \left[m^2 + \sum_\mu \sin^2 q_\mu\right]}$$
$$- \frac{64mY^2}{VN_t} \sum_{p_t q} \frac{\left[m^2 - \sin^2 p_t\right] \left[\cos p_t - 3\right] \left[\sum_\mu \cos q_\mu - 4\right] e^{-ip_t t}}{\left[m^2 + \sin^2 p_t\right]^2 \left[m^2 + \sum_\mu \sin^2 q_\mu\right]} \qquad (3.158)$$

plus terms of order Y^4. N_t is the number of sites in the Euclidean time direction on the lattice, and the sum over p_t represents the sum over fermionic lattice momentum states in that direction, as defined in appendix A.1.

3.5.1 Implementation

In the simulations of the Yukawa-Wilson model to look at its phase diagram, each Transputer simulated a separate system so that measurements of the expectation values of observables were done with a large number of different sets of

parameters. In this simulation, sets of seventeen Transputers are used to measure timesliced propagators for only a few sets of the parameters of the model. The lattice is split evenly between sixteen of the processors connected as a 4-D binary hypercube, with one extra processor controlling the others. Apart from this, the implementation is the same as before.

After an initial period of 500 iterations, to allow for equilibration and the choice of optimal run parameters, configurations were saved every 10 iterations, corresponding to 10 units of Monte Carlo time. For each of these saved configurations, columns of the inverse of the fermionic matrix M were calculated, then an average was performed over the saved configurations to produce the timesliced propagators.

To get one column of the inverse fermionic matrix, a unit fermionic source, δ, can be placed at the origin of the lattice, and the vector $X = M^{-1}\delta$ can be calculated using the conjugate gradient algorithm as described in section 1.5. Because of the linear nature of the timesliced propagators studied, then in practice the sum over the spinor degrees of freedom, as well as an average over the spatial position of the delta function source used for the inversions, could be performed by iterating the conjugate gradient algorithm until the required accuracy was achieved once for each of the timesliced propagators studied by using suitable source vectors. Thus to measure the contribution to the timesliced propagators for one of these saved configurations, a source vector, S, is constructed whose components are all zero except for those components with lattice Euclidean time coordinate equal to zero, where all elements are set to $\frac{1}{V_s}$ for G_0, and $\frac{1}{V_s}e^{i\pi x_1}$ for G_π, where V_s is the number of spatial sites on the lattice. The vector $X = M^{-1}S$ is then calculated using the conjugate gradient algorithm, and a sum is then performed on X over the spatial and spinor degrees of freedom.

As in the simulation of the model to study its phase diagram, periodic boundary conditions were used in all directions for both the scalar and the fermionic fields, except in the Euclidean time direction, where anti-periodic boundary conditions were used for the fermionic fields. This meant that the limits $Y \to 0$ and $m \to 0$ were, in principle, accessible to simulation.

	$\delta\tau = 0.3333$	$\delta\tau = 0.1$
Acceptance	0.33	0.92
Q	5.142(6)	5.151(4)
R^2	0.6071(9)	0.6080(6)
Re $P1$	1.4256(6)	1.4249(7)
Im $P1$	-0.0004(6)	-0.0014(8)
$P2$	2.0515(17)	2.0489(15)

Table 3.2: Measured expectation values of observables of the Yukawa-Wilson model with $m = 0.2$, $Y = 0.1$, and $\kappa = 0.05$ on a $4^3 \times 16$ lattice, as a function of $\delta\tau$ with total Monte Carlo time per step fixed at 1.0.

3.5.2 Program Checks

The program checks listed in section 2.4.3 were also applied here.

- Independence of the measured expectation values of observables from the time-step size, $\delta\tau$, and hence the Monte Carlo acceptance probability, was verified. See table 3.2.
- The measured expectation values of observables and the timesliced propagators were compared with values of perturbative expressions for small Y. See figures 3.5, 3.6, 3.7 and 3.8.

3.5.3 Results

Timesliced propagators were measured at two values of Y for various values of m and with $\kappa = 0$. The values of Y studied were $Y = 0.25$ and $Y = 0.5$, which, on the 4^4 lattice with $m = 0$, were in aligned and disordered phases respectively. The values of m studied were $m = 0$ and $m = 0.1$ for $Y = 0.25$, and $m = 0.2$, $m = 0.3$, $m = 0.4$ and $m = 0.5$ for both $Y = 0.25$ and $Y = 0.5$.

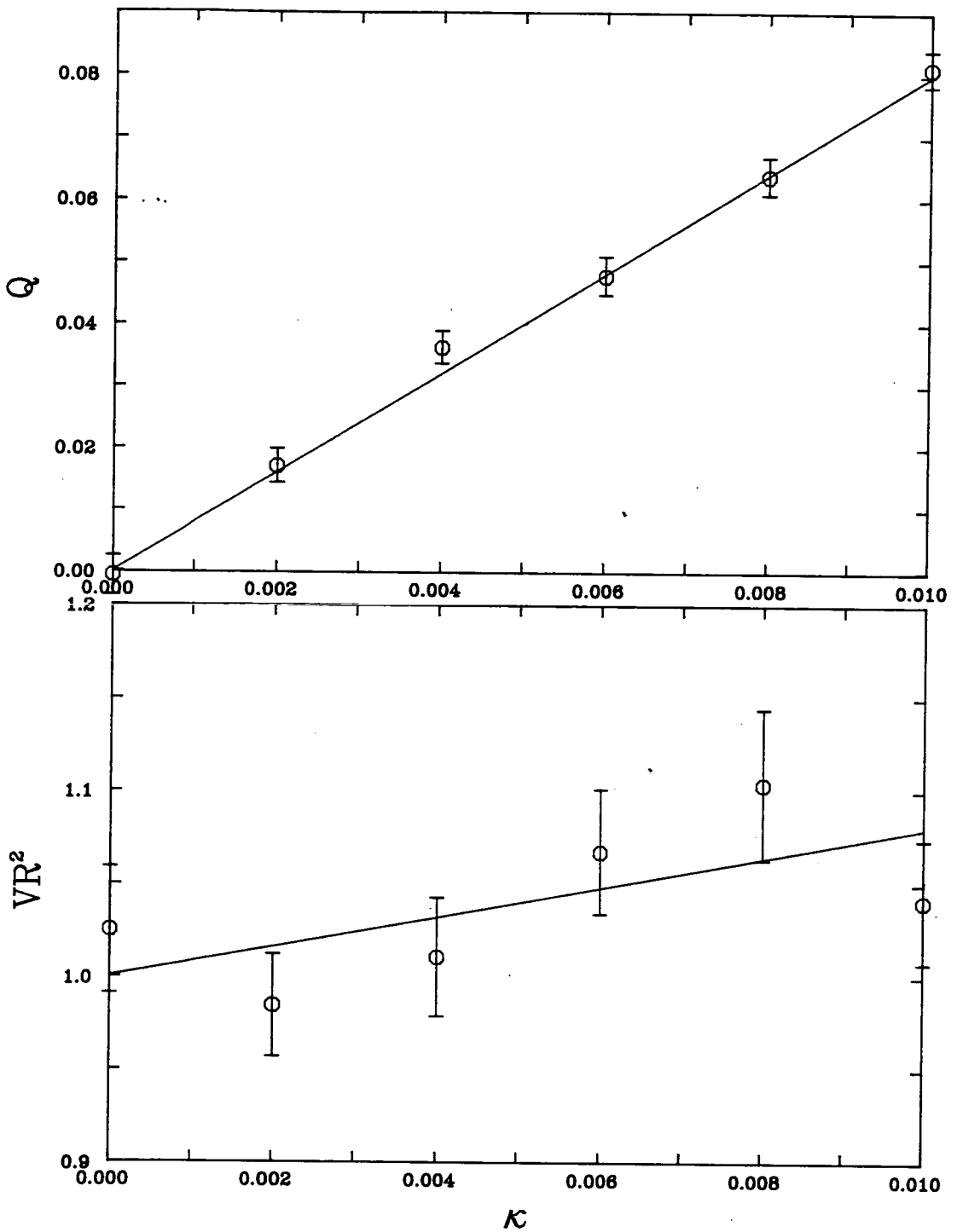

Figure 3.5: Comparison of measured expectation values with perturbative expressions for Q and R^2 when $m = 0$ and $Y = 0$ for small κ on a $4^3 \times 16$ lattice.

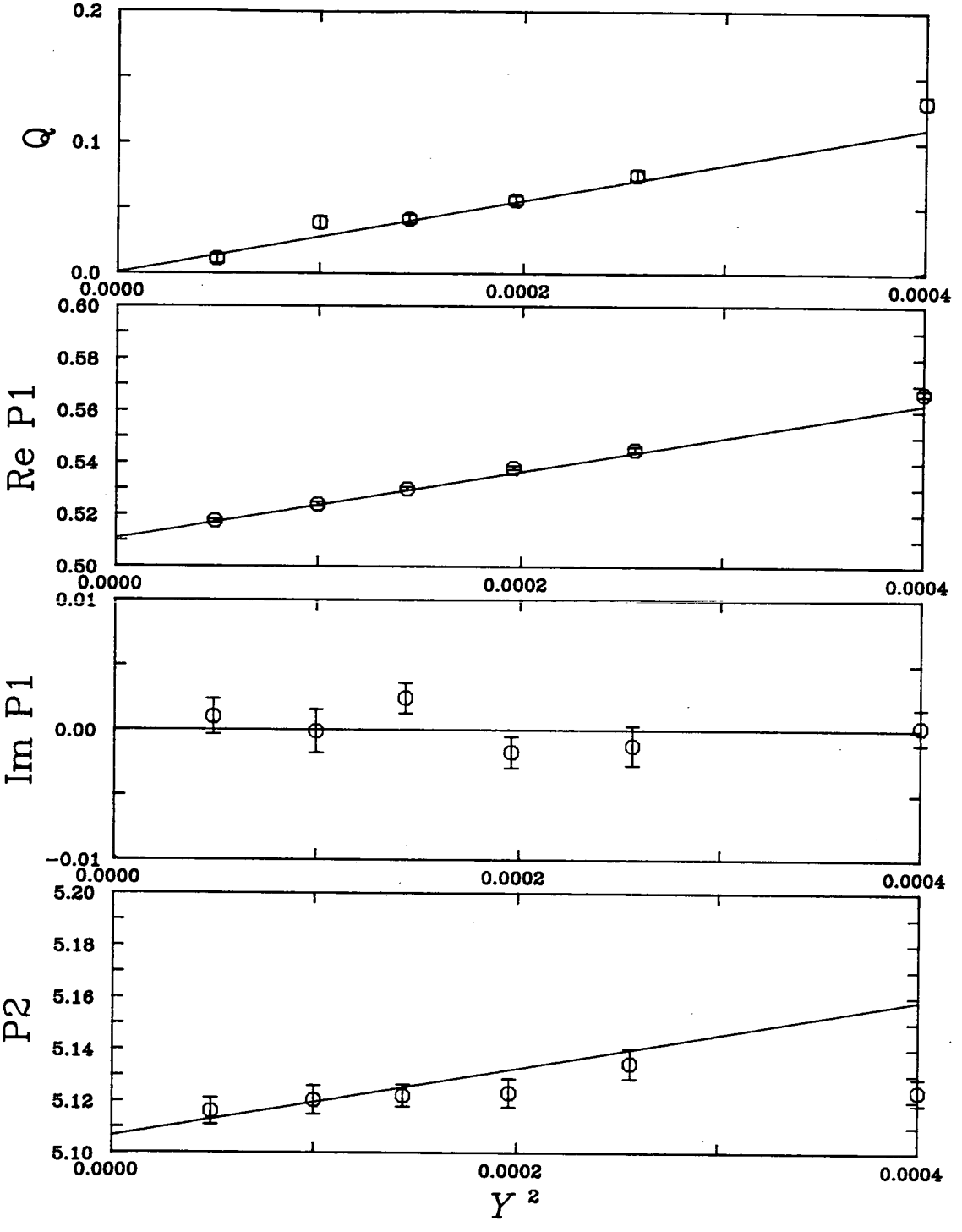

Figure 3.6: Comparison of measured expectation values with perturbative expressions for Q, $P1$ and $P2$ for the Yukawa-Wilson model when $\kappa = 0$ and $m = 0.1$ for small Y on a $4^3 \times 16$ lattice.

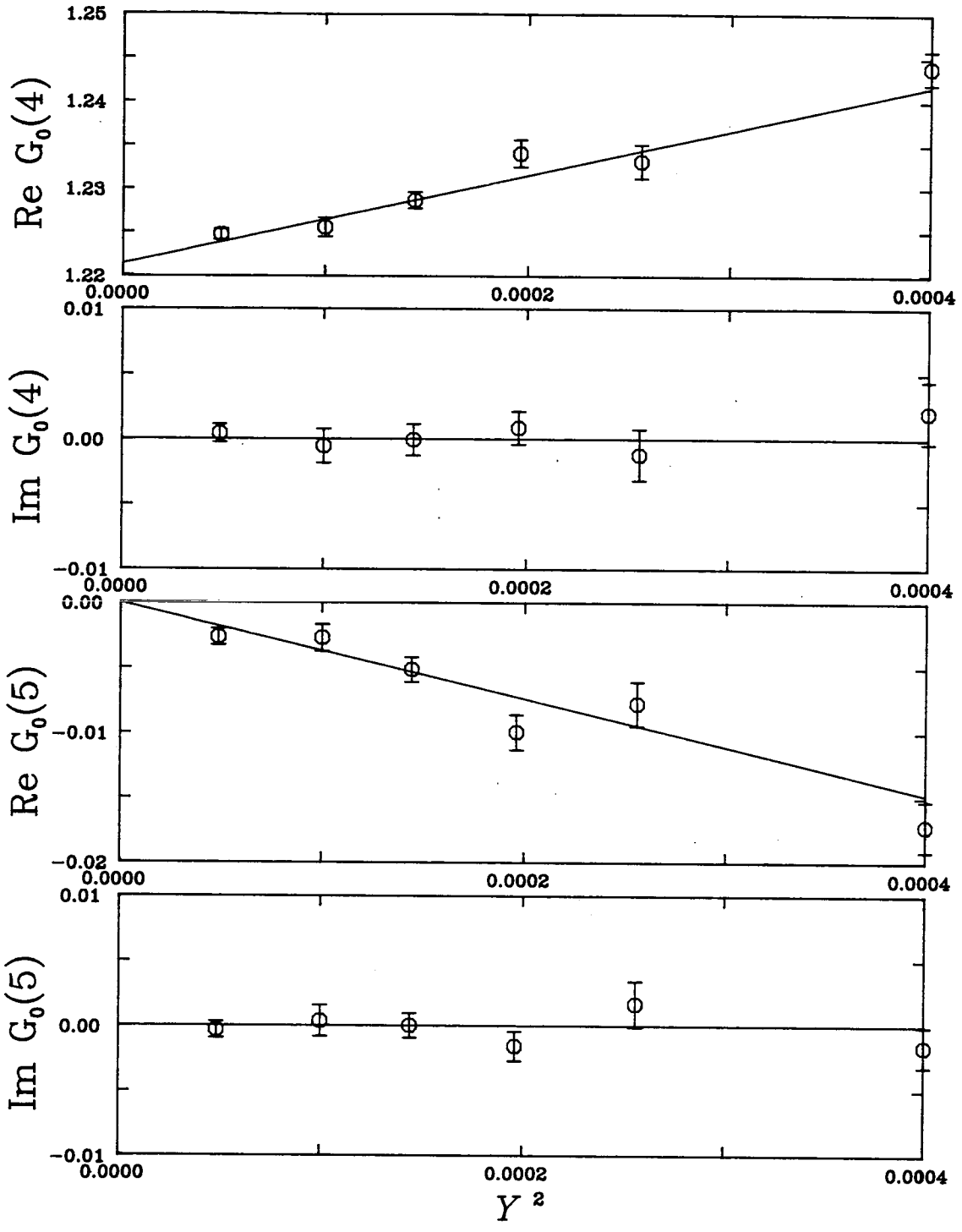

Figure 3.7: Comparison of the measured timesliced propagator, $G_0(t)$, for $t = 4$ and $t = 5$, with values of a perturbative expression for small Y with $\kappa = 0$ and $m = 0.1$ for the Yukawa-Wilson model on a $4^3 \times 16$ lattice.

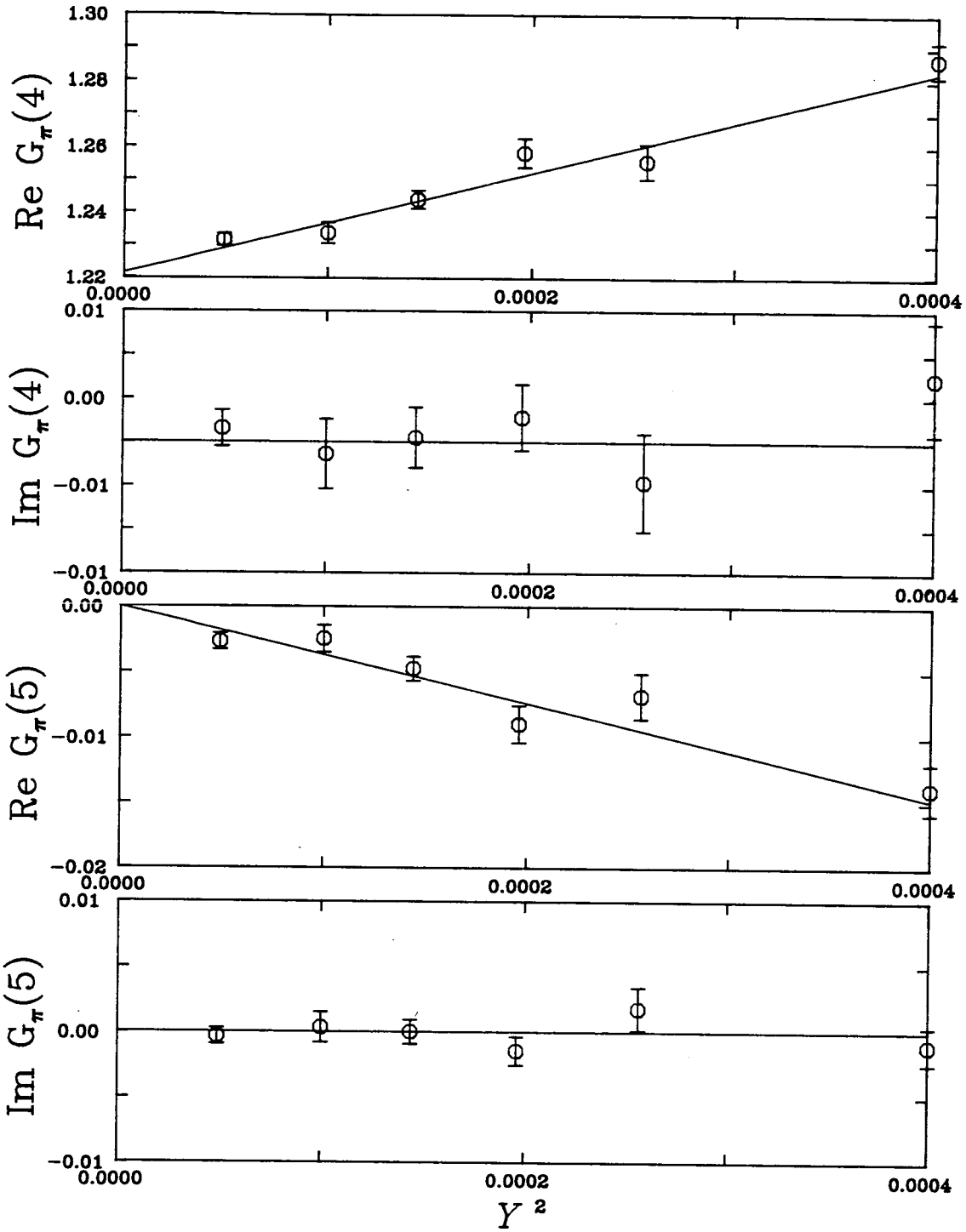

Figure 3.8: Comparison of the timesliced propagator, $G_\pi(t)$, for $t = 4$ and $t = 5$, measured in simulations of the Yukawa-Wilson model, with values of a perturbative expression for small Y with $\kappa = 0$ and $m = 0.1$ on a $4^3 \times 16$ lattice.

Fits to the measured timesliced propagators were made of the form:

$$\begin{aligned}\tilde{G}_p(t) &= A_p\left(e^{-m_p t} - e^{-m_p(16-t)}\right) \\ &\quad + B_p(-1)^t\left(e^{-m'_p t} - e^{-m'_p(16-t)}\right)\end{aligned} \tag{3.159}$$

from which fermion masses m_0 and m_π were found for $G_0(t)$ and $G_\pi(t)$ respectively. The second oscillatory term was included in the case $Y = 0.25$ to take account of the contribution to the timesliced propagators from the fermion state with momentum π in the lattice Euclidean time direction, which was required if reliable values of m_0 and m_π were to be obtained from the fits.

The fits were performed by minimising χ^2 for the fit over a selection of the timeslices:

$$\chi^2 = \sum_t \left(\frac{G_p(t) - \tilde{G}_p(t)}{\sigma_p(t)}\right)^2 \tag{3.160}$$

where $\sigma_p(t)$ is the statistical error in the measurement of $G_p(t)$, and where the sum over t is a sum over a sequence of the timeslices centred about timeslice 8. Because the set of $\sigma_p(t)$ are highly correlated, then the variance in χ^2 with fit parameters cannot be used to give reliable estimates for their errors. The errors in the fit parameters were estimated by performing the fit on timesliced propagators with a sequence of configurations removed from the average, and then looking at the variance of the best fit parameters obtained by excluding different sequences of configurations.

Because of the ill-conditioned nature of the fit problem, no reliable fits to $G_0(t)$ were possible in the case with $Y = 0.25$ and $m = 0$.

The measured timesliced propagators, $G_0(t)$ and $G_\pi(t)$, plus fits of equation (3.159) for the case $Y = 0.25$ with $m = 0.1$ and for the case $Y = 0.5$ with $m = 0.2$ are shown in figures 3.9 and 3.10 respectively. Tables of the mass values obtained from fits of equation (3.159) using a number of selections of timeslices for the fits are shown in tables 3.3 to 3.6 for the cases m_0 when $Y = 0.25$, m_π when $Y = 0.25$, m_0 when $Y = 0.5$, and for m_π when $Y = 0.5$ respectively. Figures 3.11 and 3.12 show the dependence of the measured expectation values of the observables and fermion masses obtained from the fits to the timesliced propagators as a function of the bare fermion mass, m, for $Y = 0.25$ and $Y = 0.5$ respectively.

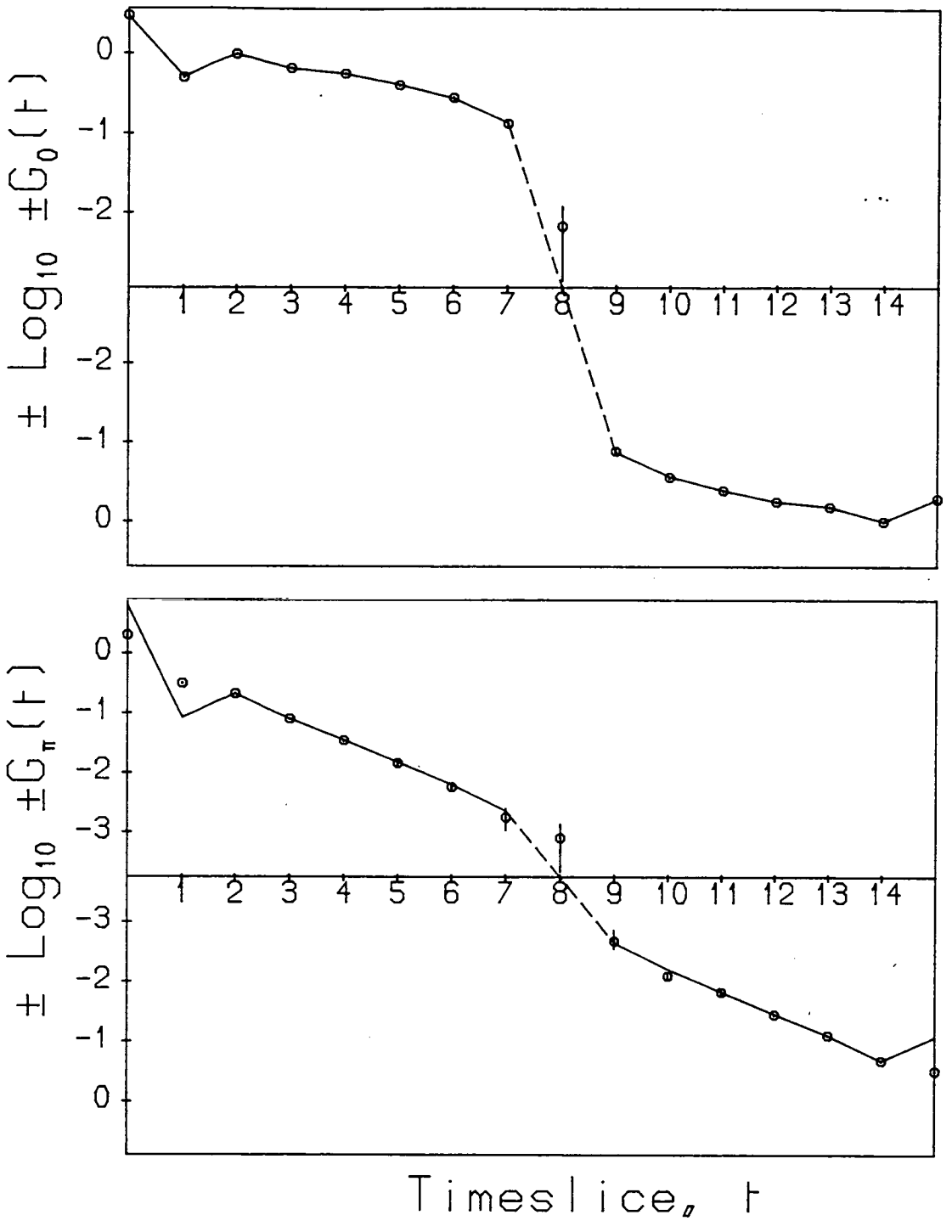

Figure 3.9: Measured zero and π momentum timesliced propagators and fits for $Y = 0.25$ and $m = 0.1$ in the Yukawa-Wilson model taken from a simulation on a 4^3 by 16 lattice. The fits shown are the best fits achieved using timeslices 2 to 14.

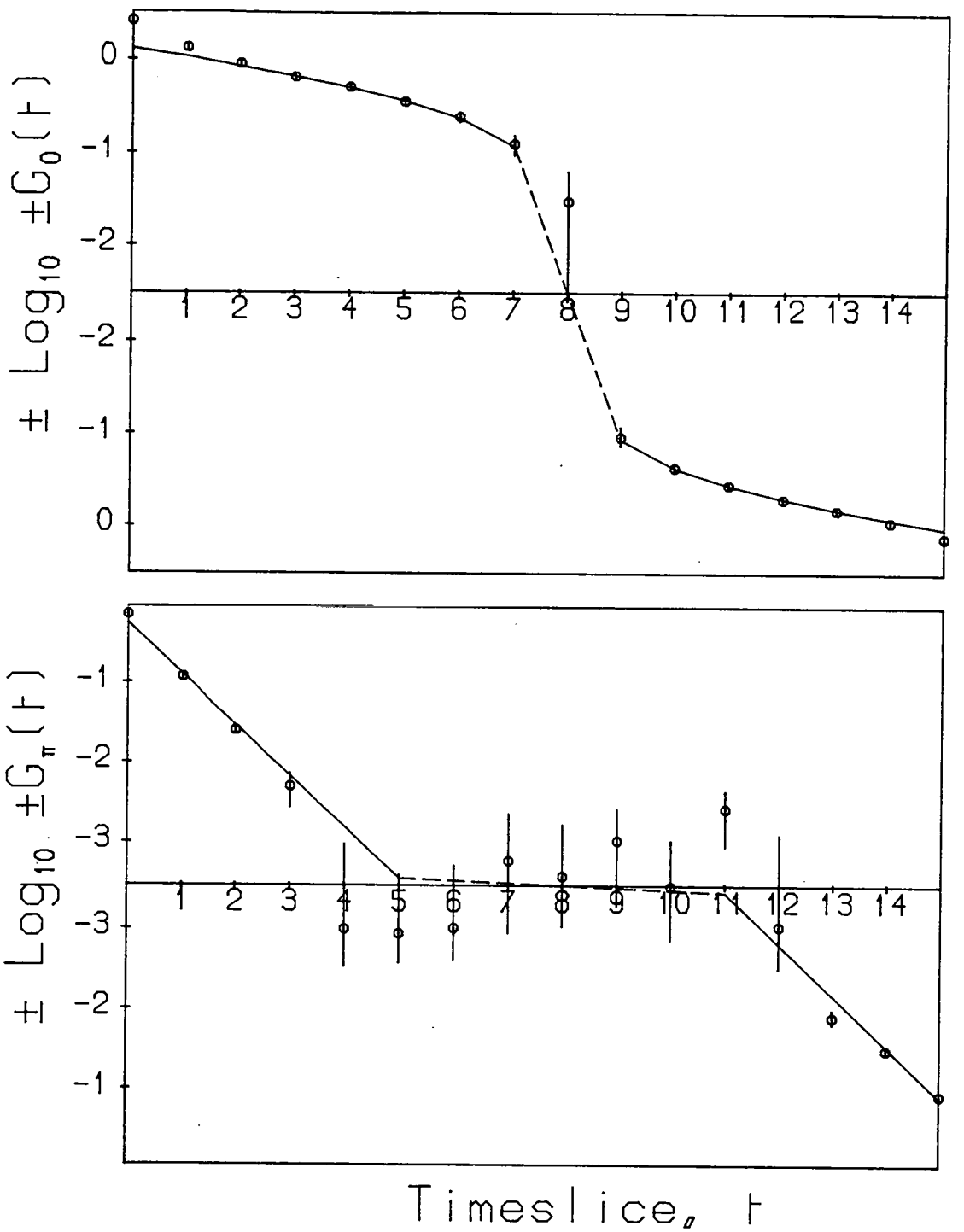

Figure 3.10: Measured zero and π momentum timesliced propagators and fits for $Y = 0.5$ and $m = 0.2$ in the Yukawa-Wilson model taken from a simulation on a 4^3 by 16 lattice. The fits shown are the best fits achieved using timeslices 3 to 13 for G_0, and timeslices 2 to 14 for G_π.

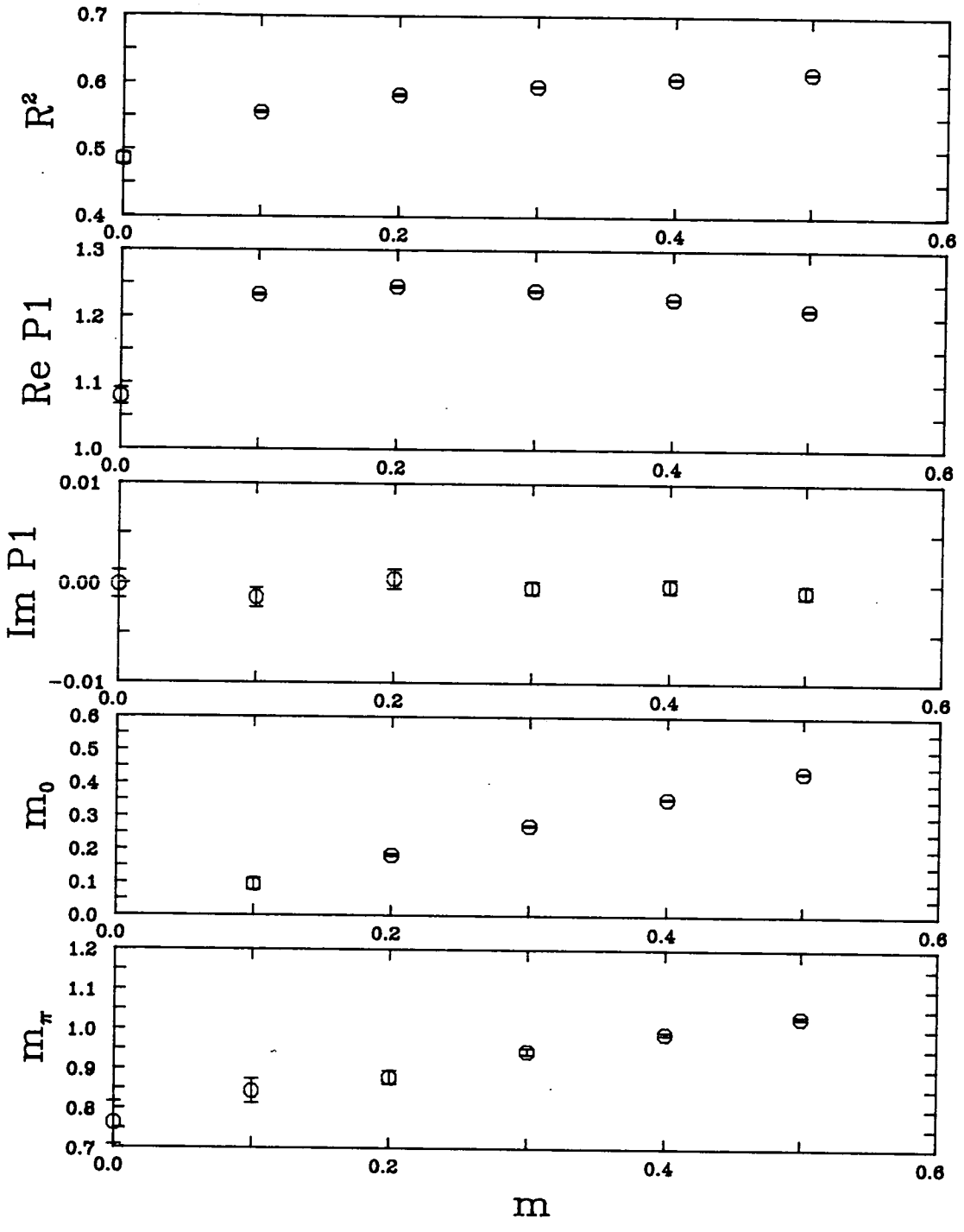

Figure 3.11: Measured expectation values of observables and fitted masses as a function of the bare fermion mass, m, for the Yukawa-Wilson model on a 4^3 by 16 lattice for $Y = 0.25$. The fitted masses are taken from fits to the timesliced propagators from timeslices 2 to 14.

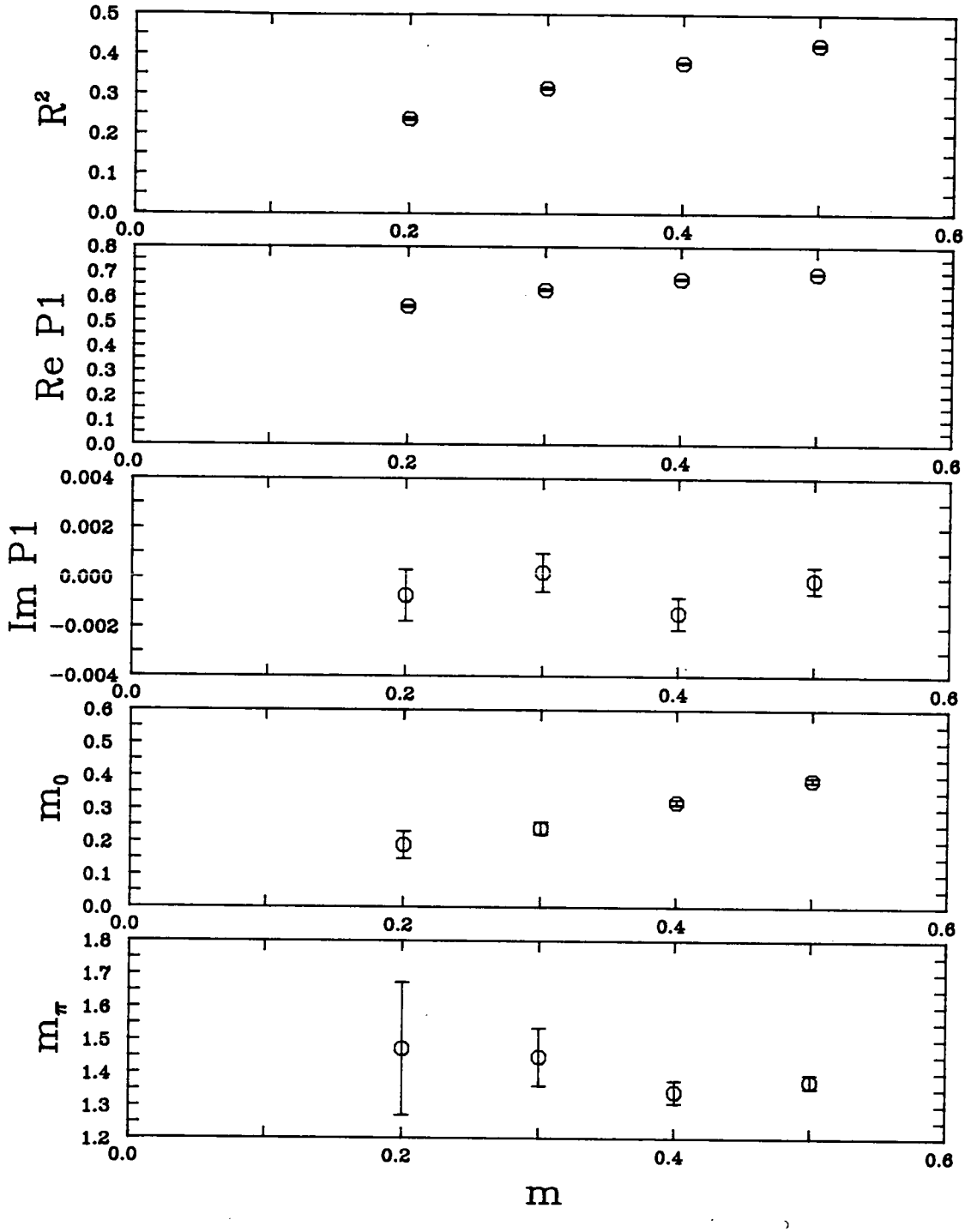

Figure 3.12: Measured expectation values of observables and fitted masses as a function of the bare fermion mass, m, for the Yukawa-Wilson model on a 4^3 by 16 lattice for $Y = 0.5$. The fitted masses are taken from fits to the timesliced propagators, G_0 and G_π, from timeslices 3 to 13 and from timeslices 2 to 14 respectively.

Bare mass	Timeslices used for fit		
m	1-15	2-14	3-13
0.1	0.093(6)	0.094(17)	
0.2	0.186(2)	0.182(4)	
0.3	0.2721(12)	0.2713(18)	0.269(3)
0.4	0.3528(7)	0.3532(13)	0.354(2)
0.5	0.4330(6)	0.4338(10)	0.4336(17)

Table 3.3: Values of the fermion mass measured from the zero momentum propagator, $G_0(t)$, of the Yukawa-Wilson model for $Y = 0.25$ on a 4^3 by 16 lattice using fits starting at timeslices 1 to 3 where possible.

Bare mass	Timeslices used for fit		
m	1-15	2-14	3-13
0.0	0.777(16)	0.76(5)	
0.1	0.8553(12)	0.84(3)	
0.2	0.892(7)	0.878(17)	
0.3	0.944(3)	0.944(8)	
0.4	0.988(3)	0.989(4)	0.994(15)
0.5	1.032(2)	1.032(3)	1.027(5)

Table 3.4: Values of the fermion mass measured from the π momentum propagator, $G_\pi(t)$, of the Yukawa-Wilson model on a 4^3 by 16 lattice for $Y = 0.25$ using fits starting at timeslices 1 to 3 where possible.

As seen in figures 3.11 and 3.12, the imaginary part of the measured expectation value of $P1$ is always consistent with zero. It was also seen that this was true of the imaginary part of the measured timesliced propagators.

Bare mass	Timeslices used for fit			
m	1-15	2-14	3-13	4-12
0.2	0.288(13)	0.23(2)	0.19(4)	0.21(8)
0.3	0.306(7)	0.264(11)	0.240(19)	0.22(4)
0.4	0.361(3)	0.328(5)	0.320(8)	0.320(16)
0.5	0.413(3)	0.388(5)	0.388(8)	0.398(11)

Table 3.5: Values of the fermion mass measured from the zero momentum propagator, $G_0(t)$, of the Yukawa-Wilson model on a 4^3 by 16 lattice for $Y = 0.5$ using fits starting at timeslices 1 to 4.

Bare mass	Timeslices used for fit		
m	1-15	2-14	3-13
0.2	1.41(6)	1.5(2)	
0.3	1.44(2)	1.45(9)	1.6(4)
0.4	1.407(15)	1.34(3)	1.28(11)
0.5	1.417(9)	1.37(2)	1.33(6)

Table 3.6: Values of the fermion mass measured from the π momentum propagator, $G_\pi(t)$, of the Yukawa-Wilson model on a 4^3 by 16 lattice for $Y = 0.5$ using fits starting at timeslices 1 to 3 where possible.

3.5.4 Discussion

At both values of Y, it is seen that the Yukawa-Wilson term induces masses of the order of the inverse lattice spacing for the fermion species that occur at non-zero momentum values for the values of m studied, but it is not clear from this simulation what happens to these masses in the limit $m \to 0$ for $Y = 0.5$. The masses of the physical fermion species, as measured by m_0, are all of order m.

When $Y = 0.25$, it is seen that the scalar sector is aligned in the limit $m \to 0$, as was seen in the simulation of the model with $m = 0$ on the 4^4 lattice, implying that chiral symmetry is not restored in this limit. It is, in fact, spontaneously broken, so that the measured expectation value of $P1$ is non-zero. This suggests, at this value of Y, that the addition of interactions between the fermions and other bosonic fields, such as a gauge field, will require that bare fermion mass tuning will have to be performed if massless fermions are to be simulated as when Wilson fermions are used.

In the simulation of the 4^4 model, in which $m = 0$, it was seen that at $Y = 0.5$ the scalar fields were disordered. In this simulation, at non-zero values of m, the scalar fields are aligned, though it may well be the case that the scalar fields become disordered in the limit $m \to 0$. If this is the case, then the breaking of the residual chiral symmetry of the model by the addition of an explicit fermion mass term induces symmetry breaking in the scalar sector, inducing excess masses for the fermion doubles.

With $m = 0$ for $Y = 0.5$, with the infra-red regulator used, chiral symmetry may well be restored, in which case the masses of the unphysical fermion doubles may well be zero, as suggested by the no-go theorem mentioned in section 1.3.2. However, this $m \to 0$ limit is only accessible to simulation because of the infra-red regulator used. Thus it may be the case that if the infra-red regulator were removed, then at $Y = 0.5$, massless fermions could formally occur in the limit $m \to 0$, when other interactions are included along with this Yukawa-Wilson term is used, even though this limit were not in practice achievable, and the doubled fermion species could still be effectively removed in the continuum limit if their masses depended on the bare fermion mass, m, raised to some power less than one if the physical fermion mass was proportional to m.

For example, figure 3.12 tends to suggest that the expectation value of R^2 is roughly proportional to m in the case $Y = 0.5$ for the smaller values of m studied. If the quantum fluctuations are ignored, then this leads to the speculation that the expectation value of $\phi(x)$ is proportional to $m^{\frac{1}{2}}$. If this is the case, then the excess masses generated for the unphysical fermion species will also be proportional to $m^{\frac{1}{2}}$, whilst the mass of the physical fermion seems to be

proportional to m.

In conclusion, a point split Yukawa term may well be the basis of a mechanism for removing the unphysical doubled fermion species from lattice simulations of quantum field theory models where fermions interact with bosonic fields without the necessity of tuning the bare fermion mass to any other value than zero.

Chapter 4

Prospects

In this short chapter I will suggest some ways in which the work described in this thesis could be extended.

As I write, the first few results from the LEP accelerator at CERN are being collected. With its ability to produce large quantities of Z_0 bosons, this will enable experimental HEP physicists to test many features of the Electroweak sector of the Standard Model. What is not so clear is whether or not any light will be shed on the scalar sector - will a Higgs boson be detected?

The work described in chapter 2 suggests that it may well be possible to construct an alternative action for the Standard Model in which no $\lambda\phi^4$ term is required, a Yukawa coupling between the scalar fields and the fermions may well be enough to ensure that spontaneous symmetry breaking occurs. The Higgs-Yukawa model of chapter 2 could easily be extended to include gauge fields to see how these affect the spontaneous symmetry breaking mechanism that occurs at large Y and to see non-perturbatively how spontaneous symmetry breaking in the scalar sector affects the gauge fields.

One of the prerequisites for relating any study of a lattice model of a quantum field theory involving fermions to real continuum physics is the removal of the unphysical doubled fermion species that are generated when fermionic fields are naively discretised on the lattice. The work on the Yukawa-Wilson model described in chapter 3 suggests a method by which this may be done without

the necessity of tuning the bare fermion mass. This Yukawa-Wilson model can easily be extended to include gauge fields, $U_\mu(x)$, which represent elements of the gauge group $SU(N)$ (or $U(1)$) and sit on the links connecting lattice sites, by a fermionic term in the action [28,29,30]:

$$\overline{\Psi} M \Psi = \frac{1}{2} \sum_{x\mu} \overline{\psi}(x) \gamma_\mu \left[\left(R + U_\mu(x) L \right) \psi(x+\mu) - \left(R + U_\mu^\dagger(x-\mu) L \right) \psi(x-\mu) \right]$$
$$+ Y \sum_{xy\mu} \overline{\psi}(x) \left[\delta(y, x+\mu) + \delta(y, x-\mu) - 2\delta(y,x) \right] \left[\phi(x) R + \phi^\dagger(y) L \right] \psi(y) \tag{4.161}$$

as well as a pure gauge term [31]:

$$- \frac{\beta}{N} \sum_{\square} \mathrm{Re\ Tr} [U_\square] \tag{4.162}$$

where the sum represents the sum over elementary square tiles bounded by links connecting nearest neighbour sites on the lattice, called plaquettes, and $U_\square$ is the ordered product of $SU(N)$ link matrices around the plaquette.

In this way the gauge fields couple directly only to one of the two handed components of the fermionic fields. With the two sets of fermionic fields used for a Hybrid Monte Carlo simulation, then if the auxiliary fields remove the unwanted fermion doubles in the continuum limit when the lattice spacing is taken to zero, there will remain only one left handed and one right handed fermion coupled to the gauge fields and one left handed and one right handed neutrino. To get just one neutrino in the continuum limit, a way must be found to simulate lattice models with non-Hermitian actions when the fermionic fields are replaced by pseudo-fermions, as then the Boltzmann-like factor $e^{-\mathcal{H}}$ that occurs in the Hybrid Monte Carlo algorithm is no longer guaranteed to be real and positive and so cannot be interpreted probabilistically.

If any lattice model of a quantum field theory is to be used to make accurate predictions about the continuum quantum field theory, then it is necessary to take the continuum limit of the lattice model. This continuum limit occurs when the lattice spacing is taken to zero. For the lattice model to have a well defined behaviour in the limit where the lattice spacing is taken to zero, then the behaviour of the system must be independent of the lattice spacing in that limit. This means that the lattice spacing must be irrelevant in the renormalisation

group sense, which can only be the case at a phase transition. Thus continuum behaviour is seen by studying the lattice models close to phase transitions on lattices of various sizes and extrapolating results to the infinite lattice limit. For models involving fermions this is wishful thinking, as the computers at present are orders of magnitude too slow to be used for simulations of lattice models on the required sized lattices using the best algorithms known to date.

It may be possible to look at the continuum limits of some pure bosonic lattice models, however, and thus the $Y = \infty$ limit of the Higgs-Yukawa model studied in chapter 2 may be amenable to study in the continuum limit, as the effect of the fermions on the scalar sector in this limit can be represented by a simple effective term in the action.

In spite of these limitations, I have been able to study models of quantum field theories on small lattices and observe phenomena not previously seen from which general conclusions can be drawn about the physical world about us.

Appendix A

Conventions Used

A.1 Fourier Transforms

This section describes the conventions used in this thesis for performing discrete Fourier transforms on the lattice.

Given the discrete version of the Dirac delta function on a regular hypercubic lattice:

$$\delta(a,b) = \frac{1}{V}\sum_{c} e^{ic(a-b)} \tag{A.163}$$

where the sum over c represents the sum over lattice sites (or lattice sites plus a constant vector), a and b are vectors on the reciprocal lattice (plus a constant), or vice versa, and V is the number of sites on the lattice. Then it is possible to write down quantities defined at lattice points, for example $\phi(x)$ in terms of sums with coefficients over momentum states:

$$\phi(x) = \sum_{p} \tilde{\phi}(p) e^{ipx} \tag{A.164}$$

where the sum over p represent the sums over the lattice directions, μ, and the allowed values of the lattice momenta p_μ where:

$$p_\mu = 0, \frac{2\pi}{L_\mu}, \cdots, \frac{2(L_\mu - 1)\pi}{L_\mu} \tag{A.165}$$

for directions in which $\phi(x)$ has periodic boundary conditions, and:

$$p_\mu = \frac{\pi}{L_\mu}, \frac{3\pi}{L_\mu}, \cdots, \frac{(2L_\mu - 1)\pi}{L_\mu} \tag{A.166}$$

for directions where it has anti-periodic boundary conditions, L_μ being the number of sites in that direction.

The inverse relation is:

$$\tilde{\phi}(p) = \frac{1}{V}\sum_x \phi(x)\, e^{-ipx} \tag{A.167}$$

where the sum over x represents the sum over sites on the lattice.

It is also possible to define the discrete Fourier transform of operators, represented by matrices on the lattice:

$$\begin{aligned}\Phi^\dagger M \Phi &= \sum_{xy} \phi^\star(x)\, M(x,y)\phi(y) \\ &= \sum_{pqxy} \tilde{\phi}^\star(p) e^{-ipx} M(x,y) e^{iqy} \tilde{\phi}(q) \\ &= \sum_{pq} \tilde{\phi}^\star(p) \tilde{M}(p,q) \tilde{\phi}(q)\end{aligned} \tag{A.168}$$

where:

$$M(x,y) = \frac{1}{V^2}\sum_{pq} e^{ipx} \tilde{M}(x,y) e^{-iqy} \tag{A.169}$$

with the inverse relation:

$$\tilde{M}(p,q) = \sum_{xy} e^{ipx} M(x,y) e^{-iqy} \tag{A.170}$$

If M is translationally invariant, i.e. $M(x,y) = M(x-y)$ then:

$$M(x-y) = \frac{1}{V}\sum_p e^{ip(x-y)} \tilde{M}(p) \tag{A.171}$$

A.2 Gamma Matrices

The Hermitian four dimensional Euclidean Gamma matrices used in this thesis are:

$$\gamma_0 = \begin{pmatrix} 1 & 0 & 0 & 0 \\ 0 & 1 & 0 & 0 \\ 0 & 0 & -1 & 0 \\ 0 & 0 & 0 & -1 \end{pmatrix}$$

$$\gamma_1 = \begin{pmatrix} 0 & 0 & 0 & i \\ 0 & 0 & i & 0 \\ 0 & -i & 0 & 0 \\ -i & 0 & 0 & 0 \end{pmatrix}$$

$$\gamma_2 = \begin{pmatrix} 0 & 0 & 0 & 1 \\ 0 & 0 & -1 & 0 \\ 0 & -1 & 0 & 0 \\ 1 & 0 & 0 & 0 \end{pmatrix}$$

$$\gamma_3 = \begin{pmatrix} 0 & 0 & i & 0 \\ 0 & 0 & 0 & -i \\ -i & 0 & 0 & 0 \\ 0 & i & 0 & 0 \end{pmatrix} \qquad \text{(A.172)}$$

corresponding to the directions t, x, y and z on the Euclidean lattice.

Also:

$$\gamma_5 = \begin{pmatrix} 0 & 0 & 1 & 0 \\ 0 & 0 & 0 & 1 \\ 1 & 0 & 0 & 0 \\ 0 & 1 & 0 & 0 \end{pmatrix} \qquad \text{(A.173)}$$

These matrices satisfy the anti-commutation relations:

$$\gamma_\alpha \gamma_\beta + \gamma_\beta \gamma_\alpha = 2\delta(\alpha, \beta) \qquad \text{(A.174)}$$

and have the trace properties:

$$\begin{aligned} \mathrm{Tr}[\gamma_\alpha] &= 0 \\ \mathrm{Tr}[\gamma_\alpha \gamma_\beta] &= 4\delta(\alpha, \beta) \end{aligned} \qquad \text{(A.175)}$$

α and β taking on the values 0, 1, 2, 3 and 5.

The left-handed and right-handed chiral projection operators, L and R, are defined as:

$$\begin{aligned} L &= \frac{1}{2}(1 - \gamma_5) \\ R &= \frac{1}{2}(1 + \gamma_5) \end{aligned} \qquad \text{(A.176)}$$

having the properties:

$$\begin{aligned} LL &= L \\ RR &= R \\ RL &= LR \\ &= 0 \\ L+R &= 1 \end{aligned} \tag{A.177}$$

With the trace properties:

$$\begin{aligned} \mathrm{Tr}[L] &= \mathrm{Tr}[R] \\ &= 2 \end{aligned} \tag{A.178}$$

Acknowledgements

I thank my supervisors Richard Kenway and Ken Bowler for their help and support and for their tireless efforts in attempting to correct my spelling and grammar.

I acknowledge the fact that David Stephenson was not only my collaborator for some of the work described in this thesis, but also the inspiration for much of the rest.

I thank Brian Pendleton for putting up with me repeatedly interrupting him to seek advice about many aspects of the work presented in this thesis. I also thank Tien Kieu for the useful contributions he made to this work.

I acknowledge the support of the SERC.

The computer simulations described in this thesis were performed on the Edinburgh Concurrent Supercomputer which is supported by SERC under grant GR/E/21810, the Computer Board, the DTI and Meiko Ltd.

Bibliography

[1] D. Stephenson and A. Thornton. Non-perturbative Yukawa couplings. *Phys. Lett. B*, 212:479, 1988.

[2] A.M. Thornton. Radially free Higgs-Yukawa model. *Phys. Lett. B*, 214:577, 1988.

[3] A.M. Thornton. A Yukawa-Wilson model. *Phys. Lett. B*, 221:151, 1989.

[4] A.M. Thornton. Fermion propagators from a Yukawa-Wilson model. *Phys. Lett. B*, To appear, 1989.

[5] M.J. Creutz. *Quarks, Gluons and Lattices.* Cambridge University Press, 1983.

[6] N. Kawamoto and J. Smit. Effective lagrangian and dynamical symmetry breaking in strongly coupled lattice QCD. *Nucl. Phys. B*, 192:100, 1981.

[7] L. Susskind. Lattice fermions. *Phys. Rev. D*, 16:3031, 1977.

[8] K.G. Wilson. Quarks and strings on a lattice. In A. Zichichi, editor, *New Phenomena in Subnuclear Physics*, page 69, Plenum, New York, 1977.

[9] H.B. Nielson and M. Ninomiya. Absence of neutrinos on a lattice I. *Nucl. Phys. B*, 185:20, 1981.

[10] H.B. Nielson and M. Ninomiya. Absence of neutrinos on a lattice II. *Nucl. Phys. B*, 193:173, 1981.

[11] S. Duane, A.D. Kennedy, B.J. Pendleton, and D. Roweth. Hybrid Monte Carlo. *Phys. Lett. B*, 195:216, 1987.

[12] M.R. Hestenes and E. Stiefel. Methods of conjugate gradients for solving linear systems. *J. Res. Nat. Bur. Standards*, 49:409, 1952.

[13] G.H. Golub and C.F. Van Loan. *Matrix Computations*, page 352. John Hopkins Univ. Press, Baltimore, 1983.

[14] J. Stoer and R. Bulirsch. *Introduction to Numerical Analysis*, page 572. Springer-Verlag, Berlin, 1980.

[15] I.S. Berezin and N.P. Zhidkov. *Computing Methods*, page 23. Volume 2, Pergamon, Oxford, 1965.

[16] J.K. Reid. On the method of conjugate gradients for the solution of large sparse systems of linear equations. In *Proc. Conf. Large Sparse Sets of Linear Equations*, Academic Press, New York, 1971.

[17] P. Concus, G.H. Golub, and D.P. O'Leary. A generalized conjugate gradient method for the numerical solution of elliptic partial differential equations. In J. Bunch and D. Rose, editors, *Sparse Matrix Computations*, page 309, Academic Press, New York, 1976.

[18] C.B. Chalmers, R.D. Kenway, and D. Roweth. Algorithms for calculating quark propagators on large lattices. *J. Comp. Phys.*, 70:500, 1987.

[19] Y. Oyanagi. An incomplete LDU decomposition of lattice fermions and its application to conjugate residual methods. *Comp. Phys. Comms.*, 42:333, 1986.

[20] P.W. Higgs. Broken symmetries, massless particles and gauge fields. *Phys. Lett.*, 12:132, 1964.

[21] P.W. Higgs. Broken symmetries and the mass of gauge bosons. *Phys. Rev. Lett.*, 13:508, 1964.

[22] P.W. Higgs. Spontaneous symmetry breakdown without massless bosons. *Phys. Rev.*, 145:1156, 1966.

[23] T.W.B. Kibble. Symmetry breaking in non-abelian gauge theories. *Phys. Rev.*, 155:1554, 1967.

[24] F. Englert and R. Brout. Broken symmetry and the mass of gauge vector mesons. *Phys. Rev. Lett.*, 13:321, 1964.

[25] G.S. Guralnik, C.R. Haglen, and T.W.B. Kibble. Global conservation laws and massless particles. *Phys. Rev. Lett.*, 13:585, 1964.

[26] R.G. Thornton. Private communication.

[27] D. Bailin and A. Love. *Introduction to Gauge Field Theory*, chapter 14. Adam Hilger, 1986.

[28] L.H. Karsten. In W. Ruhl, editor, *Field Theoretical Methods in Particle Physics*, Plenum, New York, 1980.

[29] J. Smit. *Acta. Phys. Polon. B*, 17:531, 1986.

[30] P.V.D. Swift. The electroweak theory on the lattice. *Phys. Lett. B*, 145:256, 1984.

[31] K.G. Wilson. Confinement of quarks. *Phys. Rev. D*, 10:2445, 1974.